

CLIMATE, DROUGHT, AND SEA LEVEL RISE SCENARIOS FOR CALIFORNIA'S FOURTH CLIMATE CHANGE ASSESSMENT

A Report for:

California's Fourth Climate Change Assessment

Prepared By:

David W. Pierce¹

Julie F. Kalansky¹

Daniel R. Cayan¹

**1 Division of Climate, Atmospheric Sciences, and Physical
Oceanography
Scripps Institution of Oceanography, La Jolla, California**

DISCLAIMER

This report was prepared as the result of work sponsored by the California Energy Commission. It does not necessarily represent the views of the Energy Commission, its employees or the State of California. The Energy Commission, the State of California, its employees, contractors and subcontractors make no warrant, express or implied, and assume no legal liability for the information in this report; nor does any party represent that the uses of this information will not infringe upon privately owned rights. This report has not been approved or disapproved by the California Energy Commission nor has the California Energy Commission passed upon the accuracy or adequacy of the information in this report.



Edmund G. Brown, Jr., *Governor*

August 2018

CCCA4-CEC-2018-006

ACKNOWLEDGEMENTS

We acknowledge the World Climate Research Programme's Working Group on Coupled Modelling, which is responsible for the Climate Model Intercomparison Project (CMIP), and we thank the climate modeling groups for producing and making available their model output. For CMIP the U.S. Department of Energy's Program for Climate Model Diagnosis and Intercomparison provides coordinating support and led development of software infrastructure in partnership with the Global Organization for Earth System Science Portals.

This work was supported by the California Energy Commission, Agreement Number 500-14-005. Additional support was obtained from the U.S. Army Corps of Engineers, from the U.S. Department of Interior/U.S. Geological Survey via the Southwest Climate Science Center, and from the National Oceanographic and Atmospheric Administration Regional Integrated Sciences and Assessments (RISA) Program through the California Nevada Applications Program RISA.

PREFACE

California's Climate Change Assessments provide a scientific foundation for understanding climate-related vulnerability at the local scale and informing resilience actions. These assessments contribute to the advancement of science-based policies, plans, and programs to promote effective climate leadership in California. In 2006, California released its First Climate Change Assessment, which shed light on the impacts of climate change on specific sectors in California and was instrumental in supporting the passage of the landmark legislation Assembly Bill 32 (Núñez, Chapter 488, Statutes of 2006), California's Global Warming Solutions Act. The Second Assessment concluded that adaptation is a crucial complement to reducing greenhouse gas emissions (2009), given that some changes to the climate are ongoing and inevitable, motivating and informing California's first Climate Adaptation Strategy released the same year. In 2012, California's Third Climate Change Assessment made substantial progress in projecting local impacts of climate change, investigating consequences to human and natural systems, and exploring barriers to adaptation.

Under the leadership of Governor Edmund G. Brown, Jr., a trio of state agencies jointly managed and supported California's Fourth Climate Change Assessment: California's Natural Resources Agency (CNRA), the Governor's Office of Planning and Research (OPR), and the California Energy Commission (Energy Commission). The Climate Action Team Research Working Group, through which more than 20 state agencies coordinate climate-related research, served as the steering committee, providing input for a multi-sector call for proposals, participating in selection of research teams, and offering technical guidance throughout the process.

California's Fourth Climate Change Assessment (Fourth Assessment) advances actionable science that serves the growing needs of state and local-level decision-makers from a variety of sectors. It includes research to develop rigorous, comprehensive climate change scenarios at a scale suitable for illuminating regional vulnerabilities and localized adaptation strategies in California; datasets and tools that improve integration of observed and projected knowledge about climate change into decision-making; and recommendations and information to directly inform vulnerability assessments and adaptation strategies for California's energy sector, water resources and management, oceans and coasts, forests, wildfires, agriculture, biodiversity and habitat, and public health.

The Fourth Assessment includes 44 technical reports to advance the scientific foundation for understanding climate-related risks and resilience options, nine regional reports plus an oceans and coast report to outline climate risks and adaptation options, reports on tribal and indigenous issues as well as climate justice, and a comprehensive statewide summary report. All research contributing to the Fourth Assessment was peer-reviewed to ensure scientific rigor and relevance to practitioners and stakeholders.

For the full suite of Fourth Assessment research products, please visit www.climateassessment.ca.gov. This report contributes to energy sector vulnerability assessment and supports Fourth Assessment research by providing high-resolution projections of future climate and hydrological parameters of importance to the energy system as well as probabilistic and hourly sea level rise projections, stream flows at select locations, and extended drought scenarios.

ABSTRACT

Daily temperature and precipitation over California at a resolution of 1/16° (about 6 km, or 3.7 miles) were generated to support climate change impact studies for the energy system and other sectors featured in the California's Fourth Climate Change Assessment. The data, derived from 32 coarse-resolution (~ 100 km) global climate models (GCMs), were bias corrected and downscaled using the Localized Constructed Analogues (LOCA) statistical method. The data cover 1950-2005 for the historical period and 2006-2100 for two future climate projections using medium and high greenhouse gas and aerosol emissions scenarios. Statewide, temperature is projected to increase 2-4 °C (medium emissions scenario) to 4-7 °C (high emissions scenario) by the end of this century. Precipitation shows fewer wet days, wetter winters, drier springs and autumns, and an increase in dry years as well as maximum precipitation in a single day.

Ten GCMs that closely simulate California's climate are identified for studies where all 32 GCMs cannot be used. Additional variables were downscaled for these 10, including wind speed, specific and relative humidity, and surface solar radiation. Four models that span the temperature and precipitation changes from the 10 are identified for studies that cannot accommodate the 10. Wind speed shows small decreases, while relative humidity changes are more complicated, with coastal increases but decreases inland. Surface solar radiation shows small Southern California increases in spring.

The downscaled fields were applied to the Variable Infiltration Capacity (VIC) land surface model to develop snow cover, soil moisture, runoff, water loss from plants, surface heat fluxes, and other parameters. Moisture deficit is projected to increase over much of the state, particularly Northern California and the Sierra Nevada, while top level soil moisture is projected to decrease, particularly in Southern California. Most streamflows shift to earlier in the year, with the bigger shifts experienced in basins which currently have substantial contributions from snowmelt.

Two versions of a 20-year dry spell were identified from one of the GCM simulations to investigate future drought: the original episode from 2051-2070, and one shifted earlier in the century with temperatures consistent with 2023-2042. For both, we provide downscaled temperatures and precipitation along with VIC hydrological output.

Sea level rise (SLR) projections for California were generated using a probabilistic approach employing estimates of the components that contribute to global and regional SLR, including new science on the possibility of increased contribution from Antarctica. Hourly projections of sea level at selected coastal locations were generated out to 2100 that include tides, regional and local weather influences, and short period Pacific climate fluctuations along with the aforementioned sea level rise scenarios.

The climate scenario and SLR data are available online from cal-adapt.org.

Keywords: Climate scenarios, climate change, downscaling, sea level rise, drought

Please use the following citation for this paper:

Pierce, D. W., J. F. Kalansky, and D. R. Cayan, (Scripps Institution of Oceanography). 2018. *Climate, Drought, and Sea Level Rise Scenarios for the Fourth California Climate Assessment*. California's Fourth Climate Change Assessment, California Energy Commission. Publication Number: CNRA-CEC-2018-006.

HIGHLIGHTS

- Daily, 1/16° (6 km) spatial resolution projections of precipitation, minimum and maximum temperature, specific and relative humidity, wind speed, and surface solar radiation over California were generated from multiple global climate models (GCMs) using Localized Constructed Analogues (LOCA) downscaling.
- Subsets of 10 and 4 models that do a good job simulating important aspects of California's climate are identified for situations in which using all 32 GCMs is impractical.
- Statewide warming of 2-4 °C (RCP 4.5, medium emissions scenario) to 4-7 °C (RCP 8.5, business as usual scenario) is projected by the end of the century. The warming has implications for electricity demand via air conditioning, delivery through the effects of temperature on transmission lines, human health, and agriculture.
- Mean annual precipitation is projected to increase modestly in the northern part of the state, but year-to-year variability is also projected to increase, leading to a greater incidence of dry years in future decades, which may affect state hydropower generation.
- By the end of the century under the RCP 8.5 scenario, winter precipitation is projected to increase by up to 20%, but decrease in spring and autumn by up to 20%. These changes will present a challenge to the operation of existing water storage infrastructure including reservoirs and associated hydroelectric plants, which are an important source of California's electricity.
- Daily extreme precipitation values are projected to increase 5-15% (RCP 4.5) to 15-20% (RCP 8.5), presenting challenges for storm drainage and flood control.
- The downscaled fields were applied to the Variable Infiltration Capacity (VIC) land surface model to develop snow cover, soil moisture, runoff, water loss from plants, surface heat fluxes, etc. Streamflow was derived by routing VIC runoff into selected basins' channel systems. Basins that are currently snow dominated show a shift to earlier flow as more winter precipitation falls as rain instead of snow and what snow there is melts earlier. These shifts will have further implications for the operation of reservoirs and hydroelectric energy generation in addition to those effects noted above.
- Moisture deficit is projected to increase over much of the state, but with only small changes in the Central Valley. Top level soil moisture is projected to decrease, especially in the southern half of the state.
- Two versions of a 20-year dry spell were identified (one earlier in this century, one later) for evaluation of drought impacts. Both provide downscaled temperatures, precipitation, and key aspects of the surface hydrology (runoff, snow cover, soil moisture, and so forth).
- Probabilistic sea level rise (SLR) projections were generated under RCP 4.5 and RCP 8.5, with estimates of changes in contributors to global and regional SLR, and incorporating new science on potential Antarctic ice loss. Additionally, hourly projections of sea level at selected coastal locations were generated that include tides, regional and local weather influences, and short period Pacific climate fluctuations, atop the aforementioned sea level rise scenarios.

TABLE OF CONTENTS

ACKNOWLEDGEMENTS	i
PREFACE	ii
ABSTRACT	iii
HIGHLIGHTS	iv
TABLE OF CONTENTS	v
1: Introduction	1
2: Global Climate Models	2
3: Bias Correction and LOCA Downscaling	3
3.1 Selecting Global Climate Models for Impact Studies.....	3
3.2 Downscaling Methods.....	7
3.2.1 Temperature and Precipitation.....	8
3.2.2 Humidity.....	8
3.2.3 Wind Speed.....	9
3.2.4 Surface Solar Radiation.....	9
3.3 Temperature and Precipitation Results.....	10
3.3.1 Effect of Changes in the Base Period.....	14
3.3.2 Future Changes in Temperature.....	17
3.3.3 Future Changes in Precipitation.....	20
3.4 Relative Humidity Results.....	28
3.5 Wind Speed Results.....	30
3.5.1 Santa Ana Winds.....	31
3.6 Surface Solar Radiation Results.....	39
4: VIC Hydrological Model Simulations	43
4.1 Streamflow.....	47
5: Drought Scenarios	52
6: Sea Level Rise Projections	56
6.1 Global SLR Components and Uncertainty.....	56

6.2 Regional Sea Level Rise.....	58
6.3 Expert Panel to Guide SLR Scenarios used in the Fourth Assessment	59
6.4 Probabilistic Sea Level Rise Scenarios	59
6.5 Hourly Sea Level Projections at California Coast Tide Gauge Locations	62
7: Conclusions and Future Directions	64
8: References	68

1: Introduction

Informed policy-making requires the best, most up to date scientific information possible on the problem domain. Addressing the issues of climate change in a region as climatically diverse as California is challenging, and is best done using the most physically realistic, spatially detailed climate change information available. No single projection of future climate is adequate for such a task. Rather, a suite of climate scenarios is needed, one that takes into account uncertainty in future greenhouse gas and atmospheric aerosol emissions as well as the diversity of scientific models of the Earth's climate and its response to greenhouse gas and aerosol forcing.

To address this need for climate scenarios in support of the California's Fourth Climate Change Assessment (Fourth Assessment), we have produced downscaled projections of meteorological and hydrological variables, drought scenarios, and sea level rise for California. The purpose of this report is to describe the procedures and methods used in the construction of these data. The data are aimed to inform a wide variety of applications, including energy demand (e.g., cooling), delivery (the effect of temperature on transmission lines), and supply (e.g., hydropower and photovoltaic production), human health (humidity and temperature extremes), and agriculture (e.g., drought).

The basis for these projections is a set of 32 global climate model (GCM) simulations produced by institutions across the world. To address the uncertainty in future concentrations of greenhouse gases and emissions of aerosols, we used two so-called Representative Concentration Pathways (RCPs; van Vuuren et al., 2011), which encapsulate different possible future greenhouse gas and aerosol emissions scenarios. RCP 4.5 is a "medium" emissions scenario that models a future where societies attempt to reduce greenhouse gas emissions, while RCP 8.5 is more of a "business as usual" scenario. Since global models have a coarse spatial resolution (100 km or more) that is unable to capture key features of California's landscape, we downscaled the global data to a 1/16th degree (6 km, or 3.7 mile) spatial resolution over the state, and made this finer-resolution data available for the Fourth Assessment impact studies (all data can be accessed at cal-adpat.org).

The basic meteorological and land surface data were downscaled for all 32 global climate models. However, we identified a subset of 10 models, and a further refinement to 4 models, that did particularly well in reproducing California's historical climate. The reduced sets can be used by those without the resources to use data from all 32 models. Additional key variables were downscaled from this reduced set of models, including wind speed, humidity, and surface solar radiation. These variables are important to applications that include wind power generation, wildfire, human health, and photovoltaic electricity production. Additionally, future projections of hourly sea level at several California coastal sites were constructed from several of the GCMs.

One requirement of the climate simulations and scenarios provided to the Fourth Assessment is to enable investigation of extreme, highly damaging climate changes that are possible but unlikely – e.g., low probability, high consequence outcomes. Two examples are provided, exploring extreme drought and high sea level rise. To explore extreme drought in a warmer future, two 20-year drought scenarios were produced from the downscaled meteorological and hydrological simulations: one for the earlier part of the 21st century, and one for the latter part.

A statistical approach was taken to provide a range of sea level rise scenarios. These scenarios are made using a "bottom-up" construction of sea level rise from its primary contributing components (thermal expansion of seawater, ice melt, etc.). They include extreme, but possible, scenarios of a low

probability but high consequence 99.9 percentile sea level rise, in addition to projections made using 5th and 95th percentile sea level rise scenarios that are aligned with the RCP 4.5 and RCP 8.5 GCMs. Such extreme sea level rise scenarios could affect energy, transportation, and utility infrastructure that is located along the coasts, as well as residential real estate and the tourism industry.

The purpose of this report is to provide an introduction to the downscaled data and scenarios that were produced for the Fourth Assessment, and describe the techniques and procedures used to create the data. More detailed explorations of the projected climate changes and subsequent impacts of the climate scenarios are carried out in the broad set of other studies completed as part of the Fourth Assessment project. To avoid duplication, many of the other results already presented in the Statewide and Regional reports are not repeated in this report, which describes the physical climate scenarios and methodology used to create them.

In addition to the analyzed results given in the various reports, the original climate scenario data are available online at cal-adapt.org. This web site allows readers to plot results at individual grid cells or download the climate data for their own custom analyses.

2: Global Climate Models

A robust climate assessment relies on multiple scenarios of future climate from the most current global climate models (GCMs) available. The GCM data employed here are from the Climate Model Intercomparison Project version 5 (CMIP5; Taylor, 2012), developed to support the work of the United Nations Intergovernmental Panel on Climate Change (IPCC). The CMIP5 archive, which was the most recent generation of GCMs in place when the Fourth Assessment was launched, supersedes the CMIP3 archive of GCMs used in the previous California Assessment. Any institution can contribute data to CMIP5; there is no vetting of model quality before the data is added to the archive. As a practical matter, though, the significant amount of resources needed to develop and run a GCM means that most models represent a large amount of work from many collaborating climate scientists. Uncertainty in climate change projections from different climate models arises from their inexact and differing representation of various processes, unknown rates and changes in climate forcings (e.g. rate and concentration of CO₂ and other greenhouse gases), and unknown future variations of natural climate variability such as El Niño (Hawkins and Sutton 2011).

There are more CMIP5 GCMs than CMIP3, and many of the newer models have better spatial resolution than before. At the time that work on the California Assessment climate scenarios began, CMIP5 incorporated data from approximately 40 models. However, one of the objectives of this project was to provide daily data, since many important climate impacts arise from daily extremes. For example, heat waves that affect peak energy demand and human health, Santa Ana winds, and heavy precipitation days resulting in flooding are all forms of individual daily extremes. We therefore limited the selection of GCMs to those that provided daily precipitation, and maximum and minimum temperature. This resulted in a set of 32 GCMs from both domestic and international institutions.

3: Bias Correction and LOCA Downscaling

Although GCMs form the basis of a future climate assessment, they cannot be used directly for assessing impacts. This is because GCMs have systematic errors, termed biases, in their output that can invalidate impact studies if not accounted for. For example, California state annual precipitation in a GCM may be too high, or the summer temperature might be too low. These biases are removed by a process known as bias correction; the method used here is described in Pierce et al., 2015. Additionally, global models have spatial resolution that is too coarse to be directly useful for California's needs, typically with grid cells of 100 km or more on a side. For example, current global climate models cannot adequately capture California's diverse topography, which is important to many climate impacts in the fields of energy demand, human health, water resources, agriculture, and ecosystems. Thus, selected variables projected by a GCM at relatively coarse spatial scale (100 km or more) need to be downscaled to a finer spatial resolution to inform decision making needs across diverse sectors.

3.1 Selecting Global Climate Models for Impact Studies

The large amount of data produced in this effort, ultimately about 40 TB, can be unwieldy for some impact studies to manage. Although daily data from all 32 downscaled models, under two RCPs, can be used for the most comprehensive assessment and should be considered whenever possible, this may not always be practical. Subsets of these GCM were therefore developed to provide much of the benefit of using all 32 GCMs but at a significantly reduced data volume.

A reasonable approach to reduce the number of models is to select a subset of models that perform better in simulating historical climate spatial and temporal structure at the global, Southwestern U.S., and California scales. Using this criteria, two options for reduced GCM numbers were provided.

The first option was developed by California Department of Water Resources Climate Change Technical Advisory Group, who evaluated the full set of CMIP5 models to determine which GCMs performed best in simulating historical climate means and variability related to water resources and hydrologic extremes in the California region. As described in their report (California Department of Water Resources Climate Change Technical Advisory Group 2015), 10 GCMs were identified, using a tiered set of selection criteria applied sequentially to winnow down the original CMIP5 GCMs to a set of 10. The criteria included a first screen of GCMs regarding their simulation of global climatology as developed by Gleckler et al. (2008) and provided by IPCC (2013); a second screen that evaluated regional climate and variability patterns affecting the southwestern U.S. following Rupp et al. (2013); and a third screen that evaluated California state hydrology and climate extremes and eliminated a few models whose core dynamical and numerical framework was already represented by other included models (Knutti et al. 2013).

This screening reduced the larger ensemble of 32 GCMs to a more manageable set of 10, which are listed in Table 1. The advice given to Fourth Assessment study teams was to use the 10 CCTAG GCMs shown in Table 1 if the full set of 32 GCMs was too much data to be managed or analyzed. These models are referred to below as the "10 California GCMs."

For some study teams and users of Fourth Assessment data, even the previously identified set of 10 GCMs may be too much data. Accordingly, in this work we identified 4 of the 10 GCMs from Table 1 whose projected future climate can be described as producing: 1) a "warm/dry" simulation; 2) an

“average” simulation; 3) a “cooler/wetter” simulation; 4) the model simulation that is most unlike the first 3 (for the best coverage of different possibilities). Note that all simulations show substantial future warming; the “cooler” simulation just shows less warming than other models. The procedure for identifying these 4 simulations used seven measures (metrics) covering different annual and seasonal temperature and precipitation measures. For each of the seven metrics, every model was ranked (1-10); e.g., for the summer average daily maximum temperature metric, the warmest model is assigned a rank of 1 and the coldest model is assigned a 10. The metrics were weighted according to subjective criteria as to how important we considered each metric to be when evaluating California state climate impacts. The weight of each measure is shown in the last column of Table 2 (values sum to 1). Overall, 50% of the weighting is given to temperature metrics, 40% to precipitation metrics, and 10% to variability (on the basis that greater climate variability is more difficult to adapt to). Summer temperature is spatially weighted by population since energy demand and health impacts of summer heat waves increase with temperature, while the precipitation metrics are implicitly weighted towards Northern California, which receives the greatest amount of precipitation in the state.

The model with the weighted rank closest to 1 across all metrics and both RCPs (4.5 and 8.5) is HadGEM2-ES, the “warm/dry” model. The model with the weighted rank closest to the average value across all metrics/RCPs is CanESM2, the “average” model. The model with the weighted rank closest to 10 is CNRM-CM5, the “cool/wet” model. The final selected model, MIROC5, is the one that has the pattern of rankings that is most unlike the other three models and is chosen to give better coverage of the full spread of 10 California GCM model results.

A different set of metric weightings than used here could give a different set of 4 models, depending on how different the weightings were. One exception to this is CNRM-CM5, which is a cool/wet outlier amongst the 10 California GCMs and so would likely be selected for a wide range of weightings. This sensitivity is one of the reasons why using only 4 models is less desirable than using all 10, which would give better coverage of model-projected futures. When only the four models are used because of constraints on time or resources, it should be kept in mind that the quantification of uncertainty and spread of future trajectories is less well sampled than if more models had been used.

Table 1. The 10 global climate models selected by the California Department of Water Resources CCTAG team as having a good simulation of California’s historical climate.

<i>Model</i>	<i>Institution</i>
ACCESS1-0	CSIRO (Commonwealth Scientific and Industrial Research Organization), Australia, and Bureau of Meteorology, Australia
CCSM4	The National Science Foundation, The Department of Energy, and the

National Center for Atmospheric Research, United States

CESM1-BGC	The National Science Foundation, The Department of Energy, and the National Center for Atmospheric Research, United States
CNRM-CM5	CNRM (Centre National de Recherches Meteorologiques, Meteo-France, Toulouse, France) and CERFACS (Centre Europeen de Recherches et de Formation Avancee en Calcul Scientifique, Toulouse, France)

CMCC-CMS Centro Euro-Mediterraneo per i Cambiamenti, Italy

CanESM2 CCCma (Canadian Centre for Climate Modelling and Analysis, Victoria, BC, Canada)

GFDL-CM3	NOAA Geophysical Fluid Dynamics Laboratory, Princeton, N.J., USA
-----------------	--

HadGEM2-CC Met Office Hadley Centre, Fitzroy Road, Exeter, Devon, EX1 3PB, UK

HadGEM2-ES	Met Office Hadley Centre, Fitzroy Road, Exeter, Devon, EX1 3PB, UK
-------------------	--

MIROC5 JAMSTEC (Japan Agency for Marine-Earth Science and Technology,

Kanagawa, Japan), AORI (Atmosphere and Ocean Research Institute, The Univ. of Tokyo, Chiba, Japan), and NIES (Natl Institute for Environmental Studies, Ibaraki, Japan)

Table 2. Measures (metrics) of climate model projections used in this work. Values are averaged over the state of California on the LOCA 1/16th degree (6 km) grid using the indicated spatial weighting. The final contribution of each metric to the overall rank of the model (i.e., each metric’s overall importance) is shown in the third column (“Overall metric weight”).

Metric	Spatial weighting (on 1/16° grid)	Overall metric weight
Average summer daily maximum temperature	By log of population	0.35
Annual average precipitation volume	(Implicitly Northern California weighted, since wetter there)	0.30
Average winter daily maximum temperature	None	0.15
Dry spell intensity (lowest total precipitation in 10-yr period)	None	0.10

Variability of average summer daily maximum temperature	By log of population	0.033
Variability of annual average precipitation volume	(Implicitly Northern California weighted, since wetter there)	0.033
Variability of average winter daily maximum temperature	None	0.033

3.2 Downscaling Methods

Global Climate Models (GCMs) provide only a coarse-resolution view of future climate change, with grid cells typically 100 km or more on a side. To better account for the influences of local topography and other high gradient phenomena on projected climate change, we use the LOCA statistical downscaling method (Pierce et al. 2014, loca.ucsd.edu) with a $1/16^\circ$ spatial resolution (about 6 km, or 3.7 miles), which is a more appropriate spatial resolution for assessing climate impacts in the California region (Figure 1).

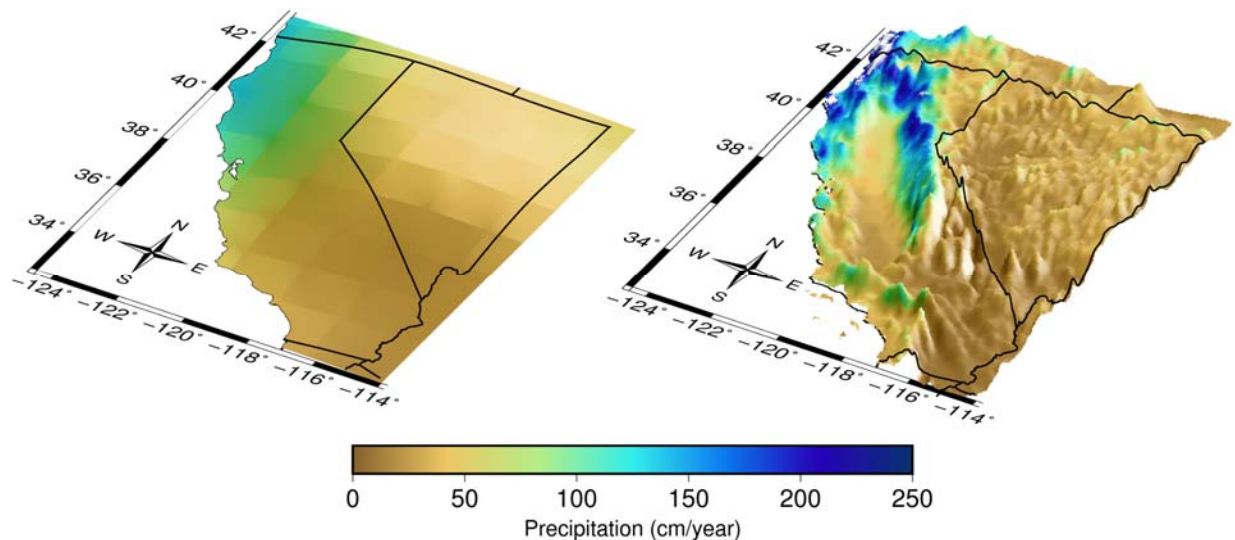


Figure 1. Annual precipitation in California and Nevada (cm; 250 cm is approximately 100 inches) in a global climate model with a resolution of approx. 160 km (100 miles; left), and after using a statistical model to account for the effects of topography at a 6 kilometer (3.6 mile) resolution (right). The global model only has a few grid cells over the entire state of California, so does not resolve the coastal mountain ranges, interior valley, or Sierra Nevada Mountains on the border with Nevada. The precipitation field in the right panel, by contrast, captures the wet conditions on the west slopes of the mountains, and the dry, rain shadow region to the east of the mountains. The vertical scale has been exaggerated for clarity, and by the same amount in both panels.

Compared to previous statistical downscaling methods used in the California Climate Assessments, LOCA is designed to better represent daily extreme weather conditions, such as intense precipitation or heat waves. Additionally, the bias correction employed in the LOCA process is designed to avoid the spurious, non-physical changes to the original GCM-predicted climate change signal that previous methods imposed (Pierce et al., 2015). As noted in that reference, the widely used quantile mapping approach (which is employed in the Bias Correction with Constructed Analogs, BCCA, and Bias Correction with Spatial Disaggregation, BCSD methods) can alter the projected winter temperature trend by up to 2°C over a century, and the summer trend by up to 1°C . Precipitation trends can be altered by up to 20 percentage points over a century in winter, and a similar amount in summer. These are large modifications compared to the original GCM-predicted trends. The trend modification imposed by quantile mapping has no physical basis, instead being a numerical artifact (Maurer and Pierce, 2013). These errors arise because quantile mapping was developed for seasonal prediction applications rather than situations where the climate is non-stationary, such as climate change over many decades.

The LOCA methodology was used to provide downscaled daily precipitation, maximum and minimum temperature (Tmax and Tmin), wind speed, specific and relative humidity, and surface solar radiation. The results for each of these separate variables is presented in the following sections.

Statistical downscaling methods such as LOCA are trained with observed historical data. The training data sets and particular methodologies for each variable will now be described.

3.2.1 Temperature and Precipitation

Changes in temperature and precipitation have implications for energy supply (hydropower), delivery (the effect of temperature on transmission lines), and demand (air conditioning loads and water pumping), as well as human health and agriculture.

The daily maximum and minimum temperature (Tmax and Tmin) and precipitation training datasets were produced and provided by B. Livneh of the University of Colorado (Livneh et al. 2015). The training data cover the domain from central Mexico through southern Canada. This data set is unique in providing daily data in Mexico, which required obtaining, quality controlling, and processing Mexican meteorological station observations. Additionally, care was taken to minimize systematic differences in the observations across international borders. The downscaled temperature and precipitation dataset may be used to investigate changes in longer term averages and changes in extreme occurrences.

3.2.2 Humidity

Humidity is important because it has bearing on human health, crops, and wildfire. For the humidity observed historical (training) data sets, we used the daily specific humidity, relative humidity (RH) maximum, and RH minimum datasets from John Abatzoglou of the University of Idaho (Abatzoglou 2011). Only 22 of the 32 GCMs saved the necessary daily surface data to downscale humidity.

The procedure for downscaling humidity is different from that used to create Tmin, Tmax, and precipitation, in that several additional variables are used in the calculation rather than just the field being downscaled. (Which is to say, downscaling precipitation requires only precipitation from the GCM, but downscaling relative humidity requires specific humidity, temperature, and surface air pressure.) Although surface air pressure is required for the humidity calculation, many GCMs only saved sea level pressure (SLP) at a daily frequency. We therefore estimated surface pressure from SLP and temperature. More details on downscaling humidity with the LOCA method are given in Pierce and Cayan 2015.

To obtain surface pressure, the original model SLP fields were first bias corrected using daily North American Regional Reanalysis (NARR) data over the period 1979-2015 (37 years). The bias corrected SLP data were bi-linearly interpolated to the 16th degree (6 km) LOCA grid cells. Interpolation was used, rather than a full LOCA downscaling of SLP, because SLP generally does not have fine-scale spatial structure. The bias-corrected, interpolated SLP was then used along with the already existing LOCA-downscaled temperature and the LOCA elevation field to produce surface pressure. Once temperature and surface pressure were available, it was straightforward to calculate RH from the downscaled specific humidity fields. Eight of the ten California models provided the full suite of variables required for calculating specific and relative humidity. We used the existing LOCA-downscaled daily maximum temperature (Tmax) to calculate the daily minimum RH, and LOCA-downscaled daily minimum temperature (Tmin) to

calculate the daily maximum RH. After downscaling, the daily RH minimum and maximum fields were bias corrected to the Abatzoglou data, and so the final available LOCA-downscaled RH values on any particular day are not identical to the downscaled specific humidity values combined with the downscaled temperature, SLP, and elevation to produce a relative humidity value.

3.2.3 Wind Speed

Wind speed is relevant to California due to wind power generation and the key role of Santa Ana winds in spreading wildfire, which can destroy electrical transmission lines and other property and infrastructure.

Due to the lack of suitable wind observations with the required spatial density to cover California, the observed historical training wind speed data set was taken from the “Card10” California Reanalysis on a 10 km grid (Card10, Kanamitsu and Kanamaru, 2007), which uses a regional spectral atmospheric model forced by NCEP reanalysis at the boundaries. The data were interpolated to the LOCA 6 km grid before downscaling. It should be noted that our analysis of Card10 shows a “blockiness” characteristic of an underlying topographic resolution that is actually coarser than 10 km, so the actual effective resolution of the surface wind training data set is not clear.

Eight of the 10 California GCMs saved the required daily wind speed data necessary for the downscaling: ACCESS1-0, CMCC-CMS, CNRM-CM5, CanESM2, GFDL-CM3, HadGEM2-CC, HadGEM2-ES, and MIROC5.

3.2.4 Surface Solar Radiation

Incoming solar radiation at the earth’s surface is important because it drives photovoltaic electricity production and is needed for many land surface modeling schemes due to its influence on evaporation, and therefore the future depiction of the effects of climate change on agriculture. Surface solar radiation was downscaled using LOCA. The training data used was surface solar radiation calculated from GOES satellite observations of cloud albedo over parts of western North America and offshore eastern North Pacific waters (Iacobellis and Cayan 2013).

Geographical coverage includes the western U.S. and Mexico and offshore region roughly 25 to 50° N, 130W to 113 W. The period of coverage is 1996-2016 (21 years), which is shorter than the other data sets we used to train LOCA. For example, the temperature and precipitation data sets were 56 years long. It is possible that some aspects of solar radiation variability were not captured by the relatively short time span of the available satellite observations.

The surface solar radiation training data ends in 2016, while the historical period for the CMIP5 global climate model data that we downscaled ends in 2005. Had we trained only on the period of overlap (1995- 2005) it would have resulted in a very short training data set. To avoid this, we time-shifted the recorded dates of the training data set to the period 1985-2005. This preserved the entire span of training data for use in the downscaling. Note that model years are not synchronized to real years, so time-shifting the training data in this way does not cause any physical synchronization problems between the observations and the simulated model fields. Of the 10 California GCMs, 9 saved the necessary daily surface solar radiation required for the downscaling: ACCESS1-0, CCSM4, CMCC-CMS, CNRM-CM5, CanESM2, GFDL-CM3, HadGEM2-CC, HadGEM2-ES, and MIROC5 (the missing California GCM is CESM1-BGC).

3.3 Temperature and Precipitation Results

As an overall summary of temperature and precipitation changes produced by each of the GCMs, Figure 2 through Figure 5 show projected mid-21st Century and late-21st Century annual mean temperature (C) and precipitation (%) changes in our region. Values are plotted for the Northern California Coast, Central Valley, and the Southern California Coast regions as defined in the California Climate Tracker (<https://wrcc.dri.edu/monitor/cal-mon/>), along with the statewide average. The changes are constructed as the difference between 30-year averages of 2035-2065 or 2070-2099 vs. the modeled 1976-2005 historical climatology. The data are drawn from LOCA downscaled daily average temperature and precipitation for each of the 32 GCMs. For comparison, the change values for the subsets of 10 California GCMs and the reduced subset of 4 GCMs are identified on the plots (red symbols and letters). When examining the plots, keep in mind that the range of projected future changes represents a combination of 1) unpredictable future natural climate variability (such as the incidence of El Niño events and La Niña events), which makes some decades warmer, cooler, wetter, or drier than others; 2) different climate model estimates of the region's climate sensitivity to increased greenhouse gases; and 3) different amounts of greenhouse gases released to the atmosphere (Figure 2 and Figure 4, vs. Figure 3 and Figure 5).

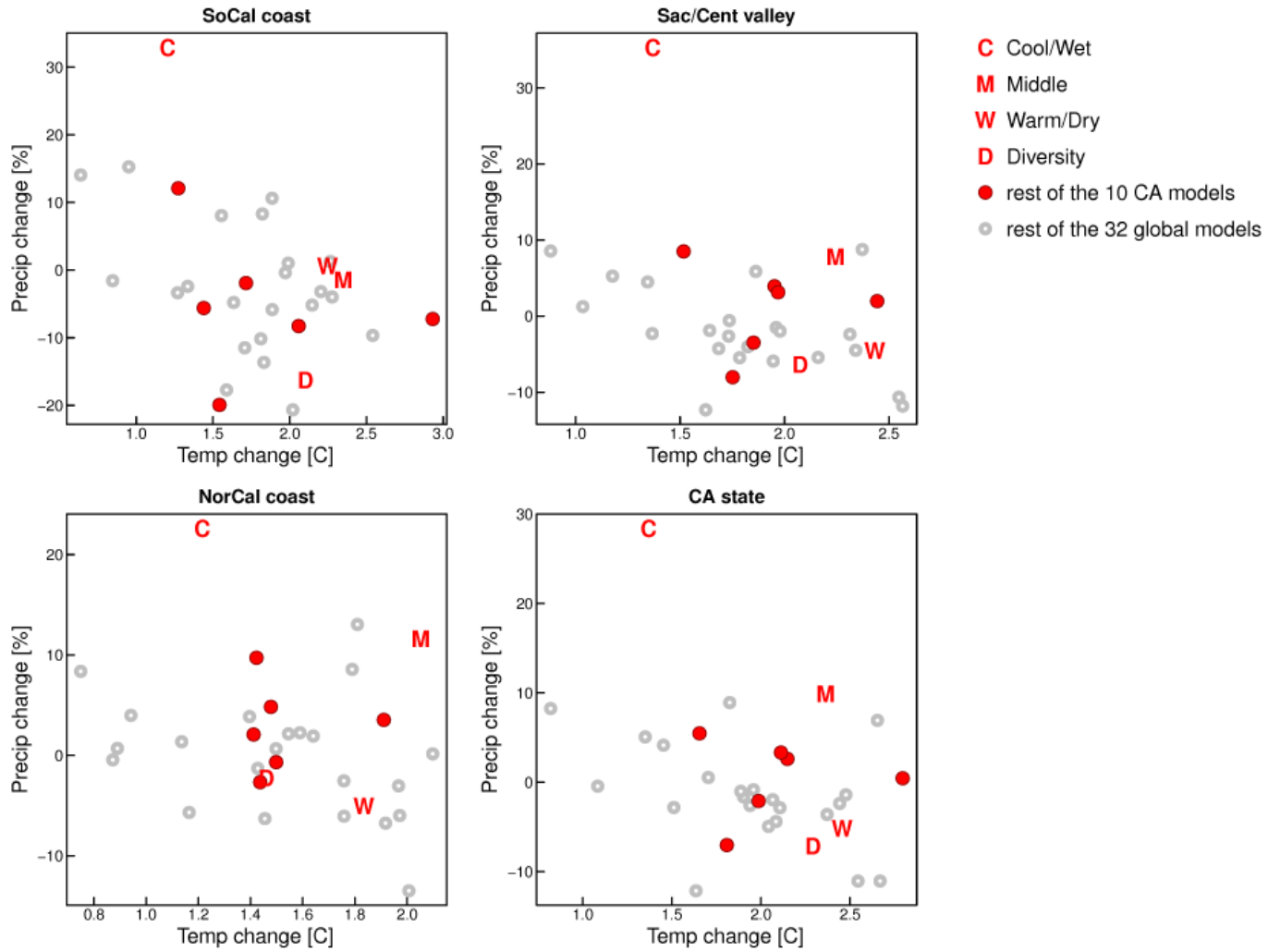


Figure 2. Combined temperature and precipitation changes in the 32 global climate models over the regions indicated. Red shows results from the 10 “California” GCMs. Red letters show the subset of the 10 California GCMs selected as being cool/wet, warm/dry, middle, and diversity (see text for details). Data is shown for RCP 4.5, mid century 2035-2065.

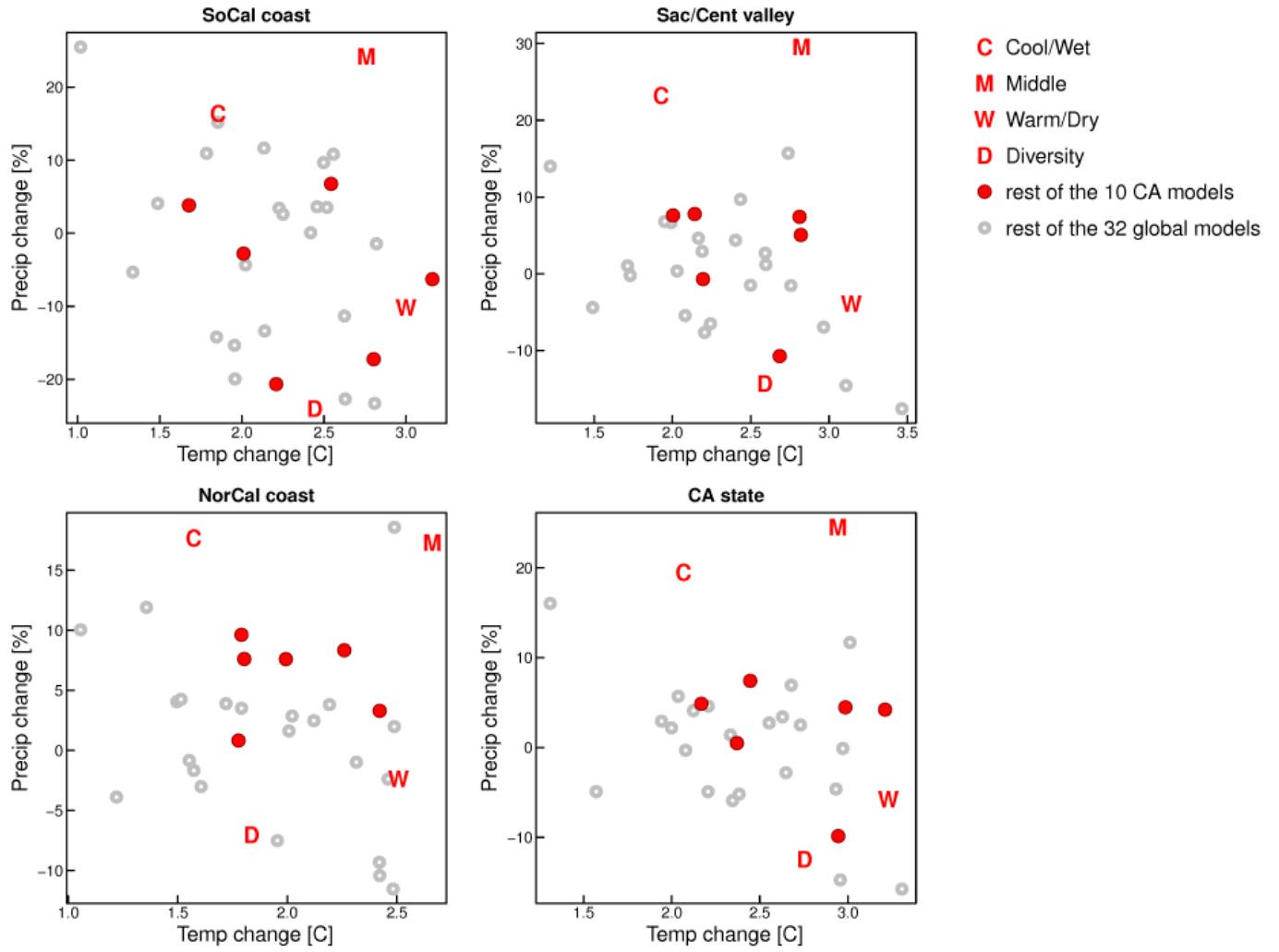


Figure 3. As in Figure 2, but for RCP 8.5 mid century (2035-2065).

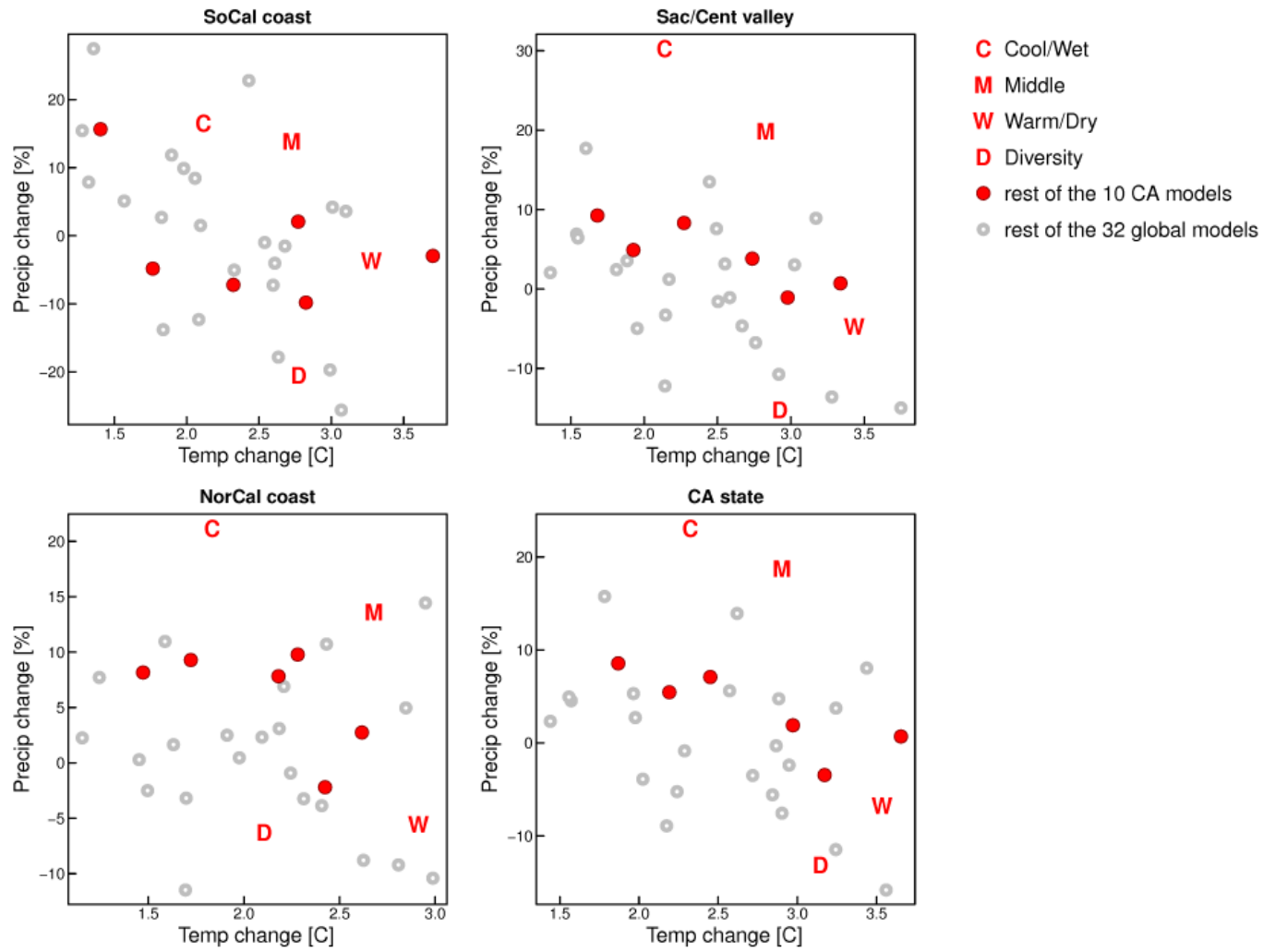


Figure 4. As in Figure 2, but for RCP 4.5 at the end of the century (2070-2099).

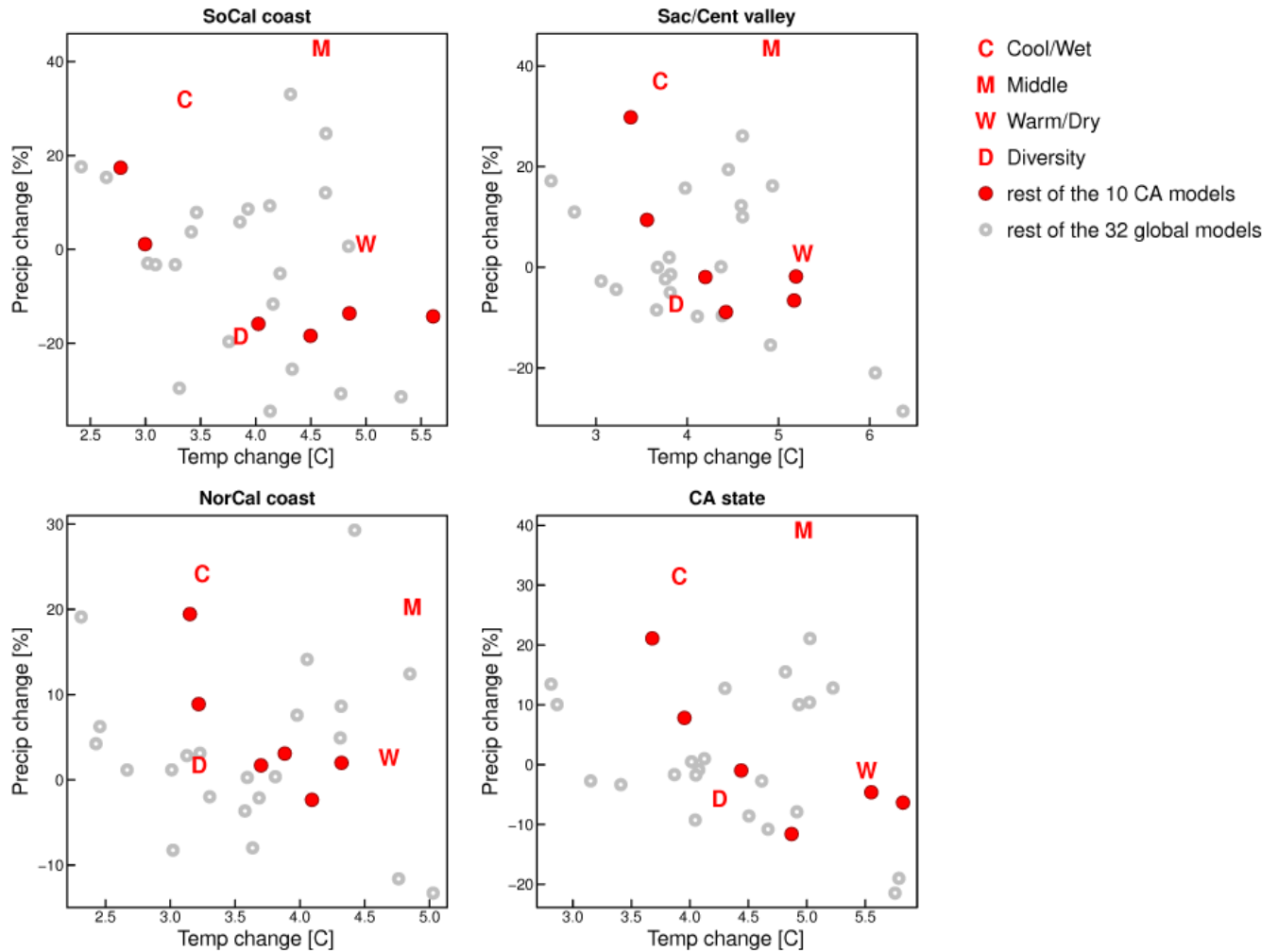


Figure 5. As in Figure 2, but for RCP 8.5 at the end of the century (2070-2099).

3.3.1 Effect of Changes in the Base Period

The Fourth Assessment historical base period is 1976-2005, while the base period used in the previous assessment was 1961-1990. This change was motivated by the additional 15 years of more recent data that is available in the 1976-2005 period. However, this change may lead to different results when compared to the previous assessment. The difference this makes in T_{min} , T_{max} , and precipitation is shown in Figure 6 as calculated by the 10 California GCMs. It is preferable to calculate this in the GCMs rather than the observations because a) using 10 models reduces the effect of random natural internal climate variability, and b) when evaluating future climate change, the model projections are compared to the *model* historical period, not the observations over the historical period. This approach reduces any errors due to residual model biases that might remain even after the bias correction process.

The shift to the later base period accounts for a 0.35 °C difference in daily maximum temperature, and a 0.29 °C difference in daily minimum temperature, with the 1976-2005 period being warmer than the earlier 1961-1990 period. The difference in precipitation is very small, however, being on the order of 0.01 mm/day out of a statewide mean of 1.29 mm/day. A rough estimate of RCP 4.5 inducing warming over the period of a century is 2 °C, which yields a temperature shift of 0.30 °C

for a 15 year segment. The change seen here, 0.29-0.35 °C, is in reasonable agreement with that expected due to climate warming, given that the warming over land proceeds at a faster pace than the global average, which is dominated by the ocean.

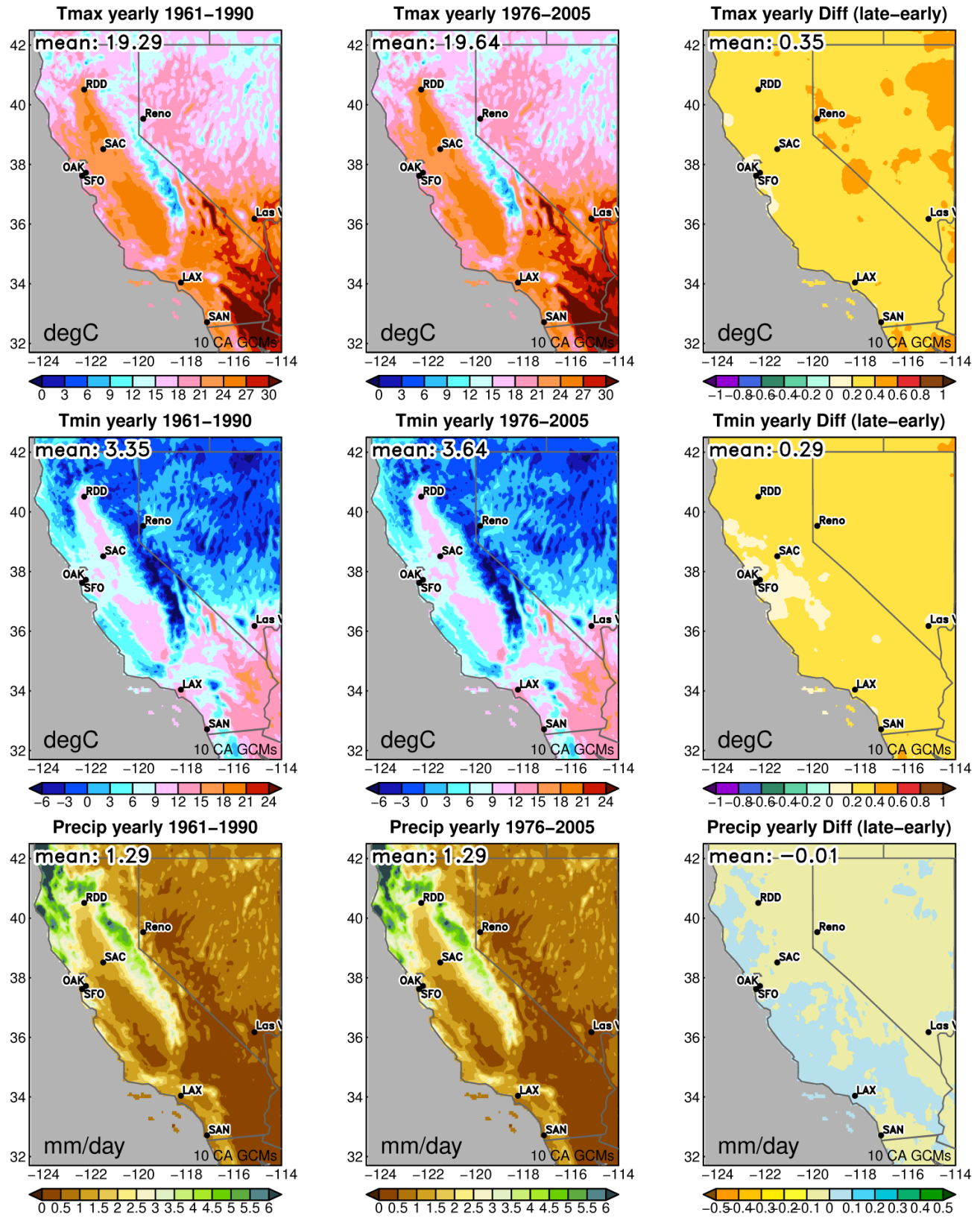


Figure 6. Top left: annual mean Tmax over the period 1961-1990 (°C). Top middle: same, over the period 1976-2005. Top right: difference, late period minus early period. Middle row: same, for Tmin. Bottom row: same, for precipitation (mm/day). Results from the 10 California GCMs.

3.3.2 Future Changes in Temperature

A key future change in climate is the generally warmer temperatures due to increased greenhouse gas concentrations in the atmosphere. The time series of statewide, annually averaged minimum and maximum temperature is shown in Figure 7. The envelope of the 10 California GCMs agrees well with the observations over the historical period. Looking ahead, the RCP 4.5 and 8.5 envelopes begin to separate around year 2060. Before 2050, the envelopes from the two RCP scenarios have considerable overlap. By the end of the century, the RCP 4.5 and 8.5 distributions are well separated, with the higher greenhouse gas emissions scenario showing, on average over the 10 GCMs, about 2.5 °C more warming in Tmin and Tmax.

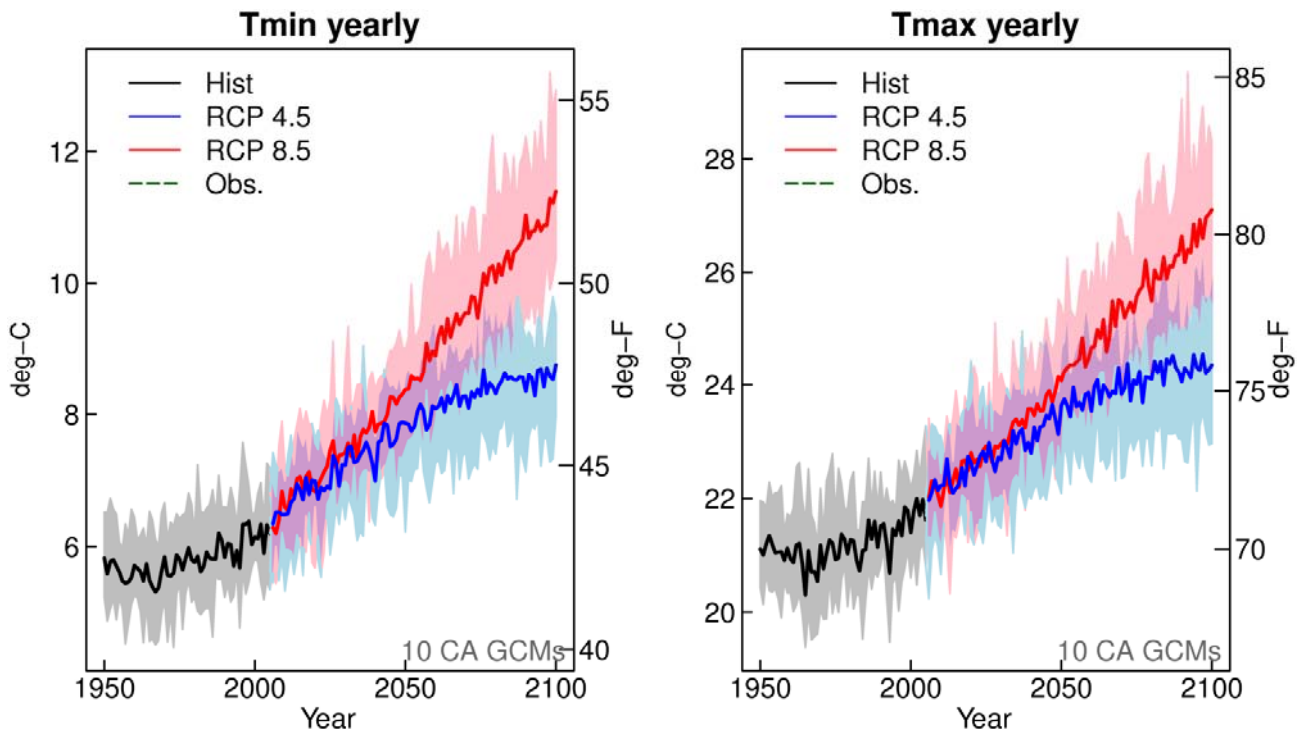


Figure 7. California statewide, annually averaged Tmin (left) and Tmax (right). The dashed green line shows the observations from Livneh et al. 2014. The grey region shows the envelope of the 10 California GCMs over the historical period. The red (RCP 8.5) and blue (RCP 4.5) lines show the multi-model average from 2006 to 2100. The pink and light blue regions show the envelope of the 10 California models over the future period, for RCP 8.5 and 4.5, respectively. This envelope represents one measure of uncertainty in the future temperature projections.

Maps of future temperature change (Figure 8) show less annually averaged warming near the coasts, which are ventilated by marine air, than interior regions. This is because the oceans warm more slowly than land due to the higher heat capacity of the ocean. As noted previously (in Figure 7), the warming around the middle of the century (middle column of Figure 8) is similar for the two emissions scenarios, but by the end of the century (right column) the two scenarios differ

markedly. In other words, what, if anything, humans choose to do about greenhouse gas emissions makes a considerable difference to the warming that California will experience.

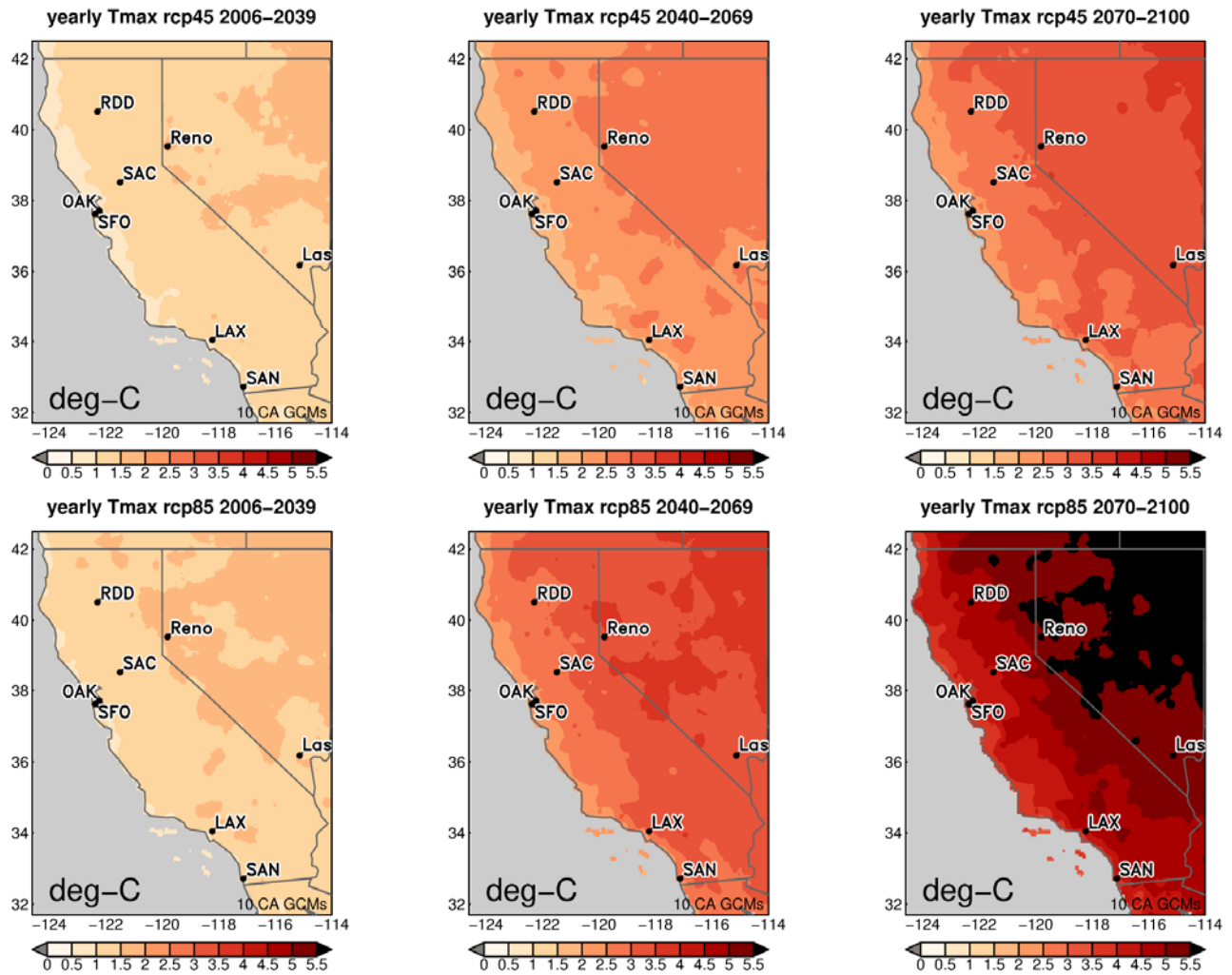


Figure 8. Future change (degrees C) in annual mean maximum temperature for early-, mid- and late-21st Century for RCP 4.5 (top) and RCP 8.5 (bottom) mapped over California region. Results are from the 10 California GCMs.

Although the mean annual changes shown up to now are an important impact of climate change, in many ways the effects of climate change will be felt most strongly at the extremes. Figure 9 shows the average hottest day of the year ($^{\circ}\text{C}$), both historically (top left) and projected at the end of the century (2070-2100) in RCP 4.5 (top middle) and RCP 8.5 (top right). The lower row shows the change with respect to historical conditions, which is the difference between the end of century and the historical values. There is a strong increase in the hottest day of the year, with values increasing by 2-4 $^{\circ}\text{C}$ for RCP 4.5 and 4-6 $^{\circ}\text{C}$ for RCP 8.5. The increases are larger in the interior region away from the California coast, similar to the gradient in mean daytime (T_{max}) warming (Figure 8).

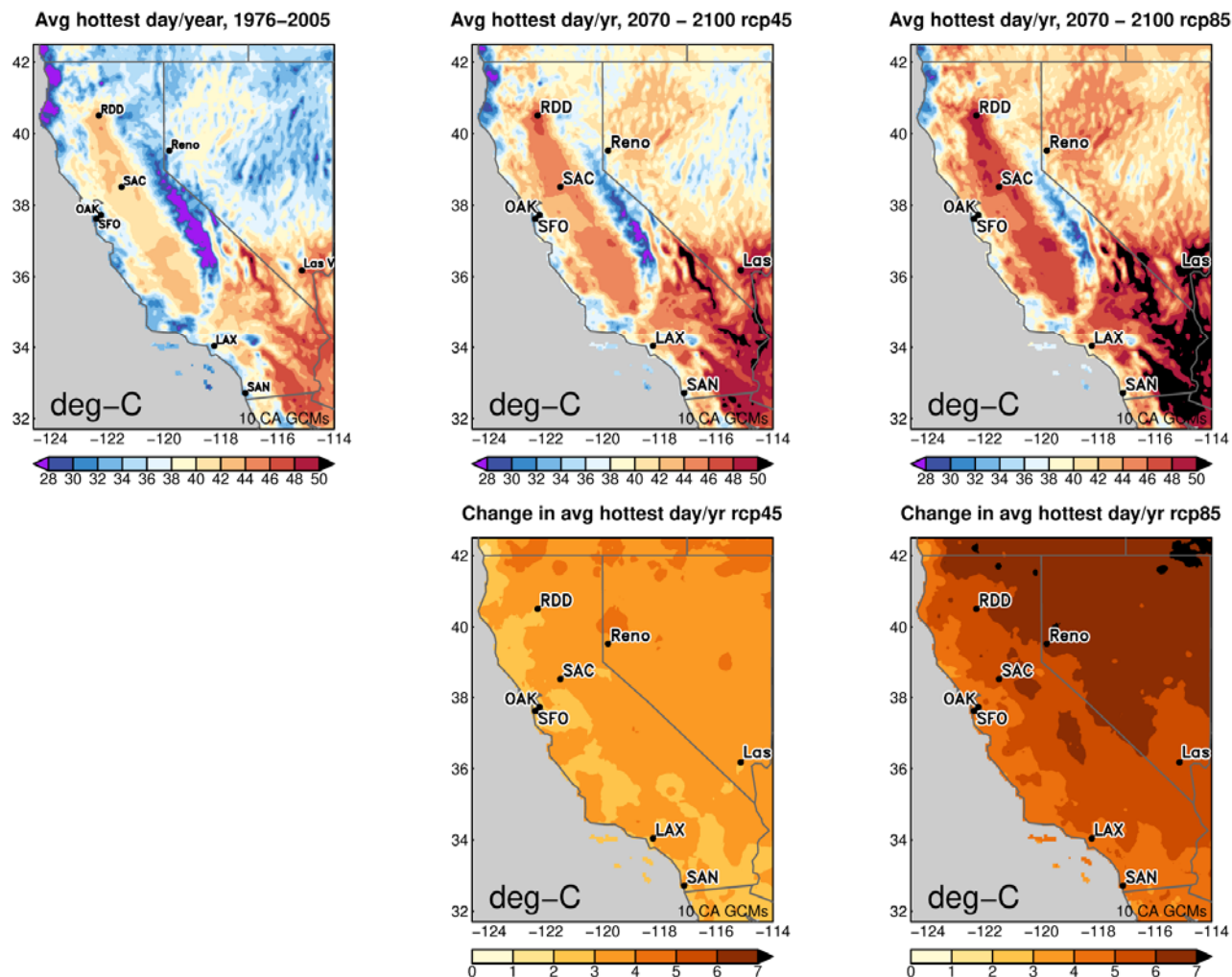


Figure 9. Top row: Average hottest day of the year (°C), averaged over 10 GCMs, for the historical period (top left) and late-21st Century for RCP 4.5 (top middle) and RCP 8.5 (top right) emissions scenarios. Bottom row: the increase (°C) of the late-21st Century over the historical values, for RCP 4.5 (bottom center) and RCP 8.5 (bottom right). Results are from the 10 California GCMs.

Increases in extreme warm days are explored in more detail at 4 locations (Sacramento, Los Angeles, Fresno, and Riverside) in Figure 10. The colored ranges show the number of days/year that reach or exceed different temperature thresholds (°C) in 2/3rds (66.6%) of years, where the thresholds are labeled in Figure 10 and identified by different colors. For example, historically Los Angeles International Airport (LAX; top right panel) has experienced less than 18 days/year ≥ 32 °C (light yellow region). However, by the end of the century with RCP 8.5 forcing, for two out of three years (66.6% of years) the same location will experience between 50 and 100 days/year ≥ 32 °C. (The third out of the three years could experience less than 50, or more than 100 days ≥ 32 °C). Projected changes for the RCP 4.5 scenario (not shown) are also substantial, but not as great as in the RCP 8.5 scenario.

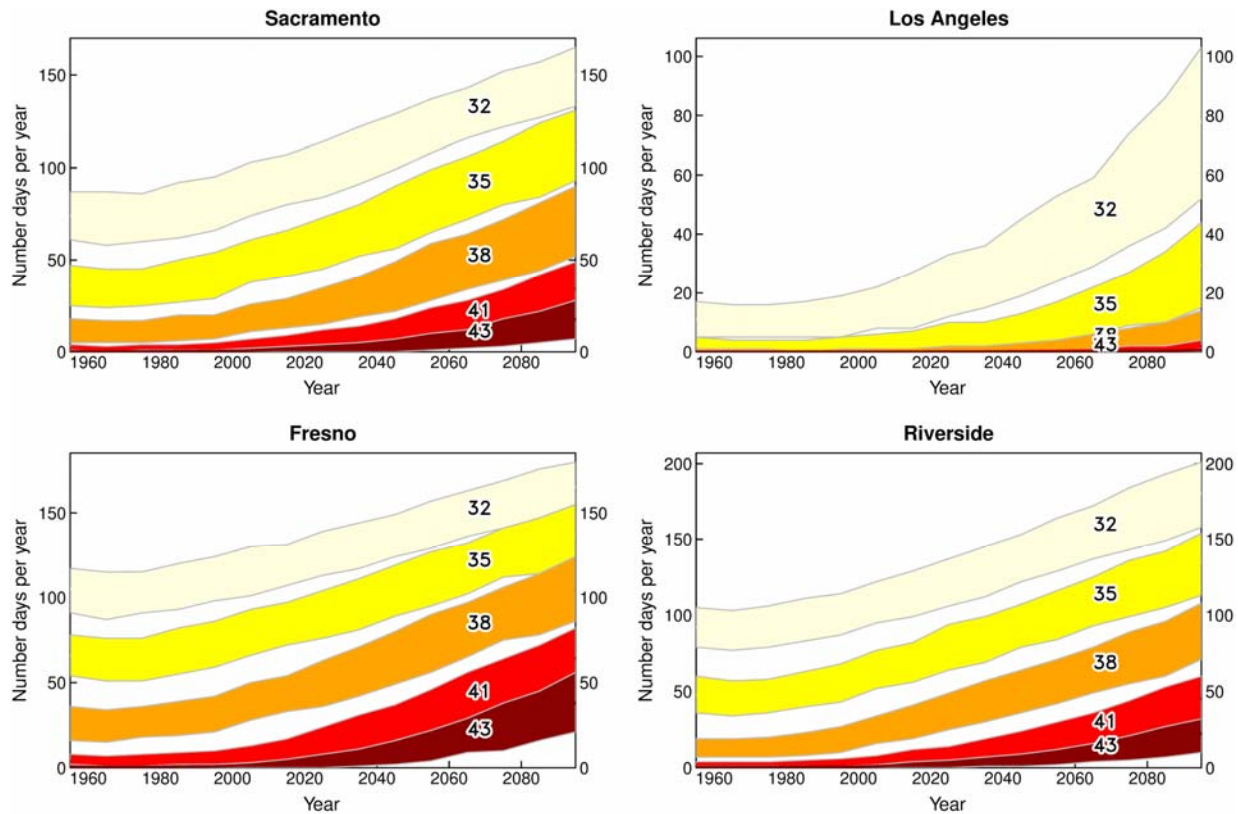


Figure 10. Projected change in the number of very hot days at 4 locations, as indicated in the panel titles. Results are for the RCP 8.5 emissions scenario. The colored areas represent the typical range in number of days per year that reach or exceed each indicated threshold (in degrees C, from 32 to 43). The values are shown as ranges that encompass 2/3rds of years (66.6% of the time). So, for instance, around year 2000, Sacramento typically (66.6% of the time) experienced between 60 and 90 days/year ≥ 32 °C (top left panel). By the end of the century, this will increase to 130-160 days/year. Approximate conversion: 32 °C = 90 F; 35 °C = 95 F; 38 °C = 100 F; 41 °C = 105 F; 43 °C = 110 F. See text for details. Results are from the 10 California GCMs.

3.3.3 Future Changes in Precipitation

Model-projected changes in precipitation are more complex than projected changes in temperature. Statewide averaged time series of future precipitation projections are shown in Figure 11. In comparison to temperature (Figure 7), where the projected temperature changes are well outside the range of historical variability, projections of 21st Century precipitation show changes that are within the range of historical variability. Also, there is less separation between the RCP 4.5 and 8.5 scenarios than was seen in temperature (the separation is more easily seen in Figure 12). The changes in precipitation have an important seasonal variation; there are modest increases projected in December, January, and February (DJF) and decreases in March, April, and May (MAM) and September, October, and November (SON). Annually, there is a projected increase of year-to-year variability in precipitation, which is due to a combination of wetter days when it does precipitate, but fewer days with precipitation. This outcome can be thought of as a sampling exercise; fewer picks of larger numbers (because fewer wet days, but more precipitation on wet days) yields greater year-to-year variability. This is explored more in Figure 17.

California

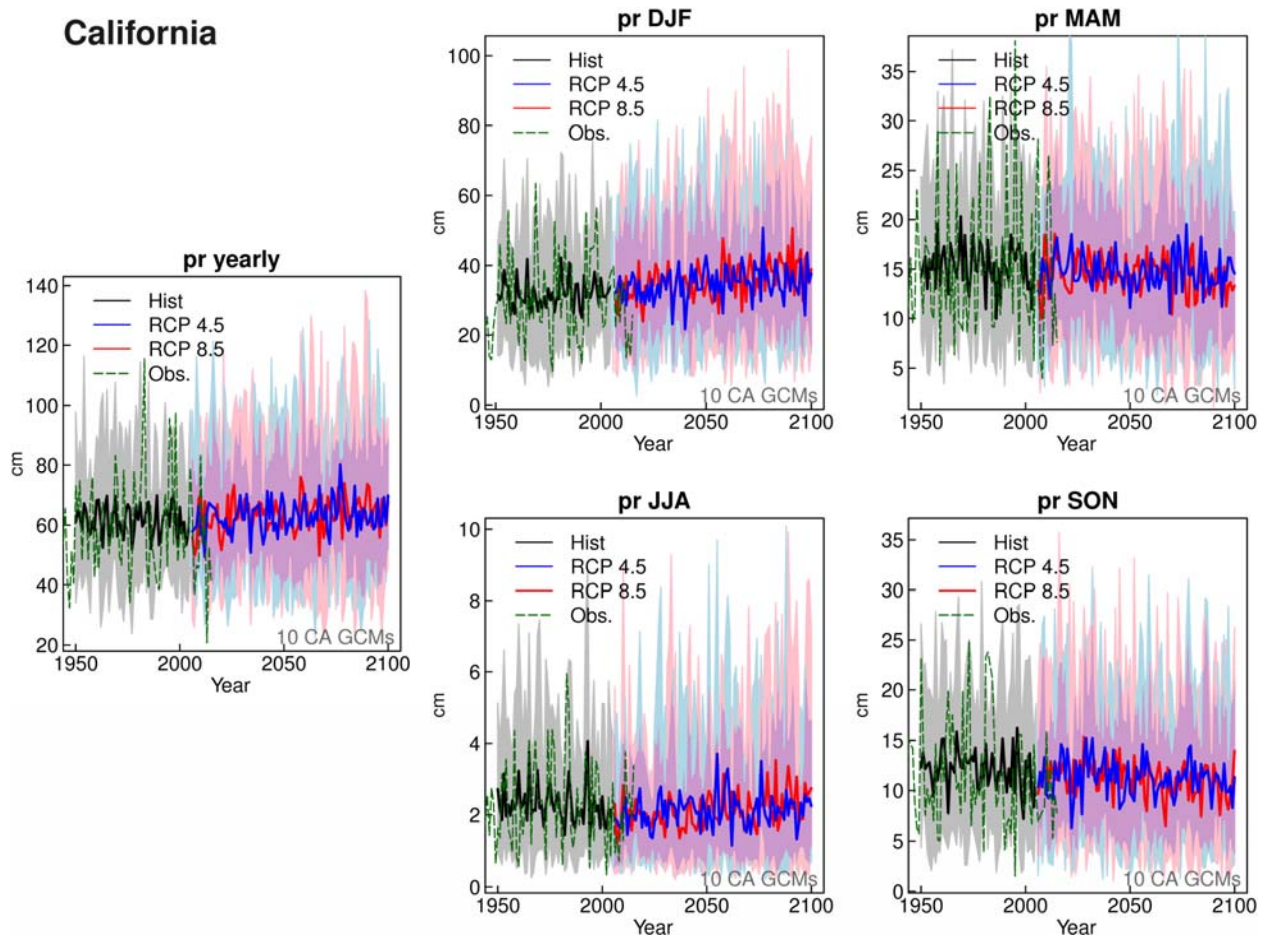


Figure 11. California statewide precipitation, annual and seasonal December-February (DJF), March-May (MAM), June-August (JJA), and September-November (SON), as simulated by 10 downscaled California GCMs. Upper to lower values of simulations shown by the colored envelope, and the mean of the 10 simulations shown by solid line; historical observations shown by dashed line. Historical simulations shown by grey envelope and black line, projected 2006-2100 values shown for RCP 4.5 (blue) and RCP 8.5 (red).

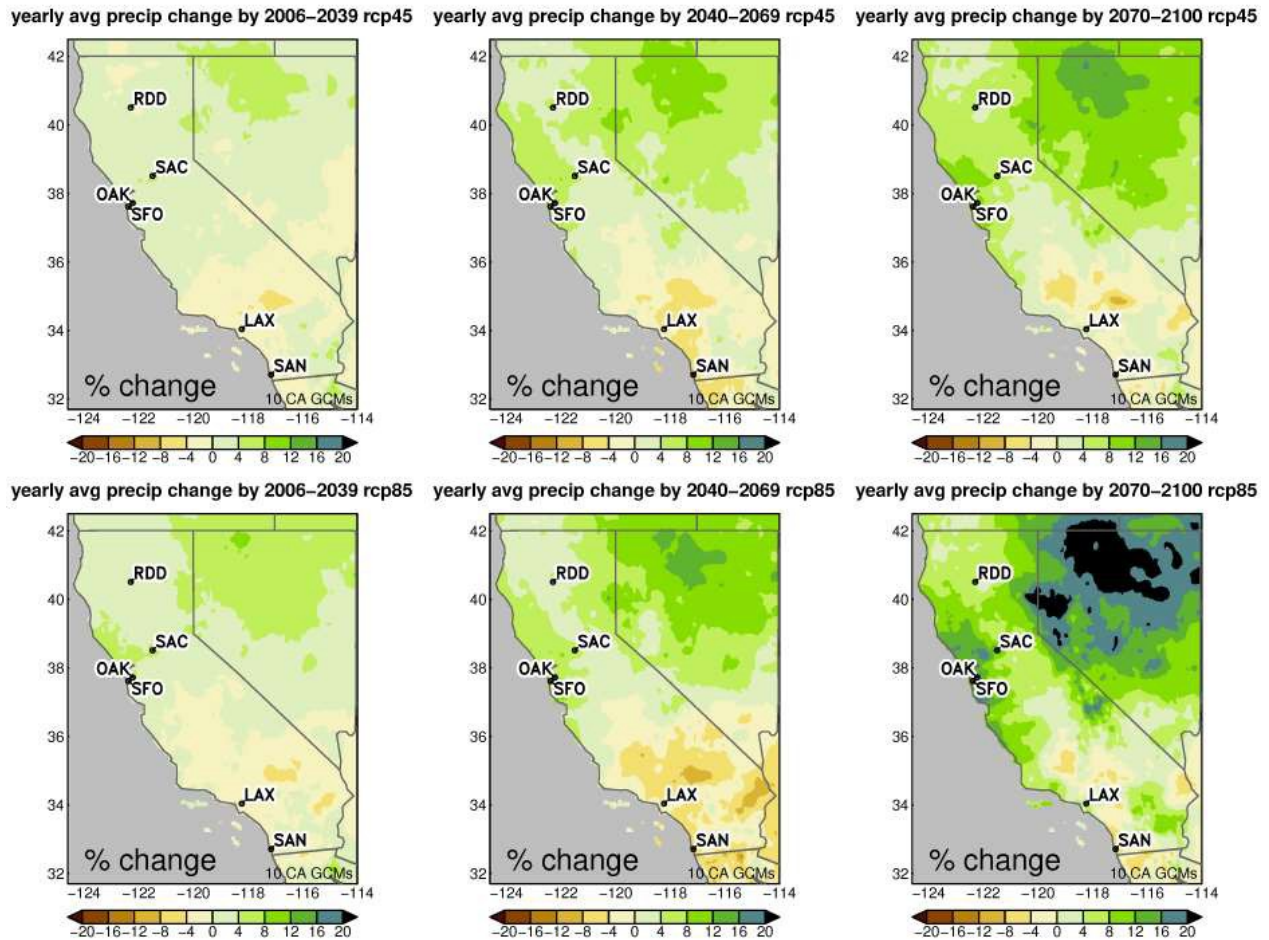
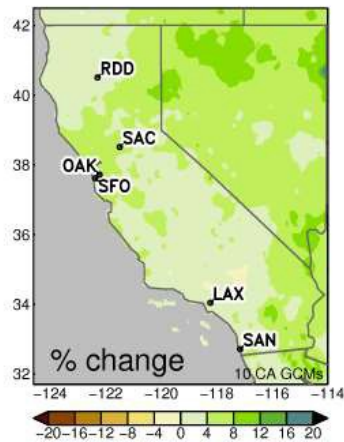


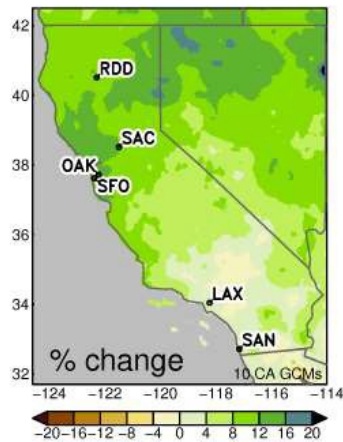
Figure 12. Change [%] in annual precipitation averaged from 10 downscaled GCMs for RCP 4.5 (top row) and RCP 8.5 (bottom row) for early-, mid-, and late-21st Century. Results are from the 10 California GCMs.

Maps of the projected statewide change in precipitation as a function of time (early, mid, late 21st century) and RCP are shown in Figure 12. It should be kept in mind that the mean changes are small compared to year-to-year variability (Figure 11), but the projections show generally wetter conditions in the northern part of the state and slightly drier conditions in the southern part of the state. The wetter conditions in the northern part of the state are more pronounced in RCP 8.5 than in RCP 4.5, especially along the central California coast, and result from an increase in the amount of precipitation on the very wettest days (e.g., Pierce et al. 2013; Polade et al. 2014). In turn, this arises primarily from an increase in water vapor in the atmosphere due to warmer global air temperatures (e.g., Lavers et al. 2015).

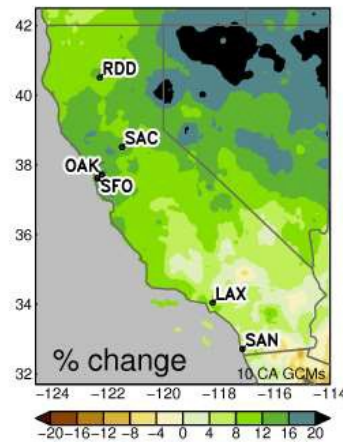
DJF avg precip change by 2006–2039 rcp45



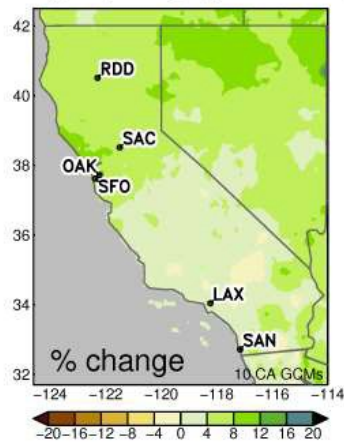
DJF avg precip change by 2040–2069 rcp45



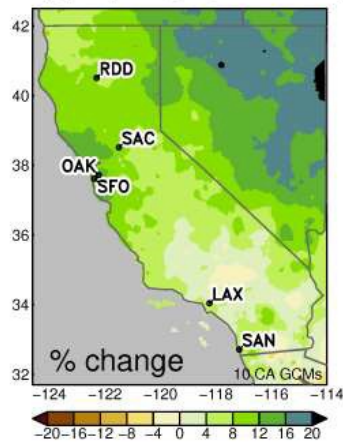
DJF avg precip change by 2070–2100 rcp45



DJF avg precip change by 2006–2039 rcp85



DJF avg precip change by 2040–2069 rcp85



DJF avg precip change by 2070–2100 rcp85

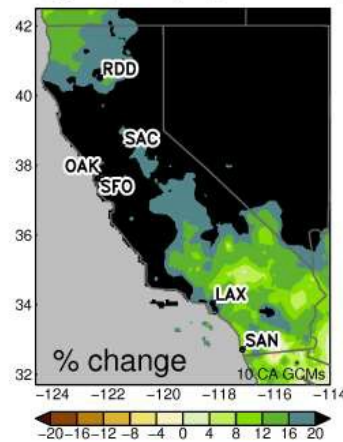


Figure 13. Change in winter (DJF) precipitation (% of historical) averaged from 10 downscaled GCMs for RCP 4.5 (below) and RCP 8.5 (above) for early-, mid-, and late-21st Century. Results are from the 10 California GCMs.

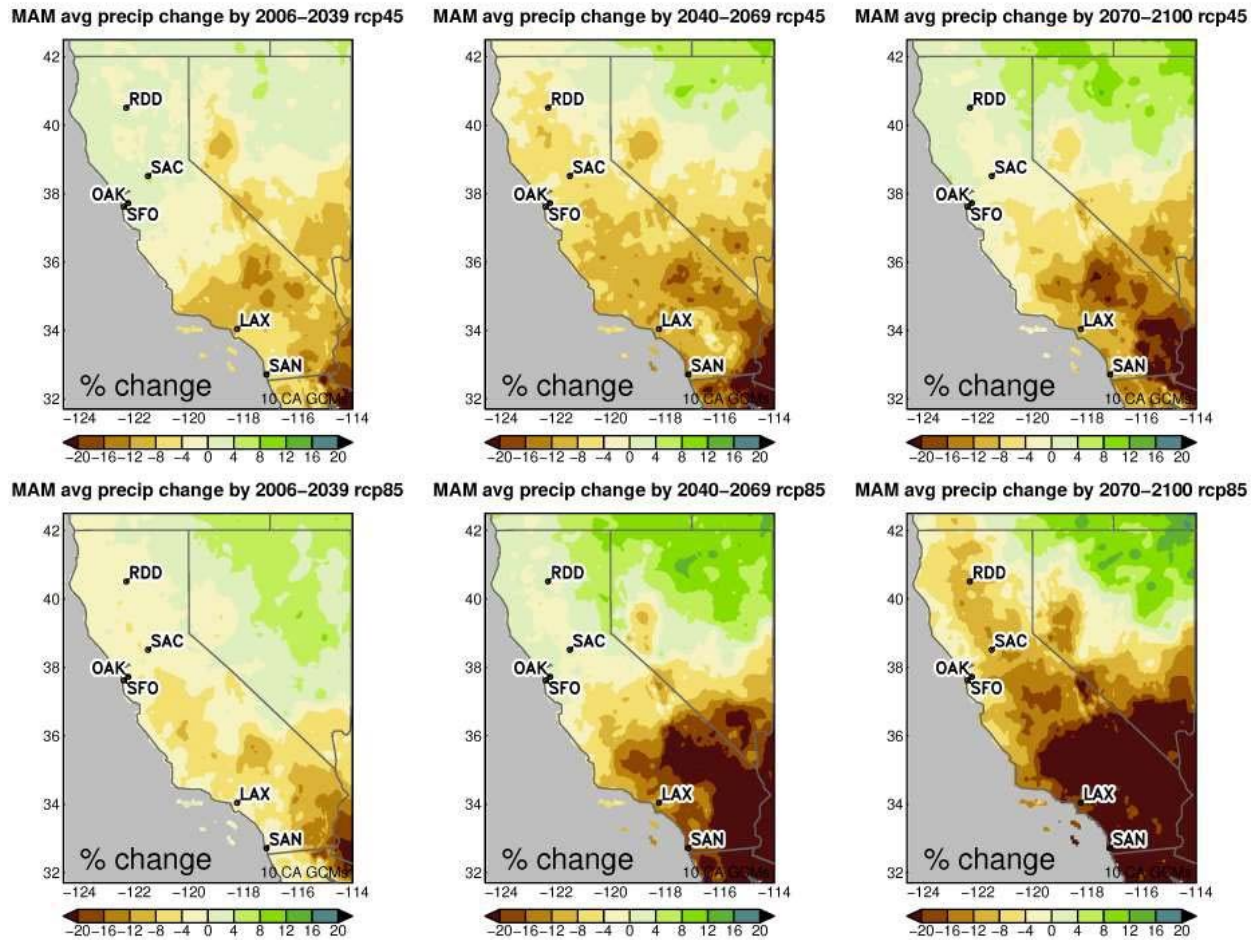


Figure 14. Change in spring (MAM) precipitation (% of historical) averaged from 10 downscaled GCMs for RCP 4.5 (below) and RCP 8.5 (above) for early-, mid-, and late-21st Century. Results are from the 10 California GCMs.

As mentioned in the discussion of Figure 11, seasonal changes are a key aspect of the future precipitation changes. This is shown in more detail by maps of the projected winter (DJF) and spring (MAM) precipitation change, Figure 13 and Figure 14 respectively (values shown are change, in percent, with respect to the historical value). Although it was shown previously that the annual changes are modest (Figure 12), the seasonal changes are more substantial. In particular, conditions become wetter in winter but drier in spring. Cancellation between these tendencies means that the annual change is small. However, the seasonal changes have important implications for the state; increased precipitation in winter could increase the chance of flooding, especially as warmer temperatures mean that more precipitation falls as rain instead of snow, and the snow that does accumulate melts faster. The decline in precipitation in spring is unfortunate, as it advances and prolongs summer dryness – a stress on natural systems and a challenge to California’s residents and economy unless the enhanced winter precipitation is retained in the state via storage.

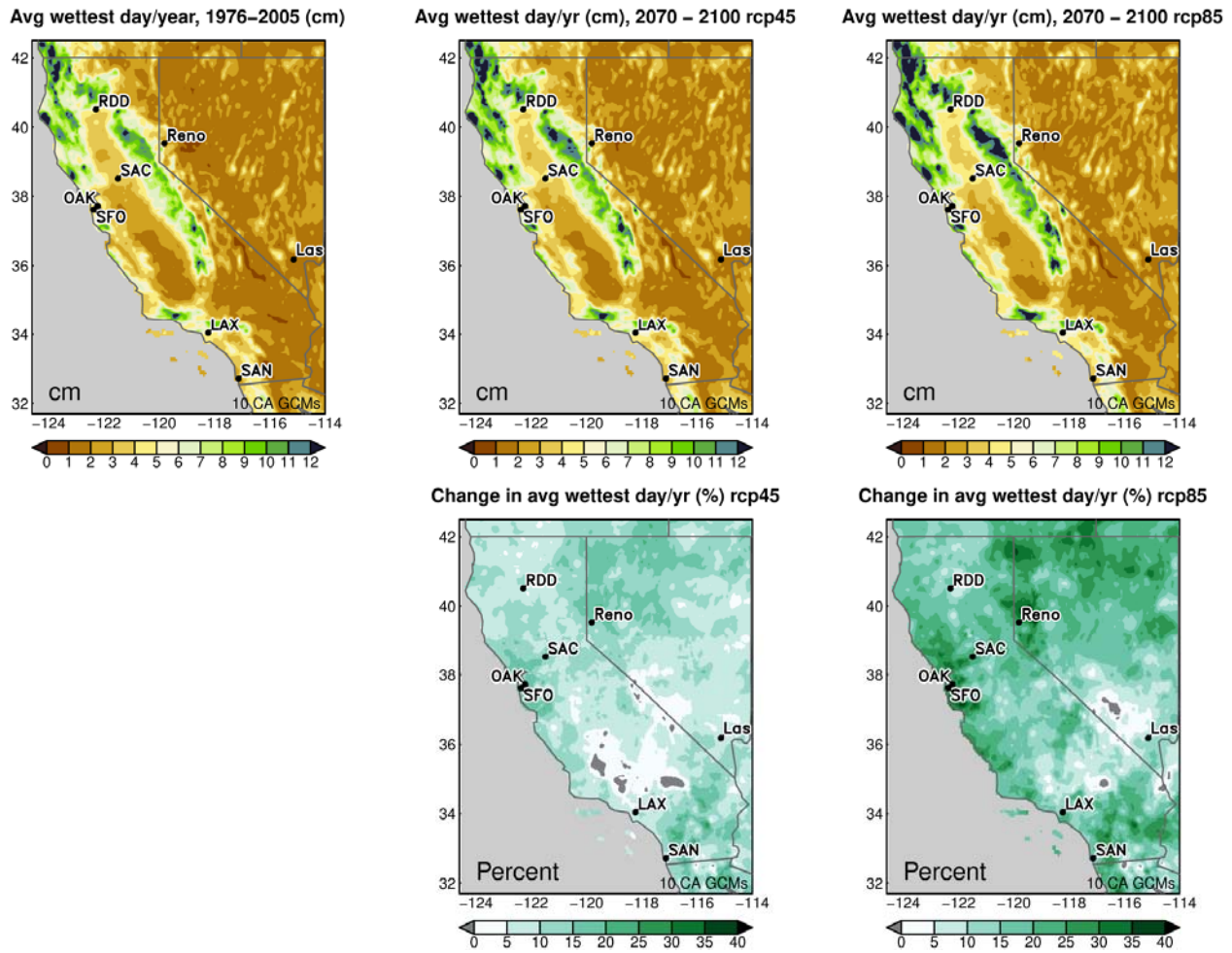


Figure 15. Average wettest day per year for historical and late-21st Century for 10 RCP 4.5 and RCP 8.5 downscaled simulations. Changes (%) shown by bottom frames. Results are from the 10 California GCMs.

As the atmosphere gets warmer, the specific humidity increases (“warmer air holds more moisture”), leading to a tendency for higher peak precipitation days in warming conditions. This is quantified in Figure 15, which shows the average wettest day per year. The wettest day is projected to increase substantially by the end of the century, especially in the RPC 8.5 scenario, where increases of 20-35% are seen in the coastal ranges. This would have important implications for flooding in the state.

Annual cycle change, California

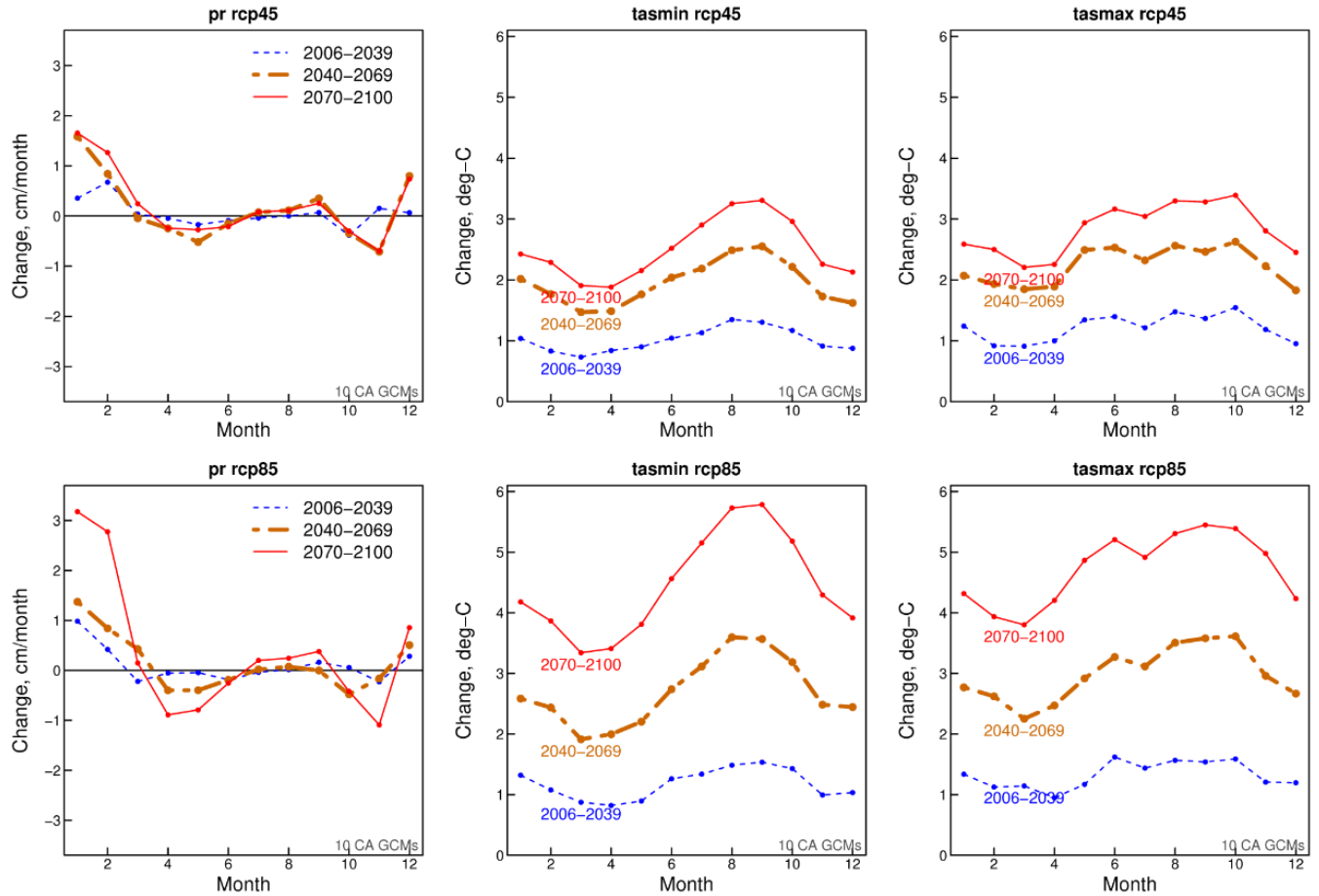


Figure 16. Changes with respect to period 1976-2005 in the annual cycle of precipitation, T_{min} and T_{max} for each month for early- (2006-2039), mid- (2040-2069), and late-21st Century (2070-2100) for RCP 4.5 (upper) and RCP 8.5 (lower). Results are from the 10 California GCMs.

Projected changes in the annual cycle of precipitation, T_{min}, and T_{max} with respect to the baseline period of 1976-2005 are summarized in Figure 16. The strong winter increase in precipitation is clear (left column), along with the decreases in spring and autumn. The models also generally project a small increase in summer precipitation. For temperature, stronger warming is seen in late summer than in spring. This is likely related to surface drying leading to more surface solar radiation going to increasing surface temperatures than to evaporating surface water (i.e., a Bowen ratio effect).

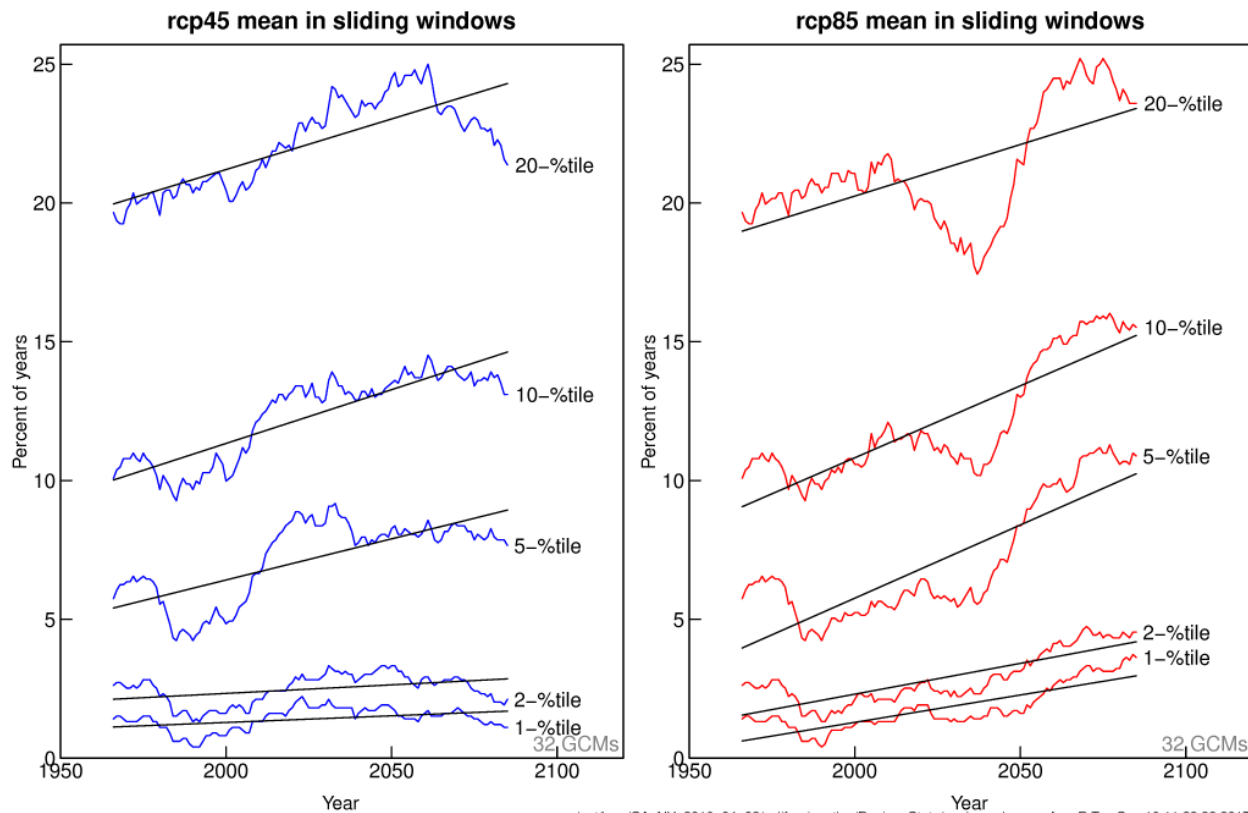


Figure 17. Frequency of dry years (% of years) for years drier than 20, 15, 10, 5, 2, and 1 percentile levels of annual precipitation. From 32 GCMs for RCP 4.5 (left) and RCP 8.5 (right). See text for details. Results are from all 32 GCMs.

Turning to the precipitation changes at lower frequencies (i.e., droughts), Figure 17 shows how the frequency of dry years is projected to change in the future, as a function of percentile of the dry years' annual precipitation (20th-percentile to 1st-percentile). Results for RCP 4.5 are shown in the left panel, and RCP 8.5 in the right panel. For example, consider the bottom line labeled "1-%tile" on the right-hand panel. It shows how often, within the 32 GCM simulations, 1st percentile precipitation years occur over the period from 1950-2100. A 1st percentile precipitation year is drier than 99 out of 100 years, so it is an extreme dry case. As expected (by definition) the example line shows that a 1st percentile dry year occurs in 1 out of 100 years (1% of years) over the historical period. However, in future decades the incidence of such years increases, reaching about 3% of years by the end of this century. The incidence of extreme dry years therefore triples in the RCP 8.5 scenario. The occurrence of dry years also increases in RCP 4.5 (left hand side of Figure 17), although not as sharply, and not nearly as much for the most extreme (1% and 2% dry years) as they did in the RCP 8.5 simulations. Results are shown for all 32 GCMs because analyzing 1-in-100-year events yields poor sampling that is mitigated by using all the available models. If only the 10 California GCMs are used (not shown), there is little increase in the occurrence of the very driest years, an example of the sampling variability across the CMIP5 GCMs.

This is a key point - even though annual precipitation changes are modest, year-to-year variability increases due to the wetter winter conditions being balanced by the drier spring

conditions. The overall result is an increase of the frequency of dry years due to greater sampling variability (fewer wet days, but more precipitation on wet days).

3.4 Relative Humidity Results

Projected changes in relative humidity (RH) mapped over the region for the eight California GCMs that saved daily humidity data are shown in Figure 18. Warmer future air temperatures increase the equilibrium water vapor pressure in the atmosphere, leading to a general increase in *specific* humidity, but *relative* humidity is a measure of the amount of moisture held in the atmosphere as a fraction of the maximum amount it can hold, the latter of which increases as temperature rises. Relative humidity changes depend on location and are controlled primarily by available surface water sources. Adjacent to the ocean, which is essentially an infinite moisture source, warmer air temperatures lead to increases in specific humidity that are often strong enough to increase RH even in the face of the warming temperatures. As a result, RH increases of up to 7 percentage points are seen along the coastal regions in winter (DJF) and summer (JJA). However, in the arid interior, far removed from any ready source of moisture, the higher saturation vapor pressure leads to RH decreases. Declines reach values of 10 percentage points in interior Southern California in spring (MAM), and in the high Sierra Nevada to Northeast California in summer (JJA). Overall annual changes are more muted, with increases of 1-3 percentage points along the coast and similar magnitude decreases inland. The interior drying could have implications for wildfire activity, while the coastal increases in relative humidity would tend to exacerbate the health impacts of warmer temperatures through the heat index, which is affected by both temperature and relative humidity.

Higher relative humidity leads to increased stress on humans during hot days, since the evaporation of sweat and resulting cooling is reduced. The top row of Figure 19 shows the historical average heat index (°C) for the 90th percentile warm day in the warm season (May through October). The 90th percentile value is equivalent to the temperature that is exceeded by an average of 18 days per 6-month warm season. The middle and right columns show the projected change in 90th percentile heat index by the end of this century for the RCP 4.5 (middle) and 8.5 (right) scenarios. Increases are of the order 3-5 °C for RCP 4.5, and 3-7 °C for RCP 8.5. Increases are greatest in the Central Valley and extreme southern desert regions and are lower along the Central to Northern California coast, where local increases in relative humidity are more than compensated for by the relatively lesser warming. The bottom row of Figure 19 shows the same results for the 99.9th percentile day, which is approximately the hottest day in 5.5 warm seasons. In the RCP 8.5 scenario in particular, the increase is stronger than seen in the 90th percentile case; in other words, the extreme value increases preferentially. The geographical pattern of changes, with greatest increases in the Central Valley and southern desert regions and less increase along the Central to Northern California coast, is similar to the 90th percentile result.

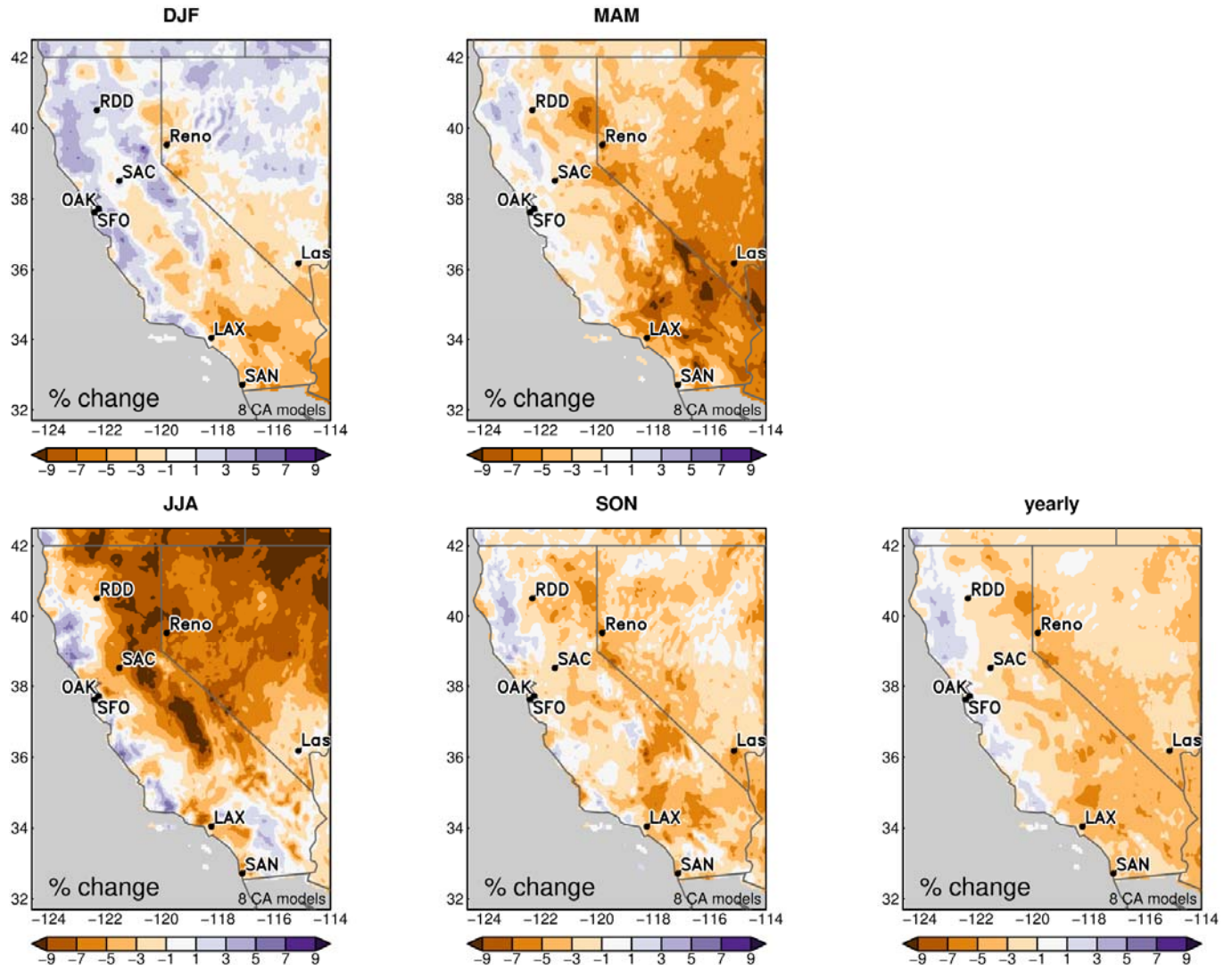


Figure 18. Change (percentage points) in seasonally and annually averaged daily minimum relative humidity (e.g. relative humidity during the warmest portion of the day) by the end of the century (2070-2100) with respect to the historical period 1976-2005. From LOCA downscaled RCP 8.5 simulations scenario using the 8 of 10 California GCMs with requisite data to calculate relative humidity. DJF= winter (December-January-February), MAM = spring (March-April-May), JJA = summer (June- July-August), and SON = autumn (September-October-November).

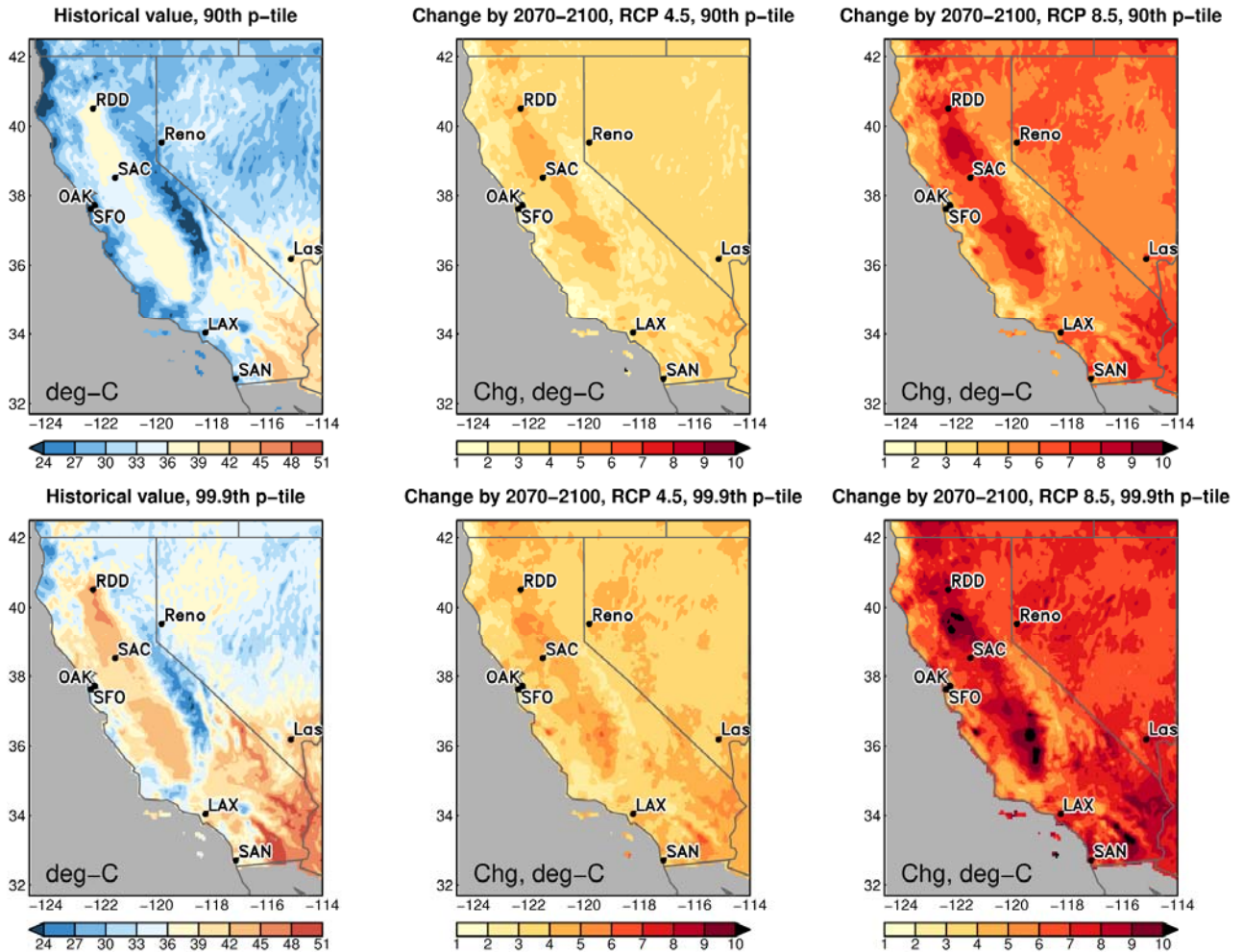


Figure 19. Top left: historical (1976-2005) 90th percentile value of the daily heat index (°C) in the warm season (May through October). Top middle: Projected change (°C) by 2070-2100 under the RCP 4.5 scenario. Top right: Change under the RCP 8.5 scenario. Bottom row: Same as top row, but for the 99.9th percentile value of the daily heat index. Computed using the 8 of 10 California GCMs with the requisite data to calculate relative humidity.

3.5 Wind Speed Results

Annually averaged changes in LOCA-downscaled wind speed at 10 meters above the surface, the standard observing height and commonly provided by GCMs, are mapped over the region in Figure 20. There is a general reduction in mean annual wind speed on the order of 2-4% for RCP 4.5, and 4-7% for RCP 8.5. Reductions are larger towards the northern part of the state.

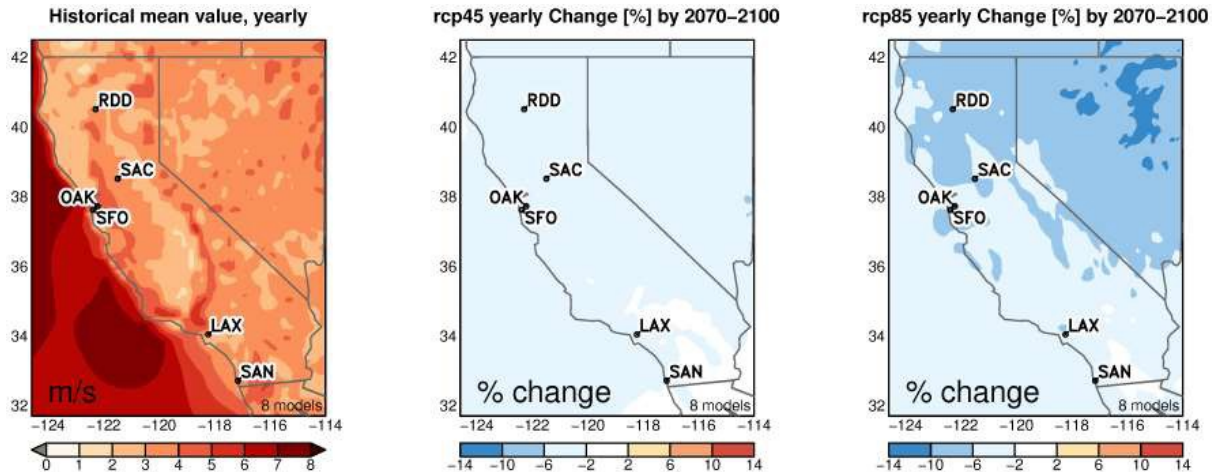


Figure 20. Left: Historical (1976-2005) mean annual 10 m wind speed (m/s) as simulated in the CaRD-10 reanalysis (Kanamitsu and Kanamaru, 2007). Middle: model-projected change in mean annual wind speed (%) by the end of the century (2070-2100) for the RCP 4.5 emissions scenario. Right: same as middle, for the RCP 8.5 emissions scenario. Computed using the 8 of 10 California GCMs with the requisite data to calculate wind speed.

3.5.1 Santa Ana Winds

Santa Ana winds are a katabatic wind that blow in an offshore direction in certain regions of Southern California, steered by the topography of the coastal hills and valleys. Santa Anas are an important feature of Southern California weather variability, since their high speed and low relative humidity can drive destructive wildfires. The climatology of Santa Ana winds is described in Guzman-Morales et al. 2016. Based on that work, we define Santa Ana winds as days where the wind speed is ≥ 8 m/s (in the middle of the “moderate” Santa Ana class in Guzman-Morales et al. 2016), relative humidity is $< 20\%$ averaged over the Southern California coastal region described below, and the day falls in the Santa Ana season, September through April.

Because only wind speed (not direction) was downscaled, winds cannot be selected based on their offshore or onshore direction. However, because of the strong correspondence of high wind speeds and low humidity during Santa Ana wind events, it is possible to use downscaled wind speed together with downscaled humidity as an adequate index of daily Santa Ana conditions. The region used for this analysis (shown in Figure 21 by the red outlines) was determined by identifying grid cells where the maximum wind speed in the CaRD10 data set (Kanamitsu and Kanamaru 2007) exceeded 15 m/s on at least one day over the period 1979-2008.

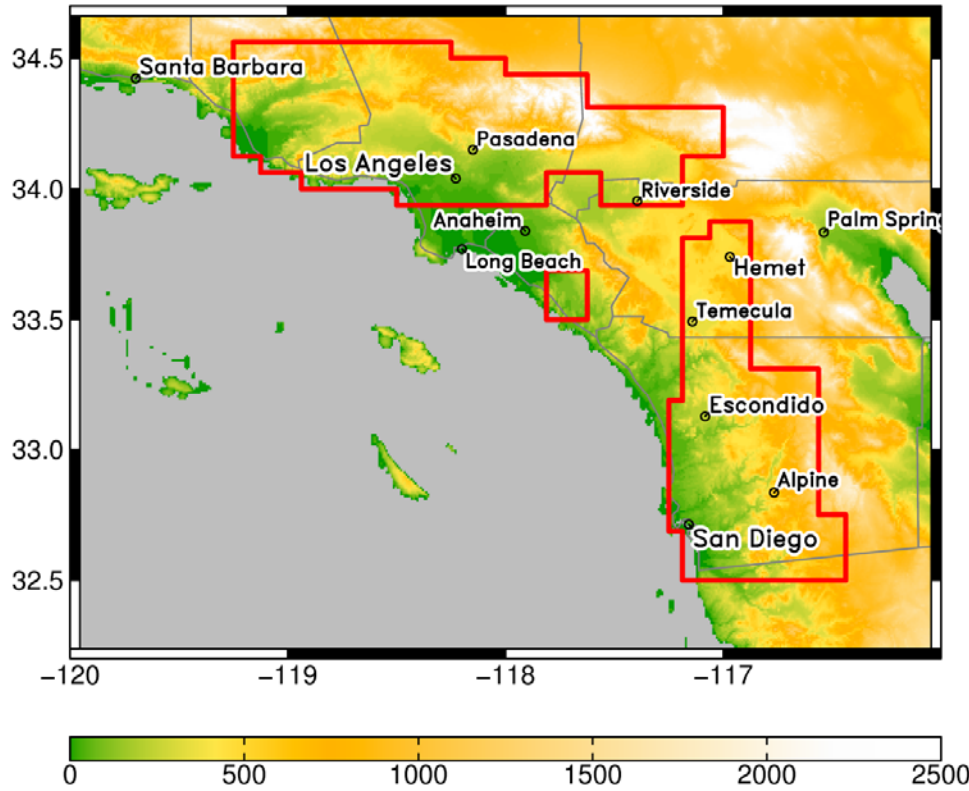


Figure 21. Southern California, showing the Santa Ana wind regions used in this analysis (outlined in red). Elevation indicated by colors, in meters. County borders are shown in grey.

The monthly climatology of Santa Ana days in the LOCA-downscaled data is shown as a function of location in our Santa Ana region in Figure 22. The peak months are November-January, although some incidents fall outside those months.

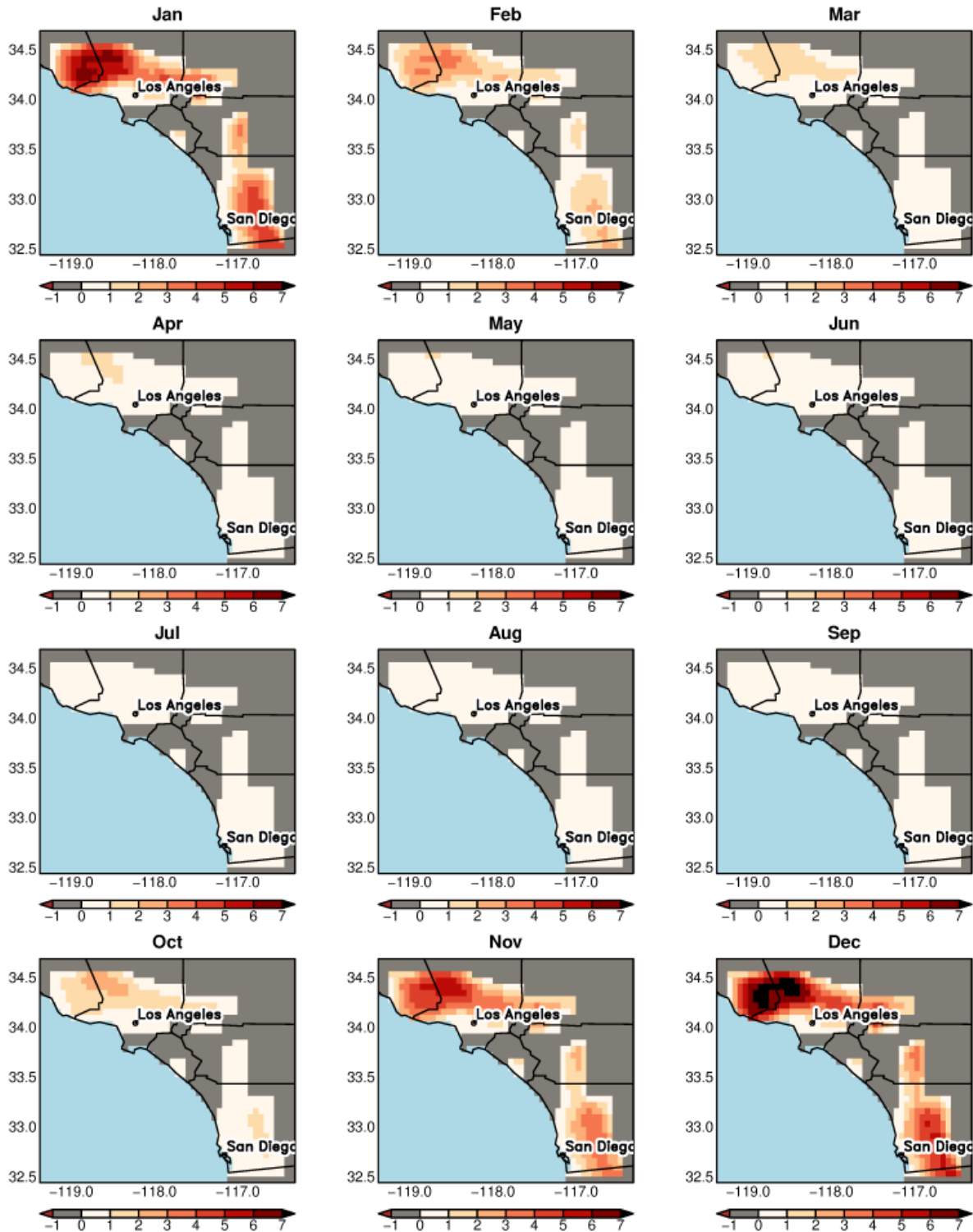


Figure 22. The incidence of days with wind speed ≥ 8 m/s and relative humidity $\leq 20\%$, the criteria taken here to be Santa Ana days. Units are mean number of days/month over the historical period. From eight LOCA downscaled GCMs. Computed using the 8 of 10 California GCMs with the requisite data to calculate wind speed.

The annual climatology of the incidence of Santa Ana days averaged over the Santa Ana region is shown in Figure 23. The amplitude and monthly distribution is consistent with the observed annual cycle found in Guzman-Morales et al. 2016. The similarity between these two results is encouraging since the Guzman-Morales et al. 2016 results are based on wind speed and direction, while the determination here is based on scalar wind speed ≥ 8 m/s and relative humidity $\leq 20\%$. As seen from the results in Figure 22, the primary Santa Ana season in the LOCA downscaled data occurs between November and January, with spatial averages over the domain exceeding 2 Santa Ana days per month. The climatological occurrence is maximum in December, with about 3.1 Santa Ana days per month on average.

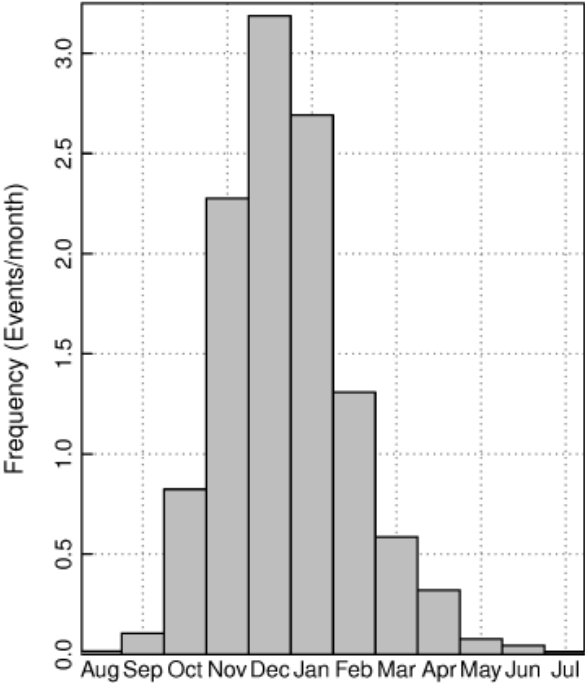


Figure 23. Histogram of the monthly incidence of days with wind speed ≥ 8 m/s and relative humidity $\leq 20\%$, taken here to be Santa Ana days. Units are mean number of days per month over the historical period. The period of coverage is 1950-2005; results are averaged over the red-outlined areas in Figure 21.

Since we define Santa Ana days in terms of wind speed and humidity, exploring future changes in Santa Ana days involves looking at changes in these two aspects of the climate. We examine how the distribution of humidity changes in Figure 24, how the distribution of wind speed changes in Figure 25, and how the joint distribution changes in Figure 26. These figures will now be described in detail.

Histograms of *relative humidity* for all days (blue) and of the subset of days with wind speed ≥ 8 m/sec (red) over the Santa Ana region, formed from all 8 models in the LOCA downscaled RCP8.5 wind speed and relative humidity ensemble, are shown in Figure 24. Only days in the September-April Santa Ana season and locations within the identified Santa Ana region are included. Of course, not all days with wind speed ≥ 8 m/sec have relative humidity below the

20% threshold, but comparing the blue lines in the top row of Figure 24 (the all days result) to the red lines in the bottom row (high wind speed days only) shows that the distribution of relative humidity on high wind speed days is more concentrated to the left compared to the distribution seen on all days (i.e., there is a tendency for high wind speed days to have lower humidity).

The rightmost column shows the difference between the distributions, future minus historical. Across all days (blue line), there is a depletion of days with relative humidity between 40 and 65%, and a corresponding gain in days with relative humidity between 20 and 40%. Focusing only on days with high wind speeds (red lines), there is a strong depletion of days with relative humidity between 8 and 60%, and a small increase in the very driest days, with relative humidity < 8%.

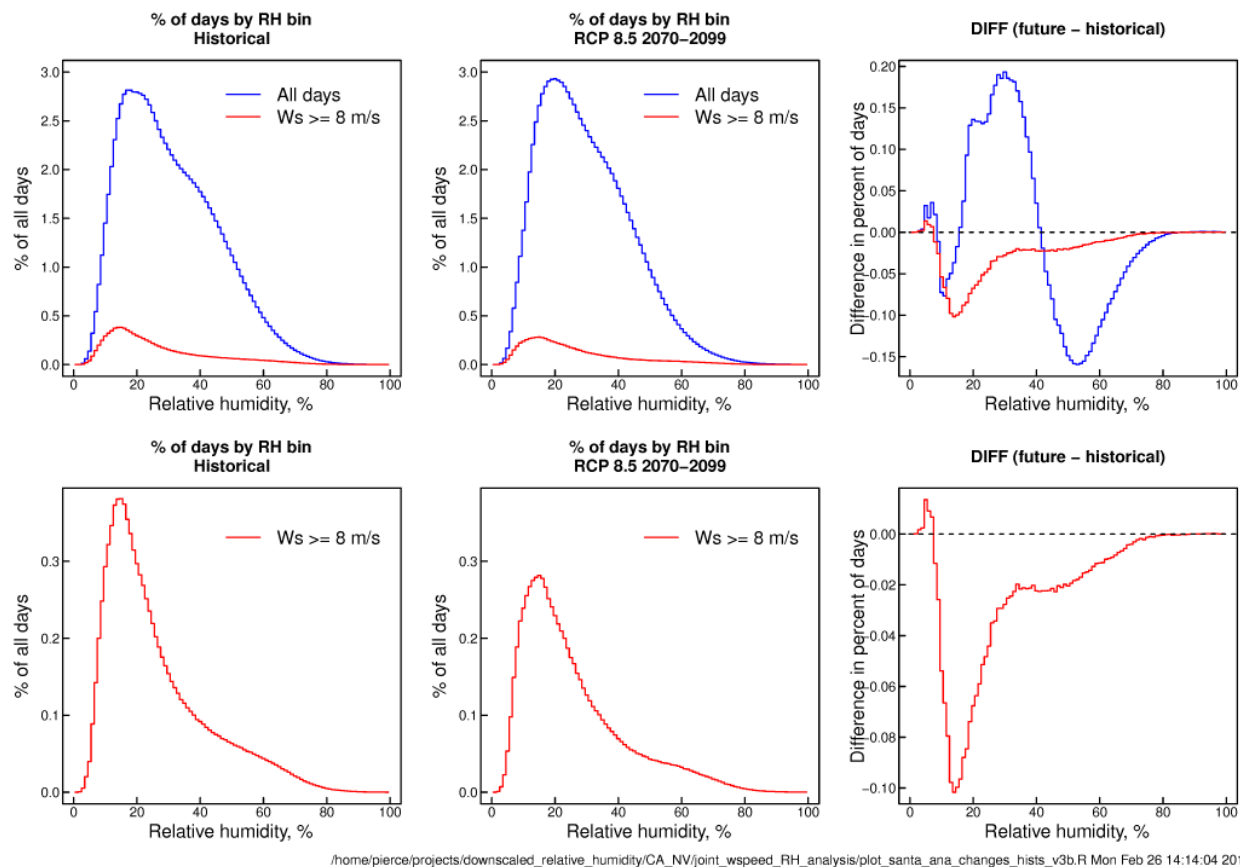
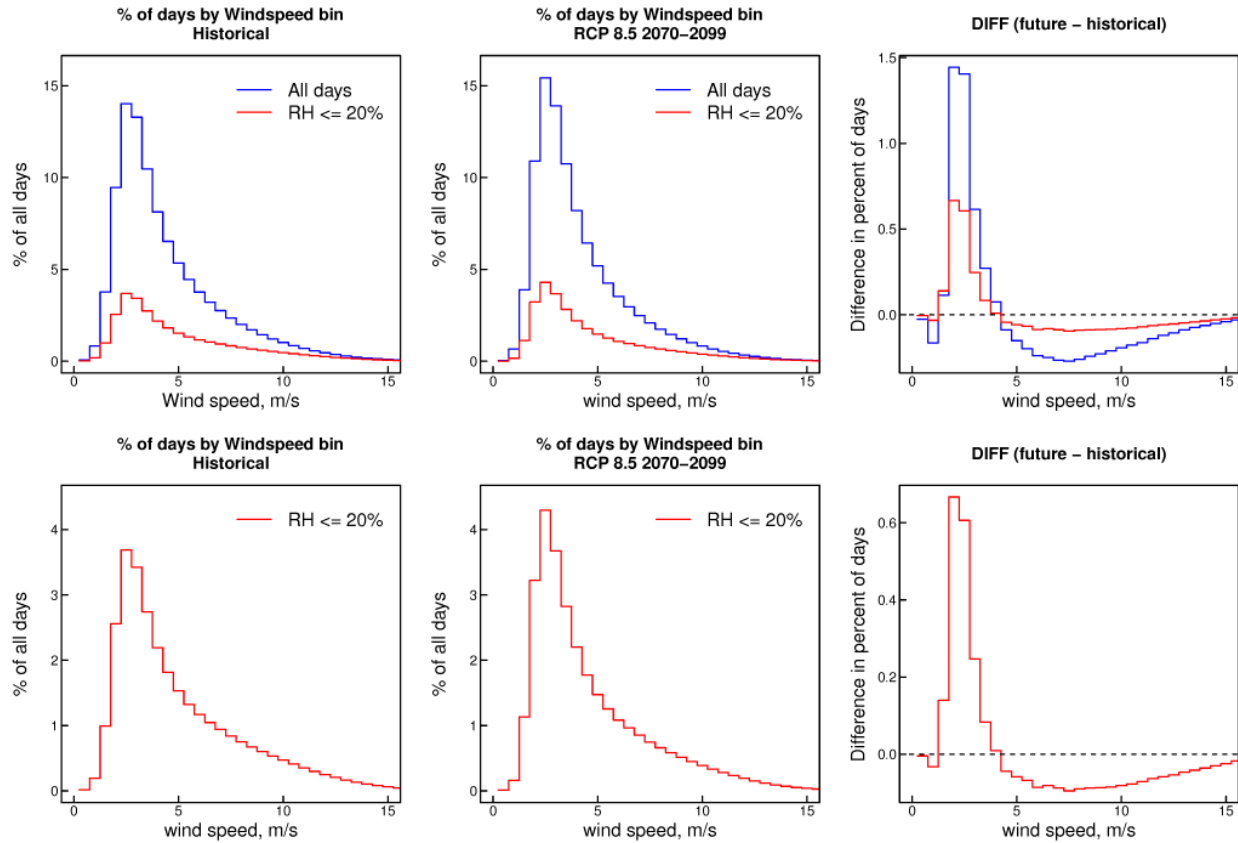


Figure 24. Histograms of relative humidity for all days (blue), and days with wind speed ≥ 8 m/s (red). Left column: Historical conditions. Middle column: Future conditions (RCP 8.5, 2070-2100). Right column: difference, future minus historical histogram. Bottom row shows the red (windspeed ≥ 8 m/s) curves on an expanded scale. Computed using the 8 of 10 California GCMs with the requisite data to calculate wind speed.

Complementary to Figure 24, Figure 25 shows histograms of *wind speed* on all days (blue) and days with low relative humidity ($\leq 20\%$; red) averaged over the Santa Ana region. The histograms show that days with wind speed ≥ 8 m/sec are relatively infrequent, constituting 9.5% of days in the historical period, and 7.5% of days in the future period (using RCP 8.5, 2070-2099). Importantly, the models project a general depletion of days with wind speed ≥ 5 m/s

(right column of Figure 25), and an increase in the number of days with wind speed between 2 and 4 m/s. This tendency is seen in both the all-day results (blue lines) and days with RH \leq 20% (red lines).



/home/pierce/projects/downscaled_relative_humidity/CA_NV/joint_wspeerd_RH_analysis/plot_santa_ana_wspeerd_change_hists.R Mon Feb 26 15:26:00 2018

Figure 25. Similar to the previous figure, but showing histograms of wind speed for all days (blue) and days with relative humidity \leq 20% (red). Computed using the 8 of 10 California GCMs with the requisite data to calculate wind speed.

The information from the previous histograms is combined and summarized in the heat map of Figure 26, which shows the ratio of incidence of future days to the incidence of historical days as a function of wind speed and relative humidity averaged over the Santa Ana region. Blue colors indicate relative humidity and wind speed conditions where the future incidences (percentage of days) decreases; orange and red colors show where the future incidence increases. The green box shows days with wind \geq 8 m/s and relative humidity \leq 20%, corresponding to our definition of a Santa Ana day. In general, there is a reduction in days with relative humidity between 30 and 70%, and an increase in the incidence in both high humidity days (which are not Santa Ana days) and very low ($<$ 5%) humidity days with wind speeds in the range of 5-15 m/s.

Using our working definition of Santa Ana days (\geq 8 m/s daily wind speed and \leq 20% relative humidity in the Santa Ana region during the period September through April; as shown in the green box in the figure), Figure 26 shows an increase in the relative frequency of such days in the lowest relative humidity bins examined, by a factor of 1.1 to 2. At more moderate 10-20% relative

humidity values, there is a general decrease in days with wind speed ≥ 8 m/s by 10 to 80%. The higher wind speed days are depleted preferentially.

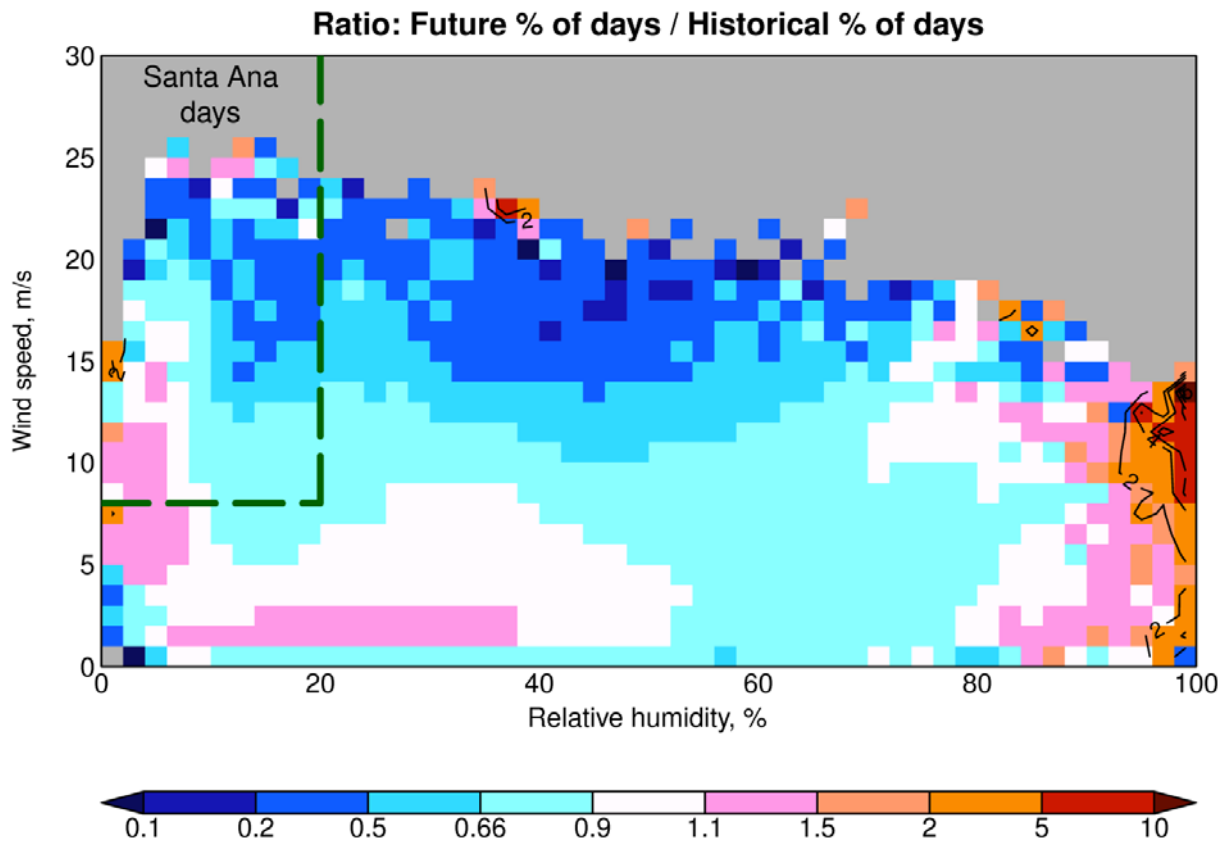


Figure 26. Ratio of the future incidence (% of days) to historical incidence of days in relative humidity-wind speed bins. The future period is 2070-2099, using RCP 8.5. The green box shows the Santa Ana day criterion used here: wind speed ≥ 8 m/s, relative humidity $\leq 20\%$. Computed using the 8 of 10 California GCMs with the requisite data to calculate wind speed.

Santa Ana winds originate in the interior, which is expected to warm more than coastal regions in the future due to the damping influence of the ocean. One might therefore expect that during Santa Ana conditions, local temperatures will experience more warming than is seen on non-Santa Ana days. This is examined in Figure 27. The top panel shows the mean (and 95% confidence interval, shaded) temperature as a function of the relative humidity on days where the wind speed ≥ 8 m/s and during the September-April Santa Ana season. The blue line is for historical conditions and the red line for the future conditions (2070-2099, RCP 8.5). There is a clear trend such that lower humidity days, associated with offshore winds, are warmer than high humidity days. This result suggests that future warming may be accentuated during low humidity days. The lower panel shows the difference between the mean curves in the upper panel: future mean minus historical mean. The results show that in the eight simulations downscaled here, future warming on Santa Ana days (RH $\leq 20\%$) will be higher than the warming on days having relative humidity between 20 and 60%. The warming on days with relative humidity $< 20\%$ ranges from 4-6 deg-C, while the warming on days with relative humidity between 20 and 60% is 3-4.5 deg-C.

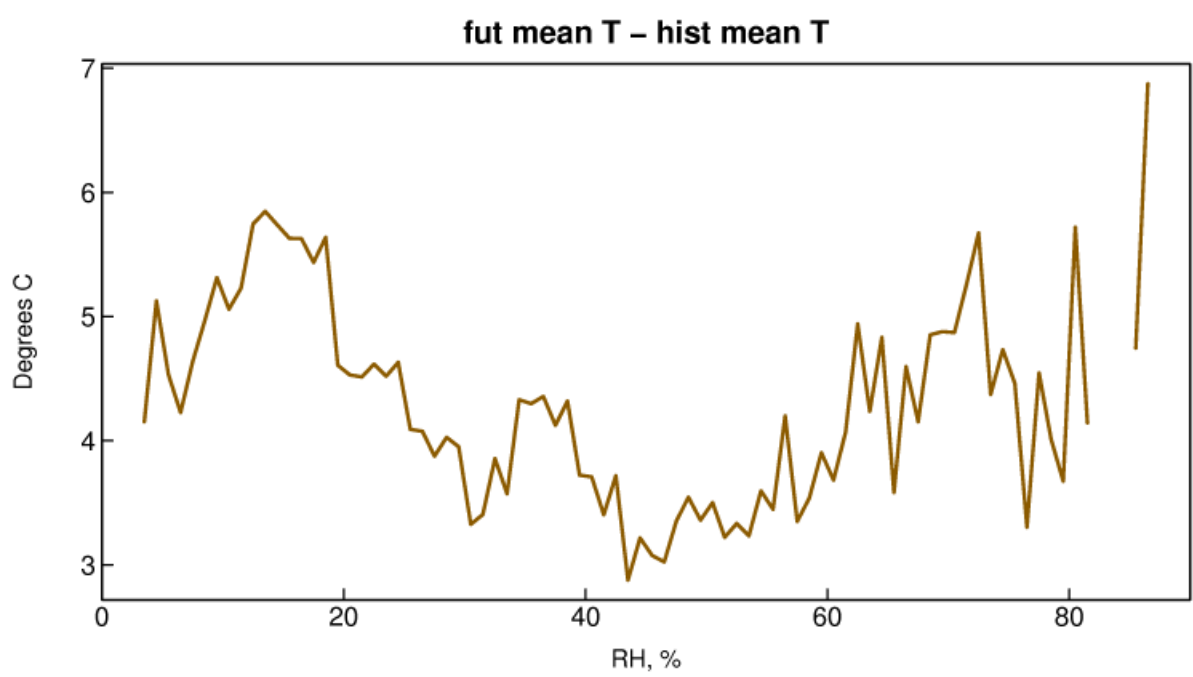
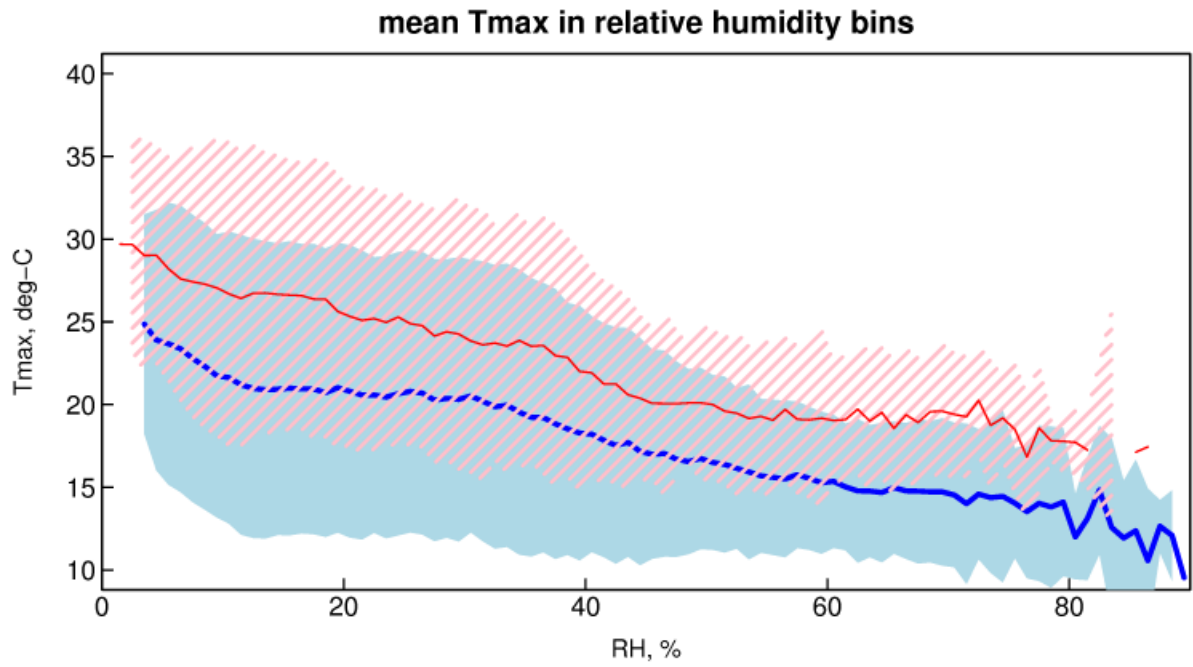


Figure 27. Upper: mean temperature as a function of relative humidity for days with wind speed ≥ 8 m/s, in the Santa Ana region, and during the Santa Ana season (Sep-Apr). The blue line shows historical conditions and the red line future conditions (2070-2099, RCP 8.5). The light blue region shows the 95% confidence interval on the historical value, while the pink lines show the 95% c.i. for the future conditions. Lower panel: The difference between the mean future and mean historical values from the upper panel.

3.6 Surface Solar Radiation Results

Projected changes in surface incoming radiation by the end of this century, mapped over the region, are shown in Figure 28 for the multi-model ensemble average over the 9 models with available surface solar radiation data. Changes are calculated with respect to a training period of 1985-2005. The models project mild increases in surface solar radiation in California in winter and spring, on the order of 2-4%. This is likely related to the decrease in number of wet days mentioned earlier. The annual average change shows a few percent increase in surface solar radiation.

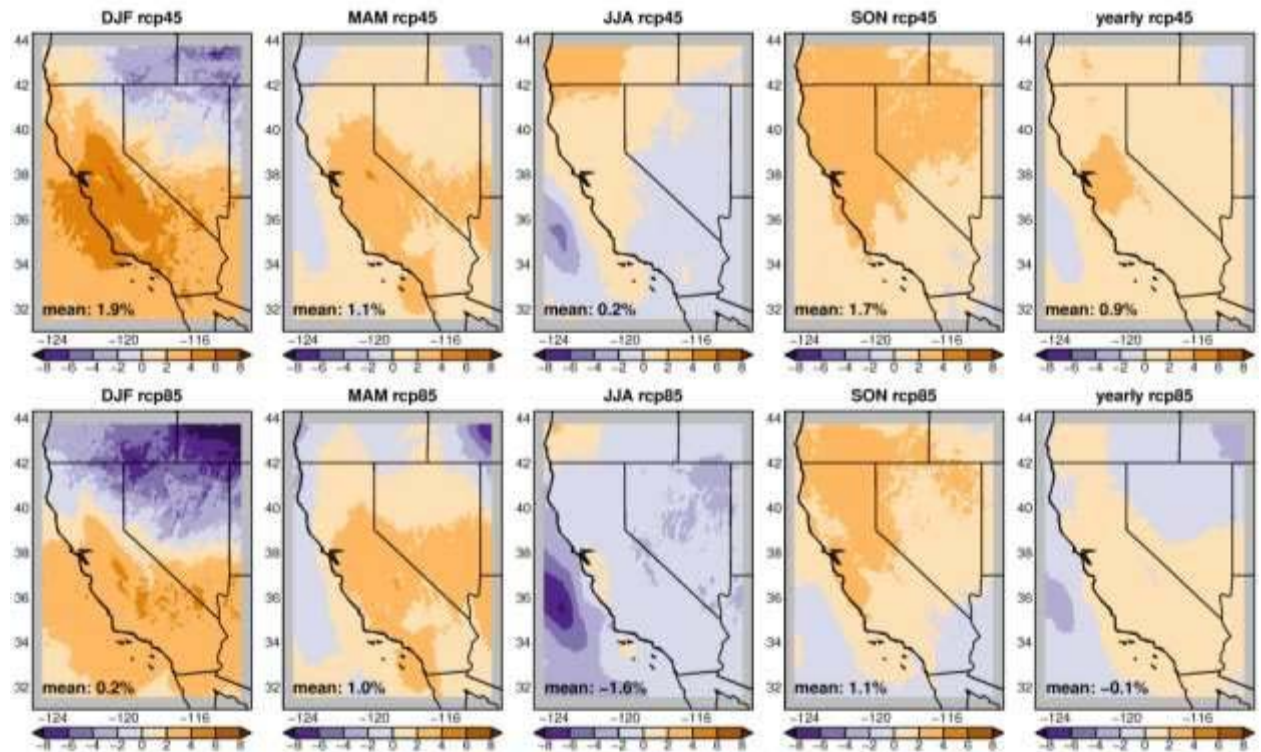


Figure 28. Seasonal and annual mean projected change in surface solar radiation [%] by the end of the century (2070-2100) with respect to the solar radiation data historical period (1985-2005), for RCP 4.5 (top row) and RCP 8.5 (bottom row). Computed using the 9 of 10 California GCMs with the requisite data to calculate surface solar radiation.

One aspect of the model projected changes that is not fully addressed by the seasonal and annual change maps is the issue of uncertainty and variability in the mean climatological change that is likely to be experienced. To address this, we use the idea of the “likely change range,” defined here as the central 2/3rds of the distribution of individual model-estimated changes in the future 30-yr mean. If the models all represent equally realistic estimates of what may happen in the future, then the 30-yr average change in surface solar radiation that the Earth experiences by 2070-2100 is twice as likely to fall within the likely change range as it is to be outside of that range.

Time series of annually averaged model surface solar radiation, along with the MMEA (darker lines), are presented in the following four figures for the grid cells corresponding to Los Angeles (Figure 29), Sacramento (Figure 30), Monterey (Figure 31), and San Diego (Figure 32). Also shown

on each panel is the likely change range computed for each RCP, 4.5 (in blue) and 8.5 (in red). The historical period is shown in black.

On a yearly averaged basis, the likely change ranges do not consistently exclude zero, although there are exceptions for particular locations and RCP's. For example, the likely change range for Los Angeles very nearly excludes zero, being generally positive.

On a seasonal basis, the only projected change that consistently (across both RCP's) excludes zero occurs in spring (MAM). Both Los Angeles and San Diego show increases in surface solar radiation (corresponding to losses of cloudiness) in spring, with a result that they are likely to receive ~2-4% more solar radiation in spring by the end of this century in either RCP scenario. Monterey and Sacramento MAM changes are positive in RCP 8.5, but the likely range includes zero for RCP 4.5.

Overall, these results suggest that natural climate variability coupled with relatively weak projected changes yield small (< 5%) future changes in surface solar radiation. In particular, the future changes are likely to be smaller than can be experienced by natural climate variability on 30-yr timescales. The only exception to this is spring in the southern part of the state, which is likely to receive 2-4% more surface solar radiation, presumably due to a reduction in cloudiness and linked to the decreased incidence of wet days in spring.

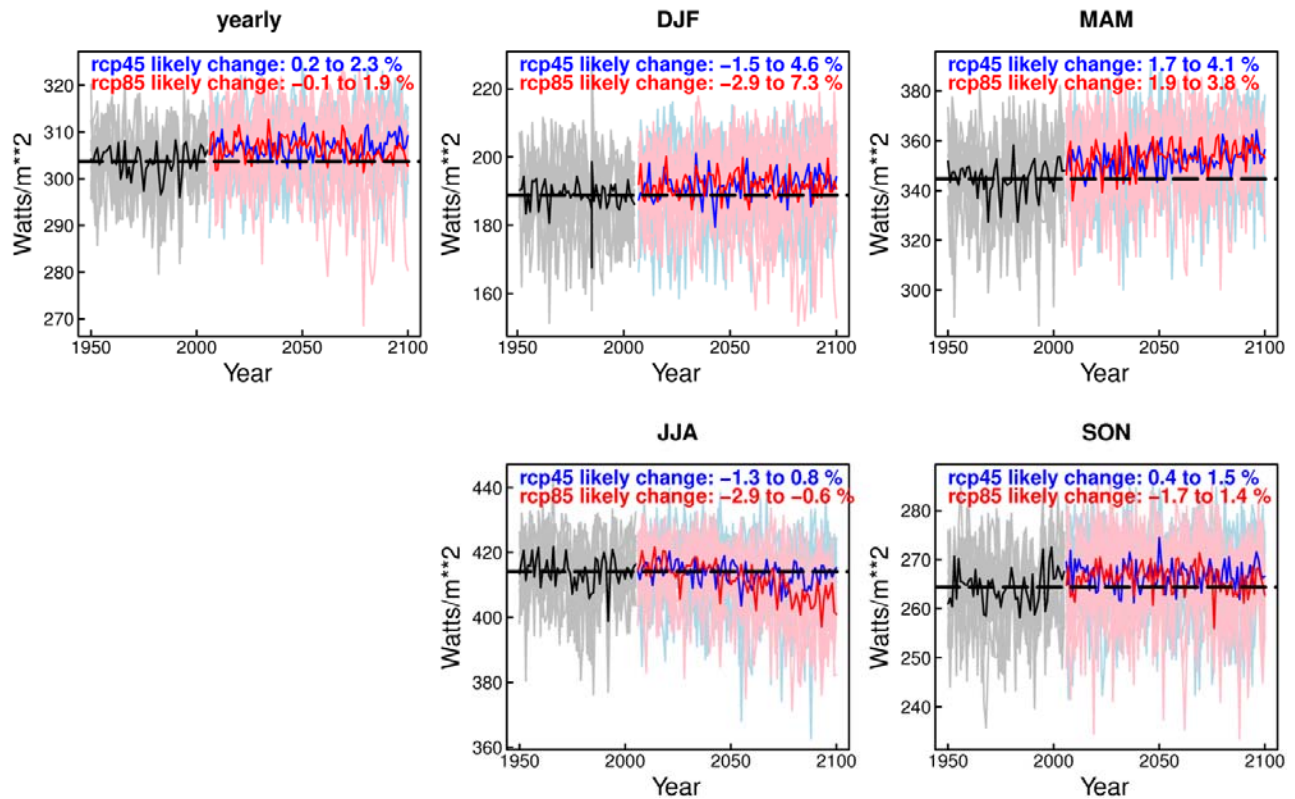


Figure 29. Time series of solar radiation: Los Angeles. Black: Historical; Blue: RCP 4.5; Red: RCP 8.5. Panels show annual (top left) and seasonal values. Computed using the 9 of 10 California GCMs with the requisite data to calculate surface solar radiation.

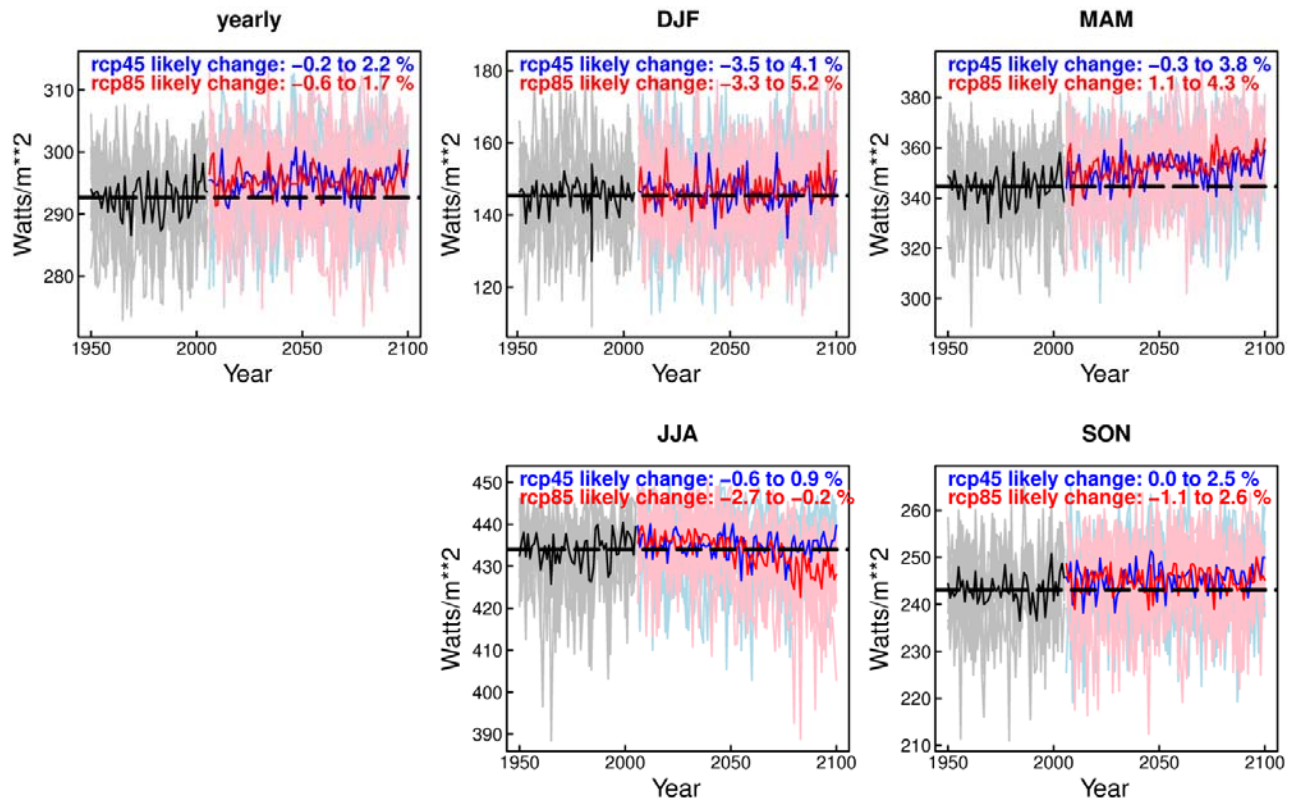


Figure 30. Time series of solar radiation: Sacramento. Black: Historical; Blue: RCP 4.5; Red: RCP 8.5. Panels show annual (top left) and seasonal values. Computed using the 9 of 10 California GCMs with the requisite data to calculate surface solar radiation.

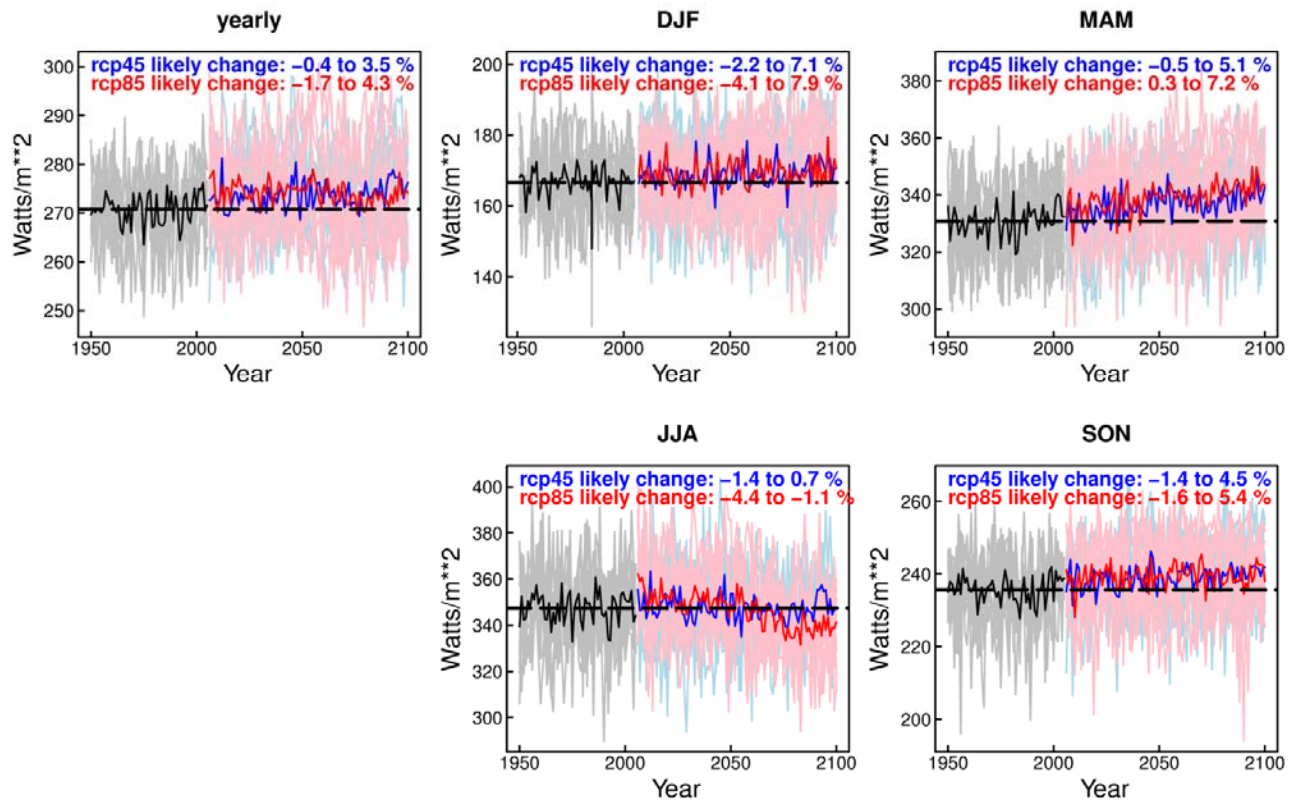


Figure 31. Time series of solar radiation: Monterey. Black: Historical; Blue: RCP 4.5; Red: RCP 8.5. Panels show annual (top left) and seasonal values. Computed using the 9 of 10 California GCMs with the requisite data to calculate surface solar radiation.

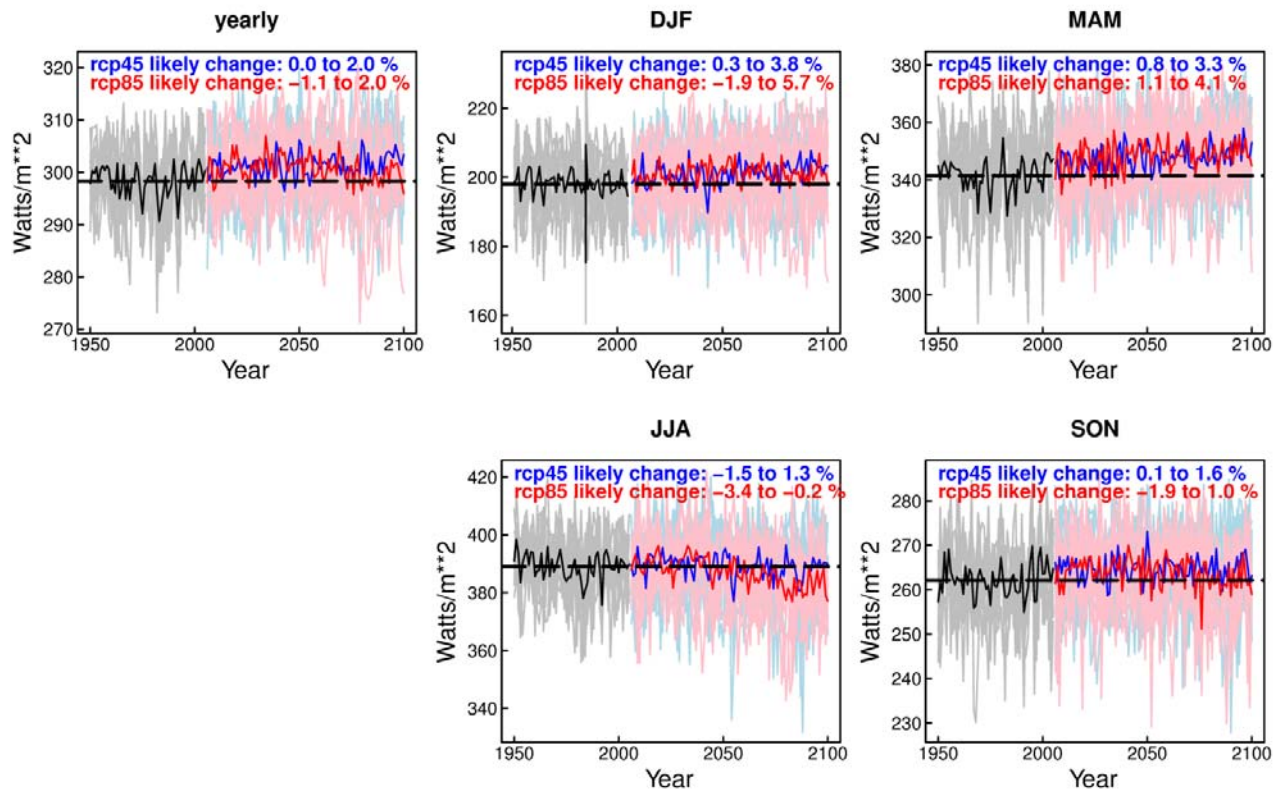


Figure 32. Time series of solar radiation: San Diego. Black: Historical; Blue: RCP 4.5; Red: RCP 8.5. Panels show annual (top left) and seasonal values. Computed using the 9 of 10 California GCMs with the requisite data to calculate surface solar radiation.

4: VIC Hydrological Model Simulations

Besides the meteorological variables provided by LOCA directly downscaling the GCM outputs, impact studies often need land surface measures of the hydrologic system, such as snow cover (for examining water supply issues), soil moisture (relevant to agriculture, ecosystems and droughts), and runoff (for flooding and water management impacts). Every GCM incorporates its own land surface model. However, modeled land surface characteristics and hydrology are highly sensitive to the spatial resolution of the model in regions with pronounced topography, such as found in California's coasts, coastal range, Central Valley, Sierra Nevada, and lower lying desert landscapes. With 32 GCMs using a variety of spatial resolutions, the GCMs are quite uneven in representing key aspects of California's land surface. Additionally, the GCMs have a range of capabilities incorporated into their embedded land surface models, including some simplistic ones that neglect processes of importance for future climate impacts. Because of these issues, we do not directly use the output from the GCMs' land surface models.

To avoid these problems, we use the Variable Infiltration Capacity (VIC) land surface / hydrology model, version 4.2.c (Liang et al., 1994), which is run using input from LOCA- downscaled fields of daily precipitation and minimum and maximum temperature. VIC balances surface and

subsurface water and energy fluxes at individual grid cells but does not include lateral processes or a stream channel system, so any routing across grid cells must be carried out subsequent to the runoff calculations. VIC has been used in numerous hydroclimate studies (e.g. Das et al. 2009; Mote et al. 2016) and is run routinely to monitor regional hydrologic variability (e.g., UCLA Drought Monitoring System for CA and NV:

http://www.hydro.ucla.edu/monitor_ca/index.html). In this application, the primary forcing variables that are input to VIC are the high resolution (1/16th degree, or 6 km) LOCA precipitation and temperature. The VIC model outputs include rain, snow, snow cover, and soil moisture content in three layers: an upper 10 cm layer, a middle layer that is usually 50cm, and a lower layer that typically ranges between 100 cm and 250 cm. VIC also calculates sublimation of water vapor from the surface, runoff, surface heat fluxes, actual evapotranspiration (ET), potential evapotranspiration (PET), and other variables. These variables are critical for impact studies in the application areas noted above, as well as for application to wildfires, agriculture, and ecosystems. On the other hand, the version of VIC used here does not include dynamic vegetation changes, so some of the projected changes by the end of the century would in actuality be accompanied by significant ecosystem shifts that are not reflected in these results. Additionally, only natural vegetation and precipitation are included; irrigated crops will experience different changes than modeled here due to the artificial water supply. However, the modeled background climate *tendencies* in absence of externally supplied water are valid.

Projected changes in runoff, annually averaged moisture deficit (AET-PET), and annually averaged upper layer soil moisture, mapped over the region, are shown in Figure 33 through Figure 35.

The mean lowest runoff year experienced in a decade declines substantially over most of California (Figure 33), relative to the historic period average driest year in a decade. Declines reach values of 30 to 50% over the southern Sierra Nevada and parts of coastal Northern California by the end of this century (Figure 33 lower right panel). So, for example, the -50% value seen over the southern Sierra Nevada indicates that runoff in the driest year in the decade 2091-2100 will, on average, be only half the runoff experienced in the driest year in a decade over the historical period. Declines in the Central Valley region are more modest, on the order of 10 to 20%.

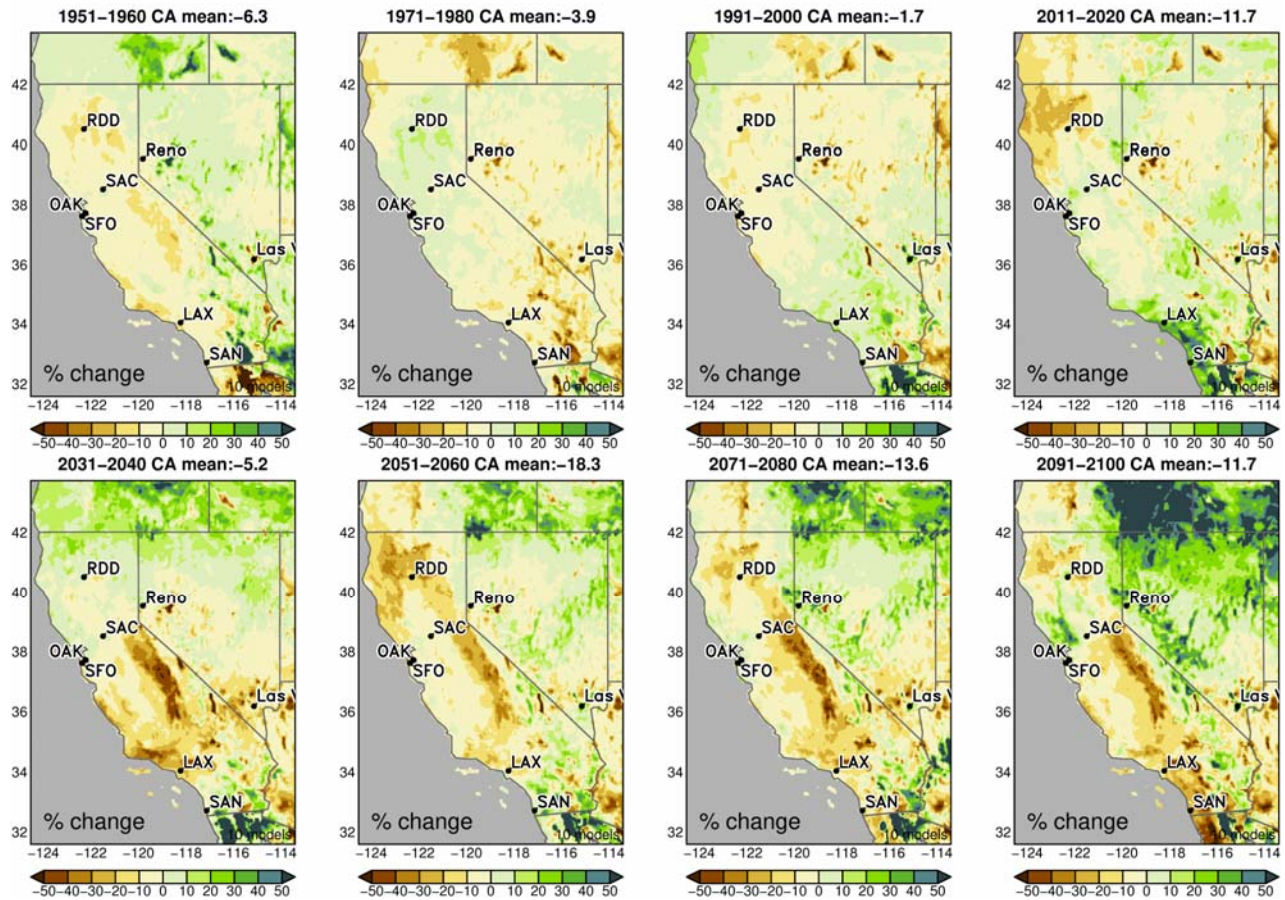


Figure 33. Difference [%] in the lowest runoff water year per decade, for the labeled decades out to the end of the 21st century, with respect to the average value over the period 1950-2005. Results are for the RCP 8.5 emissions scenario and based on the 10 California GCMs.

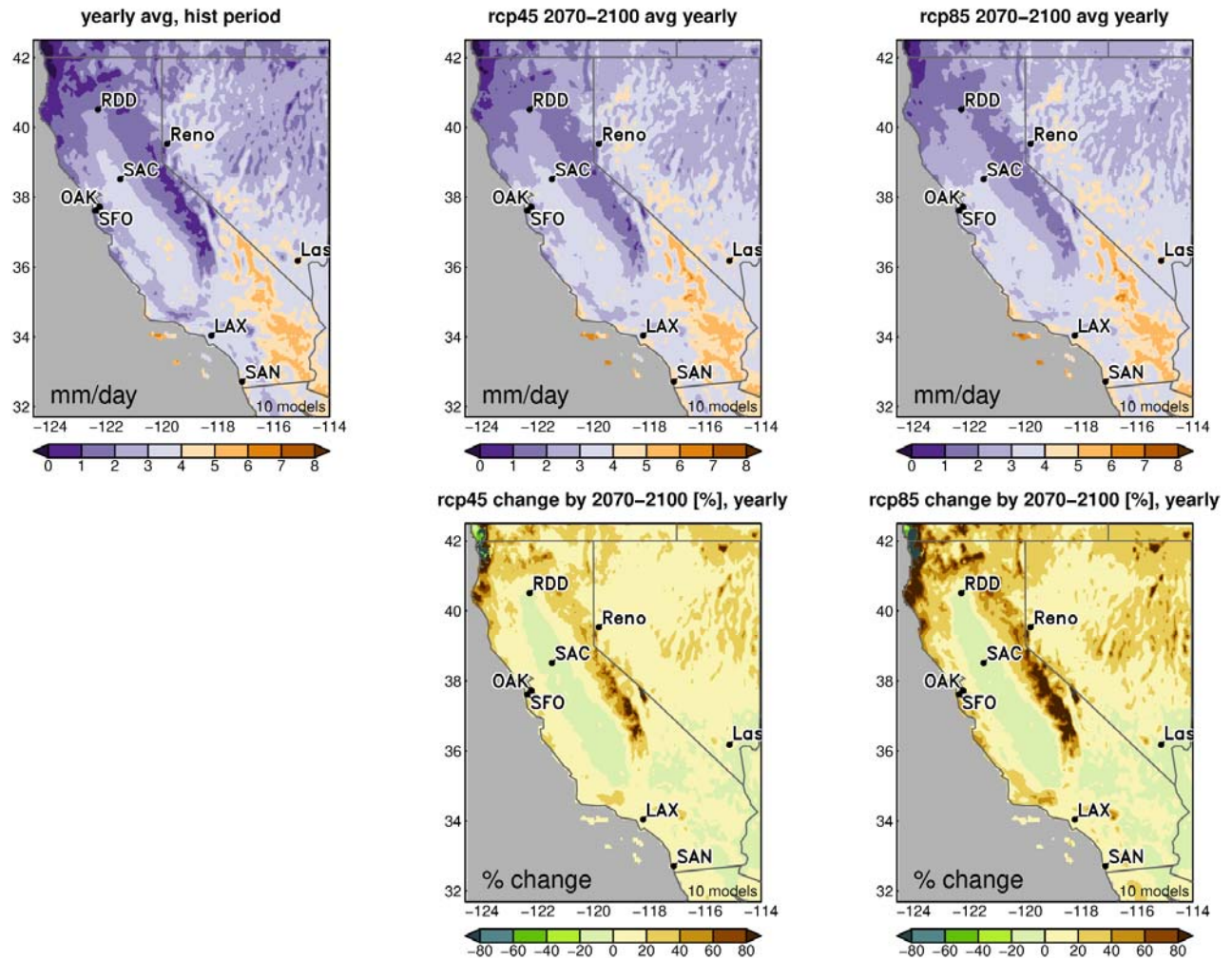


Figure 34. Top: Moisture deficit (mm/day), defined as the potential evapotranspiration minus the actual evapotranspiration (PET – AET), yearly averaged, for the historical period (top left) and end of this century for RCP 4.5 (top middle) and RCP 8.5 (top right) emissions scenarios. Bottom: changes (%) by the end of century for the RCP 4.5 (middle) and RCP 8.5 (right) scenarios with respect to the historical period. Data from the 10 California GCMs.

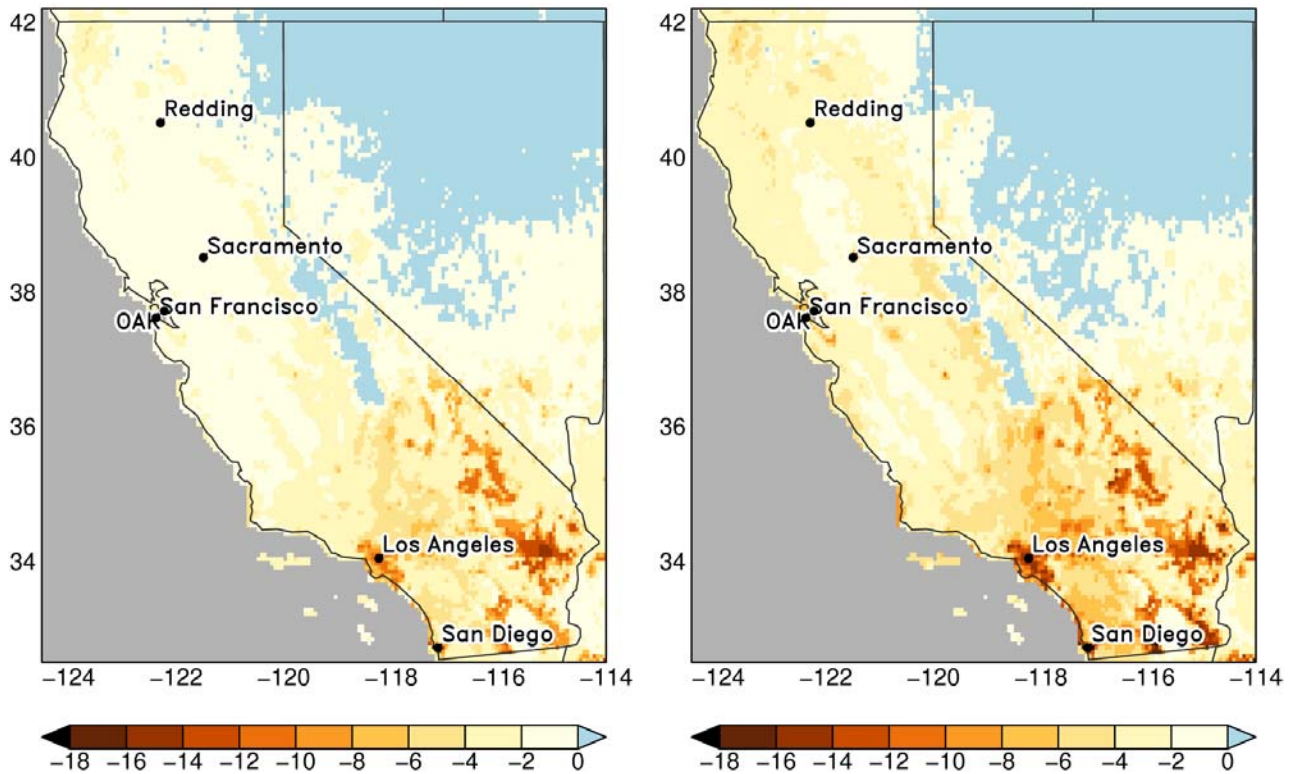


Figure 35. Change in top layer soil moisture [%] by the end of the century (2070-2100), with respect to the historical period of 1976-2005, for RCP 4.5 (left) and RCP 8.5 (RIGHT). Data from the 10 California GCMs.

Changes in the moisture deficit (Figure 34) are greatest in the southern Sierra Nevada, where increases of 40-80% are projected by the end of century. Moisture deficit declines in the future in the Central Valley because VIC includes a parameterization that increases canopy resistance, shutting off water loss from plants, at the high Central Valley temperatures that are more regularly exceeded in the future.

The top layer soil moisture (Figure 35) shows declines over most of the state, with greater declines in the southern half (6-12% in RCP 8.5, right panel) than in the northern half (2-4%). We do not show change in soil moisture at the two lower soil layers because the thickness of the layers can be chosen as a calibration parameter for the VIC model, resulting in a patchwork of soil thicknesses (and therefore projected change in moisture) where VIC has been calibrated differently in different basins. The thickness of the top layer, by contrast, is constant throughout the domain, and so more appropriate for regional comparisons.

4.1 Streamflow

To generate streamflow, surface and sub-surface (“runoff” and “baseflow”) runoff variables from the VIC hydrological model were routed using the Lohmann (1996) routing scheme for the 10 California GCMs. Currently, the routing network is only available on a 1/8th degree (12 km) latitude-longitude grid, so the VIC runoff and baseflow are calculated on the 16th degree (6 km) grid, then each 2x2 block is routed as a unit.

The routing network produces flow at 17 locations across California. However, these model-generated streamflows cannot be used directly, because the routing network and VIC hydrological model have errors. Therefore, the model-simulated flows must be bias corrected to observations before being used.

The VIC model does not include human activities such as diversions for irrigation, groundwater pumping, and the operations of dams and reservoirs. Therefore, the VIC simulated streamflows must be bias corrected using so-called “unimpaired flows”, which are flows that would have been observed in the absence of human activities. Unimpaired flows are calculated using reported diversions by the California Department of Water resources. The data were obtained from the publication “Estimates of Natural and Unimpaired Flows for the Central Valley of California: Water Years 1922-2014 (March 2016, Draft)” by the Department of Water Resources, Bay-Delta Office (hereafter referred to as the “DWR Flow Report”).

Because we bias corrected to unimpaired flows compiled in the DWR Flow Report, the locations at which the bias correction can be implemented are restricted to locations that are common to both the VIC routed flow points and the flow points compiled in the DWR flow report. We assessed this commonality by geographically over-plotting the DWR Flow Report locations and the VIC routed streamflow locations. This resulted in 11 matching CA-DWR/VIC basins, as indicated in Table 3. The total amount of flow represented by the 11 locations is 24,467 thousand acre-feet per year (TAF/yr) on average, which is 87% of the 28,100 TAF/yr total unimpaired flow in the Sacramento-San Joaquin flow region according to the DWR Flow Report. So although only 11 locations have routed and bias corrected streamflow, they represent the large majority of total flow in the basin.

Table 3. CA-DWR basin numbers (column 1), basin name (column 2), VIC routed streamflow name (column 3), and mean flow at that point (thousand acre-feet/year; column 4).

CA-DWR "UF" basin	CA-DWR Name	VIC Name	Mean flow (TAF/yr)
6	Sac R near Red Bluff	SAC_BEND_BRIDGE	8254
8	Feather R nr Oroville	OROVILLE	4376
9	Yuba R at Smartville	SMARTVILLE	2295
10	Bear R nr Wheatland	BEARCREEK	318
11	American R at Fair Oakes	FOLSOM_INFLOW	2628
14	Mokelumne R at Pardee Rsv	PRD-CAMANACHE	722
15	Calaveras at Jenny Lind	NEW_HOGAN	161
16	Stanislaus R at New Melones Rsv	N_MELONES	1177
18	Tuolumne R at Don Pedro Rsv	DPR_INFLOW	1849
19	Merced R at Exchequer Rsv	LK_MCCLURE	957
22	San Joaquin R at Millerton Rsv	MILLERTON	1730

The necessity for bias correction of the flow is illustrated in Figure 36, which shows the hydrograph (mean climatological stream flow in each month) over the historical period (1976-2005) for three example basins. These basins are shown because they illustrate the existing range in quality of the raw (original, non-bias corrected) VIC model streamflows from best to worst agreement with the observations. Each of the 11 streamflow locations was subjectively assigned a letter grade of A, B, or C depending on the agreement between the monthly hydrograph of the observations and the VIC-simulated flow at that location. Table 4 shows the grade for each of the 11 routed locations, along with the percent error in the annual mean of the simulated model flow with respect to the observed value.

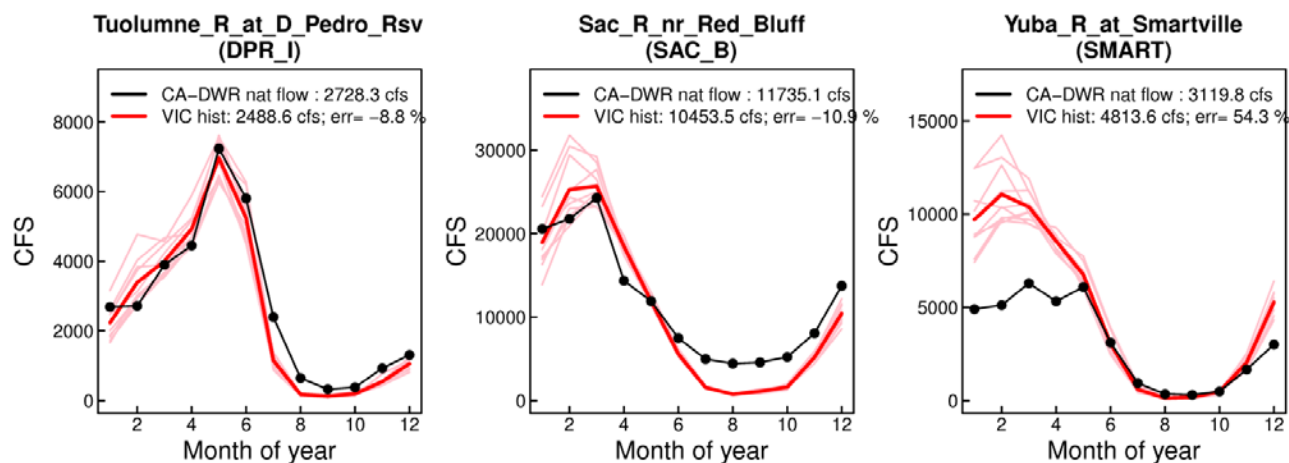


Figure 36. a) Three streamflow hydrographs illustrating the observed flows by month (black lines), and model-simulated flows by month (red lines) over the historical period (1976-2005). The left panel illustrates a Grade “A” location, where the model and simulated flows were subjectively judged to agree well. The middle panel illustrates a Grade “B” location, where agreement is medium, and the right panel illustrates a Grade “C” location, where the model-observations agreement is poor. Data from the 10 California GCMs.

The streamflow bias correction method is fundamentally the same process as used to generate the LOCA data and described in Pierce et al. 2015. The only difference implemented for streamflow is that the LOCA meteorological data were bias corrected on a daily basis, while the monthly streamflows were only available on a monthly basis. Therefore, a simpler monthly bias correction was performed on the streamflow. Other key aspects of the bias correction process were left unchanged. In particular, the future flow is calculated as the historical flow at each quantile times the model-calculated future change at that quantile. Because using only monthly data gives 30 times less data than using daily data, noise was reduced by averaging the model-predicted change factor across 3 months. I.e., when calculating the model-predicted change factor for June, change factors for May, June, and July were averaged together to reduce noise.

Table 4. The quality grade and annual mean flow error for each routed location.

UF #	Name	Obs mean flow (TAF)	Raw VIC error mean flow (%)	Quality grade*
6	Sac R near Red Bluff	8254	-14.2	B
8	Feather R nr Oroville	4376	-12.2	B
11	American R at Fair Oakes	2628	6.3	B
9	Yuba R at Smartville	2295	46.0	C
18	Tuolumne R at Don Pedro Rsv	1849	-6.8	A
22	San Joaquin R at Millerton Rsv	1730	-9.2	A
16	Stanislaus R at New Melones Rsv	1177	-2.7	B
19	Merced R at Exchequer Rsv	957	10.7	A
14	Mokelumne R at Pardee Rsv	722	19.3	C
10	Bear R nr Wheatland	318	-40.0	B
15	Calaveras at Jenny Lind	161	140.5	C

Examples of the final, bias-corrected hydrographs for two locations are shown in Figure 37, along with the bias-corrected future hydrographs by the end of the century for the RCP 4.5 and RCP 8.5 emissions scenarios. The basins included in this set (in accord with the DWR Flow Report) contain a substantial snowmelt component. Not surprisingly, most basins exhibit hydrographs having an advance of approximately 1 month earlier peak flow, due to warmer future temperatures causing a combination of more winter precipitation falling as rain instead of snow and earlier melting of the snow that does fall.

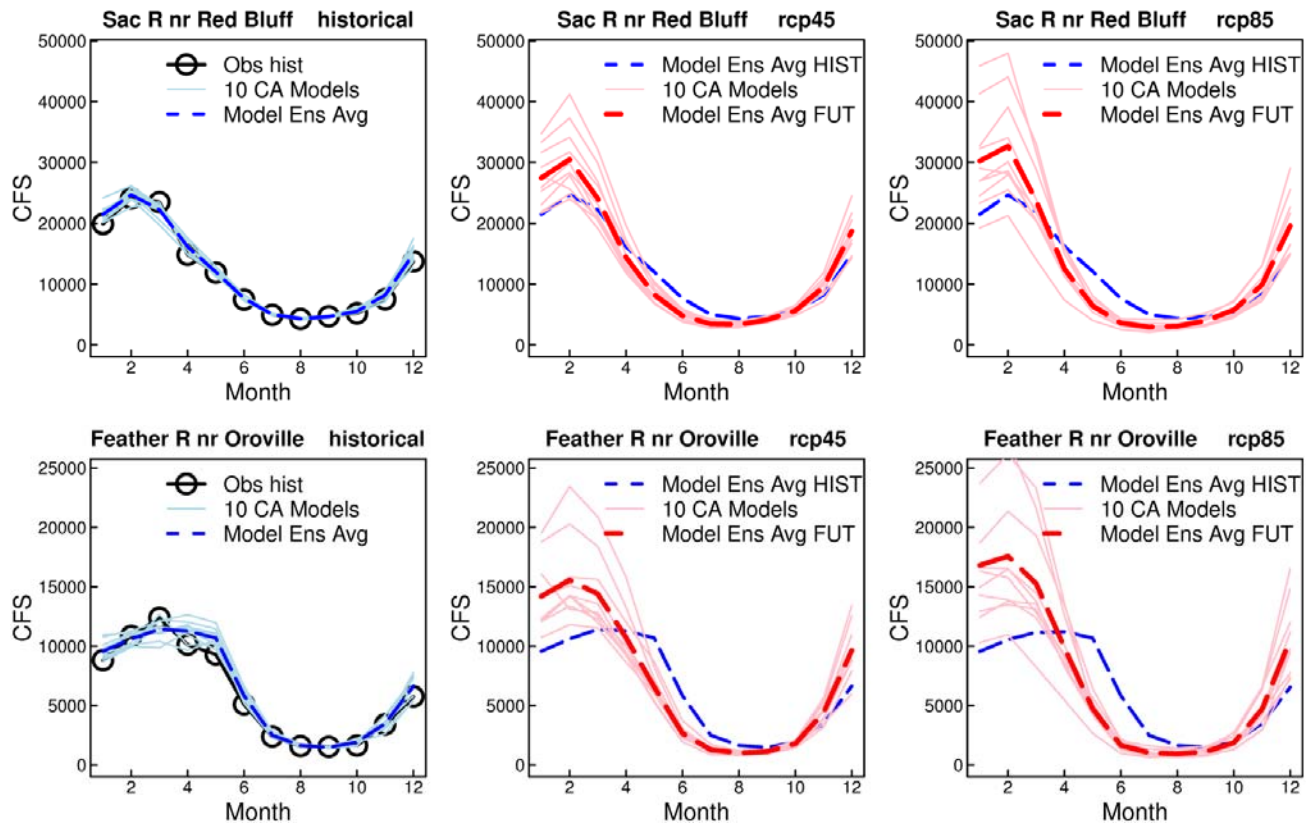


Figure 37. Each row shows a particular routed streamflow location; the upper row is for the Sacramento River near Red Bluff, and the lower row is for the Feather River near Oroville. The left column shows the observed hydrograph (black line) over the historical period (1976-2005), along with the bias-corrected model hydrographs for the 10 models that were downscaled and routed (blue lines). The center column shows the future (2070-2100) bias-corrected hydrograph for the models (red lines) using the RCP 4.5 emissions scenario, along with the observed historical hydrograph from the left column for comparison (blue dashed line). The right column shows the same as the center column, but for the RCP 8.5 emissions scenario. Data from the 10 California GCMs.

5: Drought Scenarios

California’s highly variable climate is susceptible to prolonged dry spells. A warming climate will compound drought impacts, as evidenced during recent precipitation deficits in the 2000’s Southwest drought (Colorado River basin), and during the 2012-2015 drought in California and neighboring states (e.g. Swain et al. 2014). Furthermore, recent research suggests that extended drought occurrence (“mega-drought”) could become more pervasive in future decades (e.g. Cook et al. 2015). As noted earlier, California climate projections produce greater extreme high precipitation and runoff, but they also produce more years with lower precipitation (Berg and Hall 2015) and runoff. To investigate implications of drought, an extended California drought scenario during the 21st Century was constructed. The objective was to produce an observationally-grounded, multi-year (20-year) drought scenario during the next several decades when temperatures are likely to have warmed significantly over historical climatology.

Using the observed precipitation record as provided by the California Climate Tracker Sierra Nevada and North Coast regions, the magnitude of a severe 20-year dry spell in Northern California that is consistent with prolonged historical dryness must reach deficit precipitation levels that are 80-90% of the historical median (Figure 38).

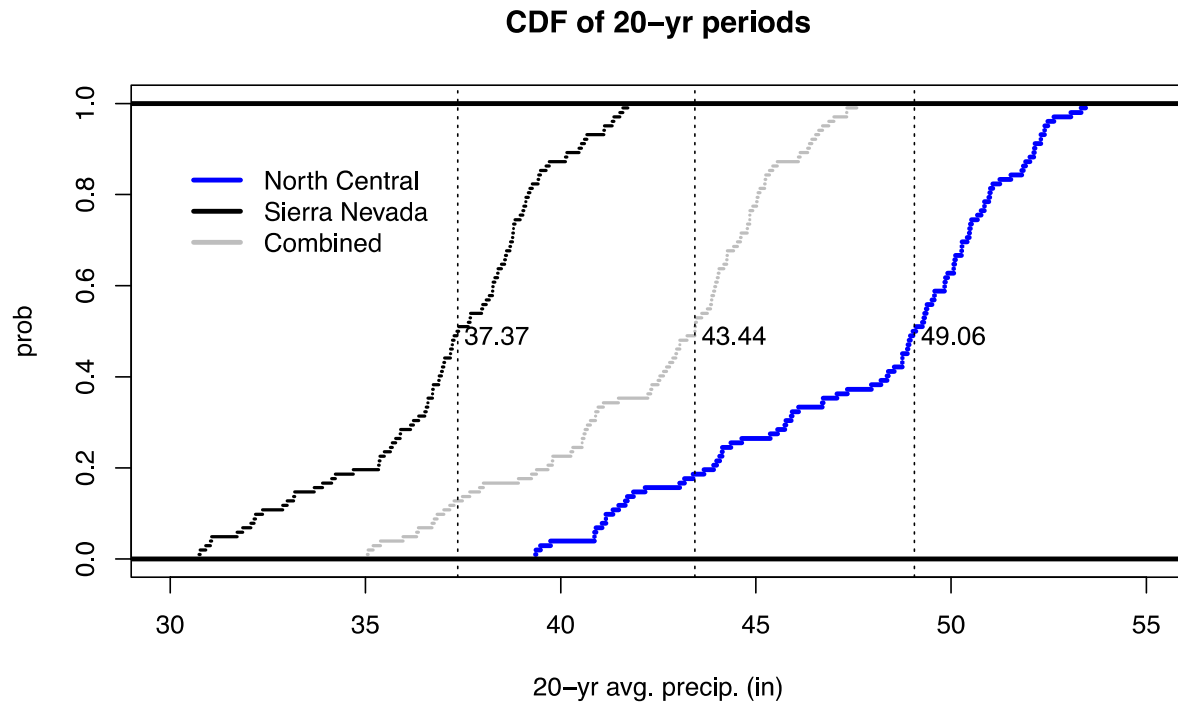


Figure 38. Cumulative distribution function (CDF) of observed (California Climate Tracker) 20-year annual avg precipitation for combined North Central and Sierra Regions (grey) has: median 20-year avg precipitation 43.4"; 5% lowest 20-year avg annual precip ~37" (85% of median); lowest 20-year avg annual precip is 35" (81% of median).

For planning, some state agency advisors sought a scenario that would portray an extended dry spell over the key water bearing regions of northern and central California. A 20-year dry spell was arrived at after discussion with these advisors and other experts. In addition, it was decided to employ a GCM based drought scenario to provide a self-consistent scenario with daily (downscaled) precipitation and temperature. To scope the magnitude of a 20-year drought scenario, the observed precipitation record was consulted via the California Climate Tracker (<https://wrcc.dri.edu/monitor/cal-mon/>). From California Climate Tracker North Central and Sierra Nevada records (1895-2015), the lowest 20-year average precipitation was 81% of historical median, while from the detrended version of these records the lowest 20-year average was 86% of historical median. To investigate the frequency and magnitude of 20-year dry spells in the models, we scrutinized the 10 California GCMs throughout the 21st Century projected climate period. A survey of individual CMIP5 GCMs run under RCP 4.5 and RCP 8.5 scenarios revealed that these simulations produced several (more than 10) 20-year extreme dry spells with magnitudes ranging from 78% - 90% of historical median. Since the GCMs produced extreme dry spells whose precipitation deficits are comparable to the greatest

20-year deficit exhibited in the instrumental record, it was decided to use a continuous segment of output from an individual GCM's dry spell to supply meteorological and hydrological information as a scenario of a future 20-year drought.

The selected extreme 20-year drought was derived from the LOCA downscaled HadGEM2-ES RCP8.5 2051-2070 dry spell, which experienced 78% of historical median annual precipitation averaged over the North Coast and Sierra California Climate Tracker regions, as shown in Figure 39. California Energy Commission and California Resources Agency advisors suggested that an early-21st Century drought was desired, so we additionally translated this dry spell from its later-mid-21st Century occurrence in the HadGEM2-ES RCP8.5 simulation to the early-21st Century period 2023-2042. The precipitation during our early 21st Century drought was daily LOCA downscaled precipitation (P) over California and Nevada in the sequence that it occurred from 2051-2070. However, the temperature (T) of the earlier 2023-2042 drought is an adjusted version of 2051-2070 LOCA daily maximum temperature (Tmax) and minimum temperature (Tmin) that takes into account climate warming over the century. Specifically, the adjustment is a subtraction of the linear change over the 2006-2100 that occurred from the 28 years that elapsed between the later (original) drought period and the earlier-(translated) drought period. The temperature adjustment was done separately for each month, and for Tmax and Tmin.

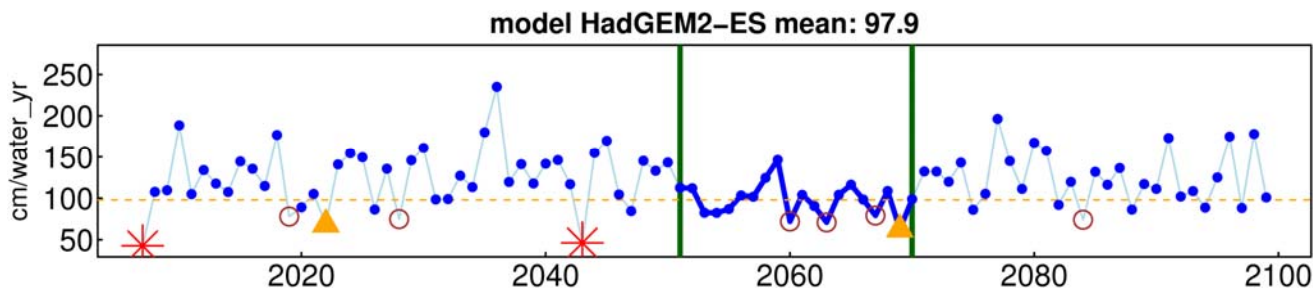


Figure 39. The 20-year drought scenario that was selected from the set of 10 California GCMs using annual precipitation in HadGEM2-ES RCP 8.5 simulation. The 2051-2070 20-year dry spell average is 78% of historical median precipitation, which is indicated by the dotted red line. Units are in scm/water year. Red asterisks, orange triangles and brown circles identify years whose precipitation falls within the 1st, 5th and 10th percentile range of bias corrected annual precipitation from all 10 of the California GCMs.

To allow further investigation of drought impacts that depend on surface hydrological conditions, VIC land surface model simulations were produced for the two dry spells. The VIC simulations were run using LOCA P, Tmax and Tmin over the period from 5 years before through 5 years after the 20-year dry spell. Selected variables, shown in

Figure 40, are averages over six selected 6 km grid cells from the North Central, Central Sierra Nevada near Lake Tahoe, and Southern Sierra Nevada. The cloud of colored lines is each of the RCP 8.5 simulations of the 10 California GCMs (including HadGEM-2 ES) run from 1950-2100, and the thick colored line is the median of the 10 simulations. Overlaid on each variable's plot is a thick red line, which is that variable obtained from the VIC run from the period enveloping the 20-year early 21st Century dry spell; this run began 5 years before and ended 5 years after the dry spell, so the red line actually covers 30 years from 2018-2047. The 20-year dry spell is identified by the grey shading. And, to mute the year to year variability, each of the simulations is smoothed with a 5-year running mean.

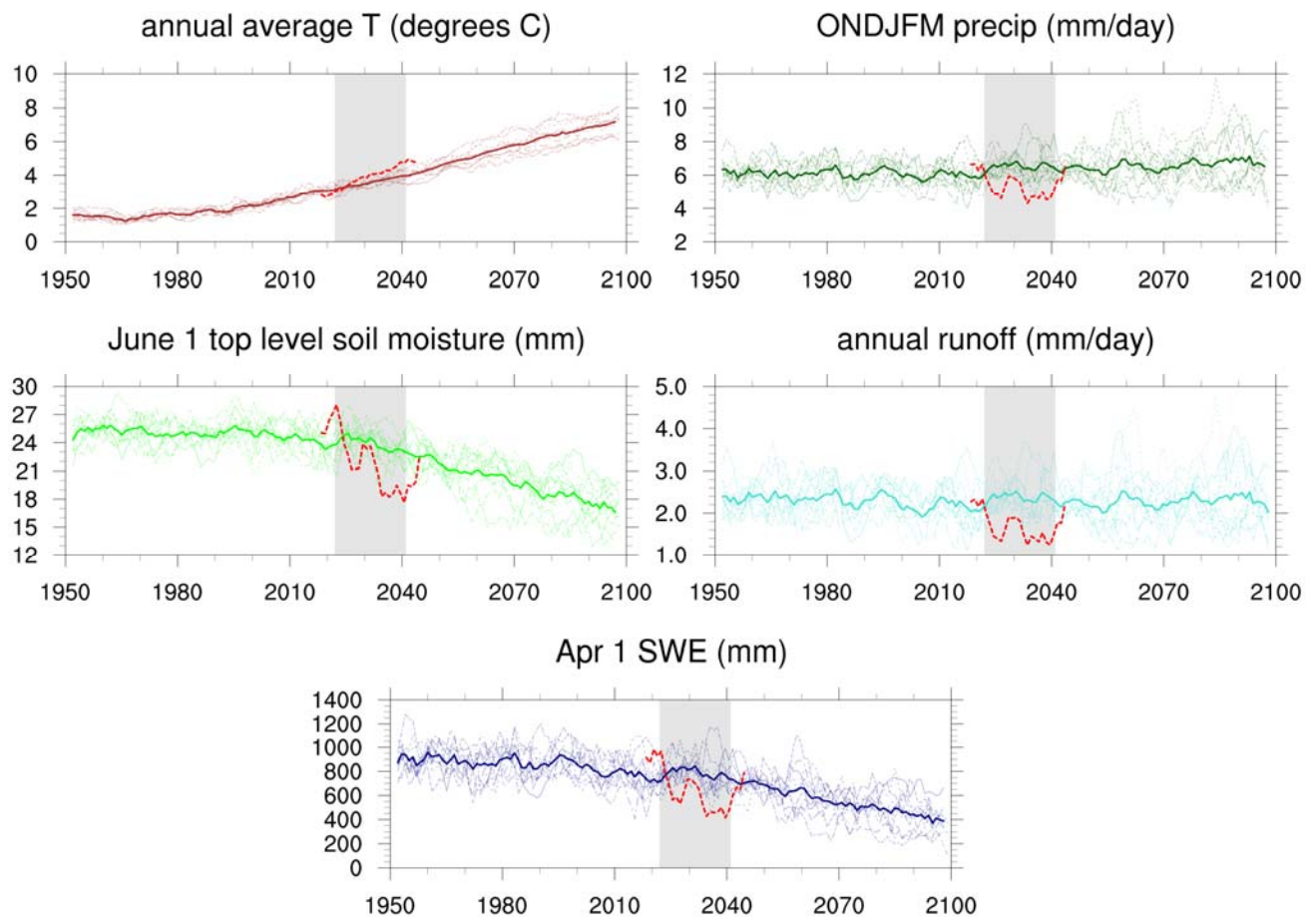


Figure 40. Hydrological Measures during the HadGEM2-ES Drought Scenario, which has been translated to 2024-2042 using a trend-adjusted temperature over northern and central California region. Individual simulations from LOCA and VIC output from each of the 10 California GCMs, including the HadGEM2-ES simulation are shown as light dashed lines whose average is shown by heavy solid line for annual temperature [°C], October-March precipitation [mm/day], VIC upper layer soil moisture [mm], VIC April 1 SWE [mm], and annual average runoff [mm/day], from top to bottom. From the HadGEM2-ES simulation, the drought is shown by the heavy red dashed line segments, delineating the period from 5 years prior to 5 years after the 20 year drought.

As required by the drought identification process, precipitation is generally low throughout the 20 year drought period, albeit with annual variations from very dry to somewhat greater than the historical median. Overall precipitation in the period is 78% of the historical median amount. Period-averaged runoff is 65% of the historical median, an amplified decline compared to the 78% precipitation reduction, but year-to-year runoff variability closely follows that of precipitation. June 1st top layer soil moisture and Apr 1st Snow Water Equivalent (SWE) also fluctuate but exhibit a significant decline from beginning to end of period. In part, this is likely the effect of increasing temperature, because SWE and early summer soil moisture trend downward as the climate warms. All variables recover to the 10 model envelope median within a few years after the 20 year dry spell ends. Comparing the effects of the early century and late century droughts, the hydrological model simulations show the growing effect of temperature on drought impacts as the climate warms. If such a drought were to occur later in the 21st

Century, the extremes in these measures and related hydrological impacts would become even more intense.

6: Sea Level Rise Projections

California has over 800 miles of coastline and coastal environments, infrastructure, and real estate is vulnerable to sea level rise (SLR). For several years, California has used the National Research Council (NRC) Report (2012) as a guiding document to plan for and protect against long-term SLR. However, since the NRC Report was published in 2012, a growing number of scientific studies have produced results describing present and future SLR that include more realistic dynamics of the components that contribute to SLR (enumerated below) and new methods to estimate regional SLR. In response to these rapidly evolving scientific findings, the State has instituted an update of this guidance to reflect recent advances in ice loss science and projections of sea level rise. As part of this process, the California Ocean Protection Council (OPC) and partners released *Rising Seas in California* (Griggs et al. 2017; hereafter *Rising Seas*), an update summarizing the latest science on SLR as it pertains to California. The report highlighted the value of using probabilistic SLR projections (Kopp et al., 2014) to estimate the likelihood of a given amount of sea level rise throughout the next century. The report also summarizes the contribution of polar ice sheets to SLR over the next century. The uncertainty of the contribution of ice sheets, in particular Antarctica, to SLR has increased in large part due to a recent study by DeConto and Pollard (2016; hereafter DP2016).

DP2016 incorporates new understanding of ice-loss processes in an ice sheet model to estimate contributions to global sea level from Antarctica. The DP2016 results introduce the possibility of global and regional SLR outcomes under higher greenhouse gas emissions scenarios that are greater than most previous upper bound estimates.

Regarding the magnitude of SLR on a yearly basis, the scenarios developed here employ recent methods and include updated SLR projections by developing probabilistic SLR projections for California that use the Kopp (2014) methodology, but are augmented to include results for Antarctica based on DP2016. The method here uses an ensemble of Antarctica ice sheet loss results from DP2016 for the contribution of Antarctica to sea level rise (Kopp et al., 2017). It is not asserted that these results are better than Kopp (2014) simulations without DP 2016, as was presented in the Griggs et al. 2017 *Rising Seas* report, but they do provide a lens into possible increased SLR over the second half of the 21st Century. We note that the methods employed to obtain probabilistic sea level rise projections discussed below are different than the LOCA downscaling that is discussed in the above sections.

6.1 Global SLR Components and Uncertainty

Global SLR projections include the contribution from five different components: the thermal expansion of the ocean, meltwater from glaciers, pumping of continental ground water and impounding of water that would otherwise flow into the oceans, and contributions from the large ice sheets on Antarctica and Greenland. Each component of global SLR has uncertainty that is based upon the amount the component can contribute to SLR as well as how well the response of the component to warming is understood. The contributions to SLR from extraction (or sequestration) of land surface water is the smallest of the components. Glacial melt will

continue to contribute but will probably decline to low levels as glaciers disappear during the 21st Century. The thermal expansion of the ocean has, over the 20th Century, been the largest contributor to SLR, and is projected to continue to be a primary contributor through the 21st Century. Greater than the uncertainty of SLR from thermal expansion is that from the Greenland and Antarctica ice sheets, the two most uncertain components of SLR (Figure 41).

The range of possible contributions from ice sheets is large because they have the potential to significantly contribute to SLR in large catastrophic episodes. Such events are difficult to model since they are uncommon and therefore infrequently observed, and involve ice loss dynamics that are complex and likely non-linear (Vaughan and Arthern, 2007).

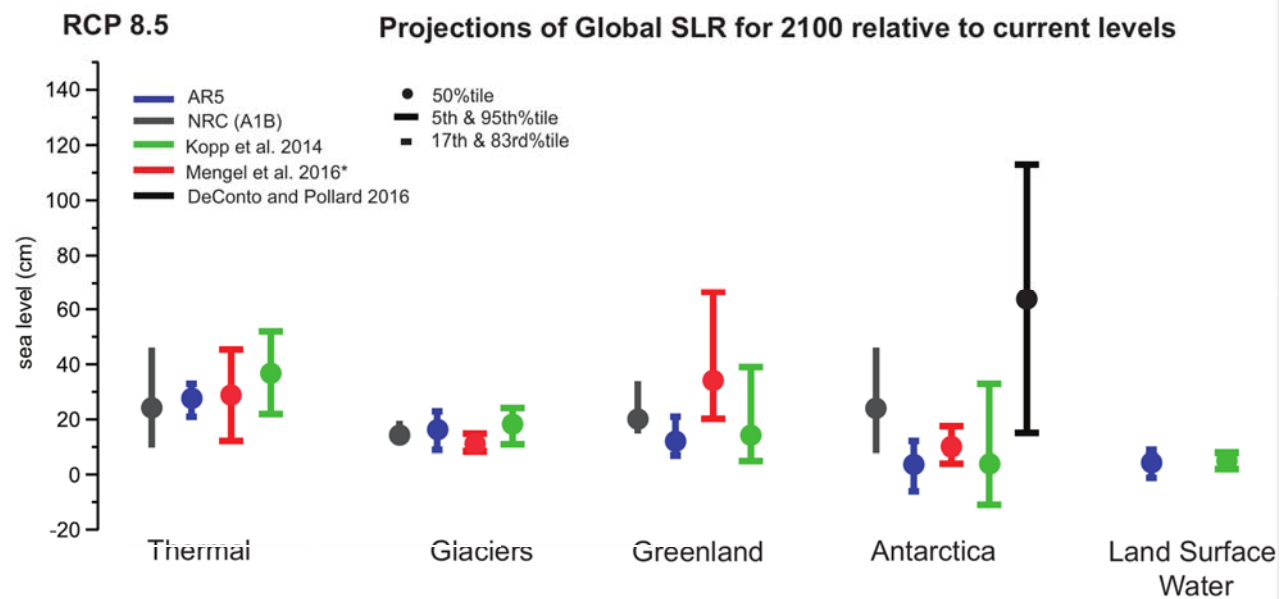


Figure 41. Projected contributions to Global SLR for 2100 (relative to current levels) from previous SLR assessments. The present study uses the results from Kopp 2014 (green lines) for all contributions except Antarctica. DP2016 (black line) is used in place of Kopp 2014 in this study. Range of AR5 estimates is the 17th and 83rd percentiles; ranges of other estimates is the 5th and 95th percentiles. For the NRC projections, the reported range is shown, though these values are not associated with percentiles.

The contribution to SLR from Antarctica is more uncertain (and potentially larger) than that from Greenland according to a survey amongst experts (Bamber and Aspinall, 2013). Antarctica is divided into West and East Antarctica by the Transantarctic Mountains. The uncertainty is largely due to West Antarctic Ice Sheet (WAIS) instability (Rignot et al. 2014) and lack of understanding regarding the dynamics and rate of potential ice sheet collapse. The East Antarctic Ice Sheet (EAIS) is not thought to be unstable and is likely the least susceptible to climate change on a centennial time scale. DP2016 included new dynamics in an estimate of Antarctica ice sheet mass loss that, under higher rates of global warming, would result in the WAIS contributing much more to SLR within the latter half of the 21st Century (and beyond) than had been previously estimated.

The new dynamics included in DP2016 account for atmospheric and oceanic warming that provokes fracturing within the ice sheet due to the refreezing of water and the collapse of ice

shelves. Higher amounts of warming therefore results in high rates of ice loss and attendant SLR under higher global warming scenarios during the latter half of the 21st Century. DP2016 validated their model by comparing their results to paleo sea levels reconstructed from proxy evidence in two separate periods when global sea underwent a sharp rise. These two periods are the last interglacial (~125,000 years ago), when temperatures are estimated to be 0-2 °C above current temperatures, and the Pliocene (~3 million years ago), when carbon dioxide concentrations are estimated to be similar to today. The median result from the DP2016 is approximately 70 cm greater contribution to SLR from Antarctica at the end of century under RCP 8.5 than found in Kopp et al. 2014, which used the results from AR5 for the likely range of Antarctic contributions to SLR (17th-83rd percentiles) and responses from Bamber and Aspinall (2013) for probabilities outside of this range. The DP2016 results await additional modeling and continued observationally based studies, but in discussion with a panel of experts organized to offer opinions on the SLR scenarios construct (described below), the consensus view was that these model results should be included. The point was made that the DP2016 results should be considered as a low probability scenario occurring in a high-emissions (RCP 8.5) case.

6.2 Regional Sea Level Rise

Regional SLR includes the global signal described above as well as regional effects from ocean dynamics, plate tectonics, and (in certain locations) changes due to decreases in the ice sheet mass' gravitation attraction. Changes in the ocean circulation can affect local sea level by causing water to accumulate or disperse along a coast due to winds. For example, multi-year changes in the Pacific trade winds and North Pacific atmosphere and ocean variations associated with the Pacific Decadal Oscillation (PDO) have been linked to anomalously higher and lower sea levels along the California coast (Bromirski et al. 2011; Merrifield 2011; Zhang and Church 2012; Hamlington et al., 2016). Local SLR also includes changes due to plate tectonics, including the sinking or uplifting of plates due to geological activity and glacial isotactic adjustment, and the rebounding of the Earth's crusts as a result of the removal of the weight of the ice sheets. The Earth's crust does not respond uniformly, with some areas sinking and other areas ascending. Currently the Earth is undergoing this process in response to the last ice age (~18,000 years ago) and will continue to be affected in this manner as ice sheets melt due to climate change. Along California's coast, projected regional SLR is relatively uniform from Arena Cove on south, whereas farther north, the SLR is projected to be ~25 cm less (figure 42). In addition to these large spatial processes, there are local processes that might cause a specific location to subside or uplift (Simms et al., 2016).

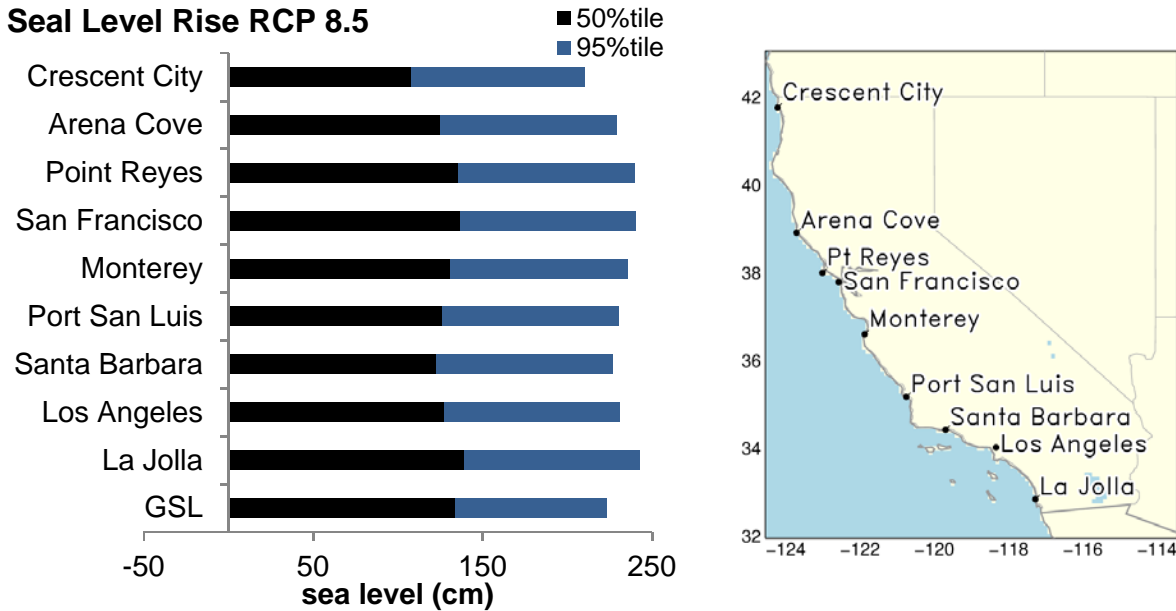


Figure 42. 50th and 95th percentile SLR projections under RCP8.5 scenario for nine California tide gauge sites by year 2100, along with that for global sea level (GSL). The sites are listed from north to south (top to bottom) and follow the map on the right. These are the same stations that hourly projections were modeled.

6.3 Expert Panel to Guide SLR Scenarios used in the Fourth Assessment

Prior to preparing the SLR scenarios for the Fourth Assessment, the authors, in response to advice by program managers at the California Energy Commission and other state officials involved in the Fourth Assessment, solicited input from a panel of 7 experts who provided feedback via a teleconference. The panel supplied guidance on the methods proposed to develop the SLR scenarios and the latest science, supported using a probabilistic approach to develop SLR projections, and indicated that the new findings of DP2016 were significant. The panel agreed that although the DP2016 was the first study to include the relevant new dynamics and the approach represented therein is still emerging science, the results were important enough to include in the probabilistic projections (Cayan et al., 2016).

6.4 Probabilistic Sea Level Rise Scenarios

Using the input from the expert panel, probabilistic SLR projections were developed courtesy of Robert Kopp, and based on the methodology of Kopp et al. 2014 with the modification of using the recent DP2016 results for the Antarctic Ice Sheet contribution. The science-decision making interface, and the relevance of the potential Antarctic contributions and their insertion into a quasi-probabilistic framework to policy and decision making, is described by Behar et al. (2017). The Kopp et al. (2014) method creates a time- dependent probability distribution of the different components of SLR and uses a Latin hyper-cube method to sample the different components to calculate resultant total SLR probabilities. This process assumes that the components are independent of each other because the response of the different components might not be correlated. For example, a 2°C temperature increase might affect ocean circulation in a way that

contributes a local negative SLR tendency even while ice sheet melting increases under the warming conditions, giving a positive SLR tendency.

The estimated probability density functions of each of the five primary global SLR components are developed based on the current research on how the individual components have responded historically to climate variability and projected to respond to future climate change. The land surface water contribution to SLR is based upon population estimates (Rahmstorf et al., 2012). The projected contribution from glacier and ice caps is based upon regional modeling of the response of glaciers and ice caps to changes in temperature and precipitation (Marzeion et al., 2012). The oceanographic processes, including both thermal expansion and dynamical changes, are based on global climate models. Contribution from Greenland ice sheets are based upon the most recent Intergovernmental Panel on Climate Change Assessment report (“AR5”), for the median and likely (17-83 percentiles) range. Outside this range, estimates are based upon expert elicitation (Bamber and Aspinall, 2013). The Antarctic contribution is based on the DP2016 model developed using estimated Pliocene sea levels above present day between 5-15 meters and without any adjustment to ocean temperature. Local sea level changes from tectonics and glacial isostatic adjustment were extrapolated (by Kopp) from tide gauge data.

The different greenhouse gas emission scenarios do not start to show a significant difference in SLR until around 2060 (Figure 43).

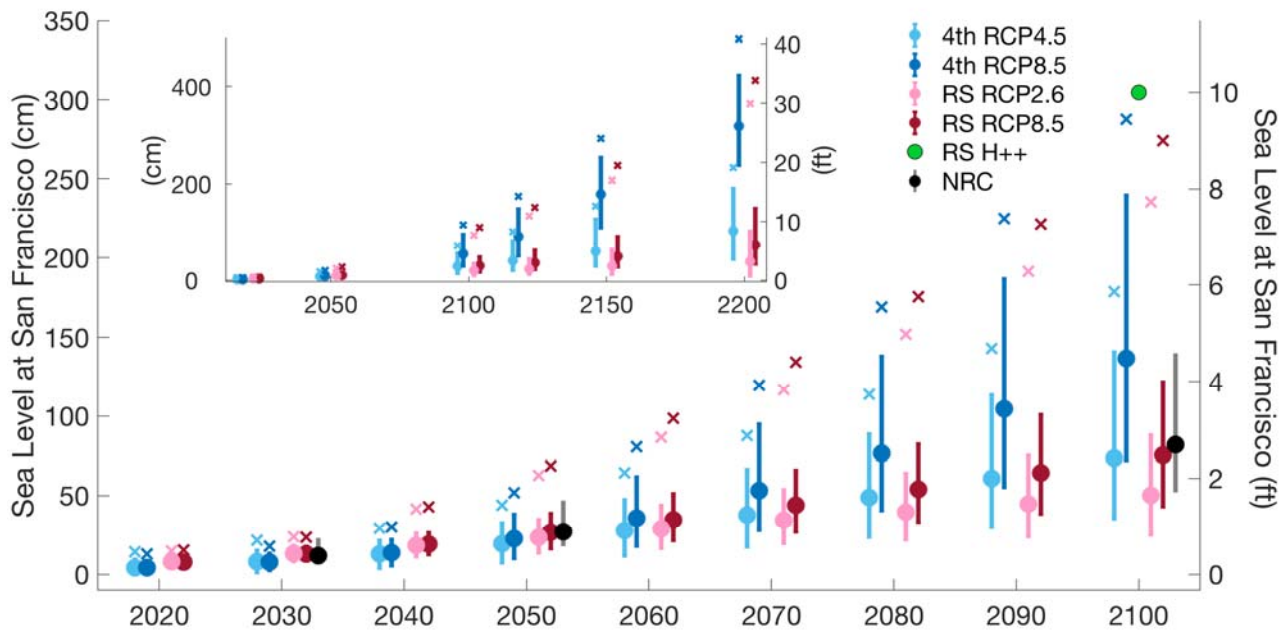


Figure 43. SLR projections, which include the DP2016 results, from R. Kopp after Kopp (2014) for each decade for RCP 4.5 (light blue) and RCP 8.5 (dark blue) for San Francisco over the 21st Century. The red and pink lines and symbols represent the results from *Rising Seas* using RCP 2.6 (pink) and RCP 8.5 (red) as well as H++ (large green dot). NRC is represented by the black dots and grey lines. Each decade’s estimate is shown as a range from 5th to 95th with circles representing the 50thtile and crosses representing the 99.9th percentile. Inset shows projections carried out to year 2200.

The range between the 5th and 95th percentiles increases with time, primarily due to the large uncertainty in the ice sheet response to climate change. The 99.9th percentile, shown at the top of the envelope in **Error! Reference source not found.**, is considered the maximum that is physically possible. Note that the 99.9th percentile is different from the H++ projection, which is from the *Rising Seas* report and is a single projection of 3.05 m (10 ft) of SLR by 2100 (Griggs et al., 2017). Projected increases in SLR are not constant in time, and by 2200, the median SLR for RCP 8.5 is more than five times its amount in 2100 (**Error! Reference source not found.**, inset graph). The probabilistic SLR median projections from all RCP greenhouse gas scenarios made here are lower than the *Rising Seas* and NRC committee values at 2030 and 2050 by about 5 cm, but the RCP 8.5 median value at 2100 is 137 cm, 47 cm higher than the NRC committee value and 61 cm higher than the *Rising Seas* RCP 8.5 value (Table 5).

SLR scenarios provided by the NRC, OPC *Rising Seas* guidance, and the present Fourth Assessment effort each developed sea level rise from a “bottom-up” approach that estimates SLR from its major contributing components. The Fourth Assessment scheme places a heavier reliance upon recent Antarctic ice loss modeled by DP2016 than did the *Rising Seas* projections used to revise the State Sea Level Guidance. Thus the mid-range estimates presented here are somewhat greater than those in *Rising Seas* by the end of the century. Major methodological elements of these different projection schemes are shown in Table 6.

Table 5. SLR projections for CA (NRC) and for San Francisco (*Rising Seas* and Fourth Assessment) for the different RCPs. Similar to figure 43, the NRC is the committee value and the range while *Rising Seas* (RS) and Fourth Assessment are the 5th, 50th (in bold) and 95th percentiles. All values are in cm above 2000 level. Projections are similar for other locations throughout CA south of Cape Mendocino.

	2030 (5 th - 50 th -95 th) (cm)	2050 (5 th - 50 th -95 th) (cm)	2100 (5 th - 50 th -95 th) (cm)
NRC	7- 12 -23	18- 27 -52	52- 82 -140
RS (RCP 2.6)	8- 12 -18	13- 24 -35	25- 50 -88
RS (RCP 8.5)	8- 13 -18	16- 27 -39	43- 75 -122
Fourth Assessment (RCP 4.5)	1- 8 -15	7- 20 -33	35- 74 -141
Fourth Assessment (RCP 8.5)	2- 8 -14	10- 23 -38	72- 137 -240

Table 6. The differences in methodologies used to generate SLR projection for California in recent reports.

Report	Greenhouse Gas Scenario	Method
NRC, 2012	B1 A1F1	Model projections, observations, Expert Recommendations
Rising Seas, 2017	RCP 2.6 RCP 8.5	Kopp et al., 2014; quasi-probabilistic projections
Fourth Assessment, 2018	RCP 4.5 RCP 8.5	Kopp et al., 2014 with ensemble results from DP2016 substituted for Antarctica

6.5 Hourly Sea Level Projections at California Coast Tide Gauge Locations

The long term SLR projections developed above establish the base sea level, upon which operates a spectrum of shorter-term sea level fluctuations. These shorter-term fluctuations, ranging from hourly to decadal, are caused by astronomical tides, weather and wind patterns, and El Niño Southern Oscillation events. The open coast tidal range in California is up to approximately 3 m from high to low tide. The tidal time scales that are important for California are semi-diurnal, diurnal, semi-monthly, semi-annually and 4.4 years, and are well known (and predictable) many decades in advance. Anomalies of sea level above or below the predicted tides result from barometric pressure, wind, and wind wave effects, e.g. during winter storms. These non-tidal anomalies (Bromirski et al. 2017) along the California coast rarely exceed 0.7 m in amplitude when excluding the effects of waves, but can reach over 1.5 m when including wave induced surge (Cayan et al., 2008). As mentioned previously, El Niño events have the largest seasonal to interannual impacts on sea level heights with amplitudes of 10-20 cm.

Following the methods in Cayan et al. (2008), hourly sea level projections using a base line of the probabilistic SLR projections were developed for the Fourth Assessment. Hourly projections were made for locations with a reliably continuous coastal tide gauge record that begins before 1984 (Figure 42). The sea level projections were derived from short period climate and weather data extracted from a subset of global climate models and various RCP-based SLR scenarios (described above). The modeled sea level includes contributions from astronomical tides, weather influences from wind and barometric pressure, shorter period climate fluctuations (e.g. El Niño and other climate patterns), and long period (decade to century timescale) change over the region from global SLR.

Eight of the 10 California GCMs were used to provide the hourly sea level estimates, the same eight as used for the wind downscaling (section 3.2.3). First, the daily climate and meteorological variables (wind, sea level pressure, ocean temperatures) needed to predict local sea level at each of the selected California tide gauge stations were extracted from the eight models and bias corrected using methods developed for the LOCA downscaling procedure (Pierce et al., 2015).

The bias corrected daily values were then converted to hourly data using an archive of historical observations to relate daily averages to hourly fluctuations. The El Niño/Southern Oscillation component was estimated using a regression equation that related the monthly Niño 3.4 sea surface temperatures to the smoothed sea levels at California’s tide stations. Lastly, these components were combined to synthesize the hourly sea levels based on the probabilistic SLR projections.

Envelopes of projected daily maximum sea level at La Jolla constructed from the eight GCM simulations and using the RCP 4.5 and RCP 8.5 scenarios, illustrated over the range of 50th to 95th percentile levels of regional SLR projections, are shown in

Figure . Values are expressed as departures from the year 2000 mean sea level value at La Jolla. The Figure also shows the annual maximum of the daily maxima from the highest (99.9th percentile) of the RCP 4.5 and RCP 8.5 simulations. Through 2050 the most extreme maximum sea level event is approximately 40 cm (1.3 ft) above the historical maximum of 1.55 m (5.1 ft). However, by the end of the century there is a larger spread of projections, with the high projections under RCP 8.5 and the 95 percentile showing a maximum event at approximately 370 cm (12 ft). As a companion to Figure 44, the hours of exceedance over La Jolla’s historical maximum of 1.55 m (5.1 ft) above mean sea level is shown in Figure 45.

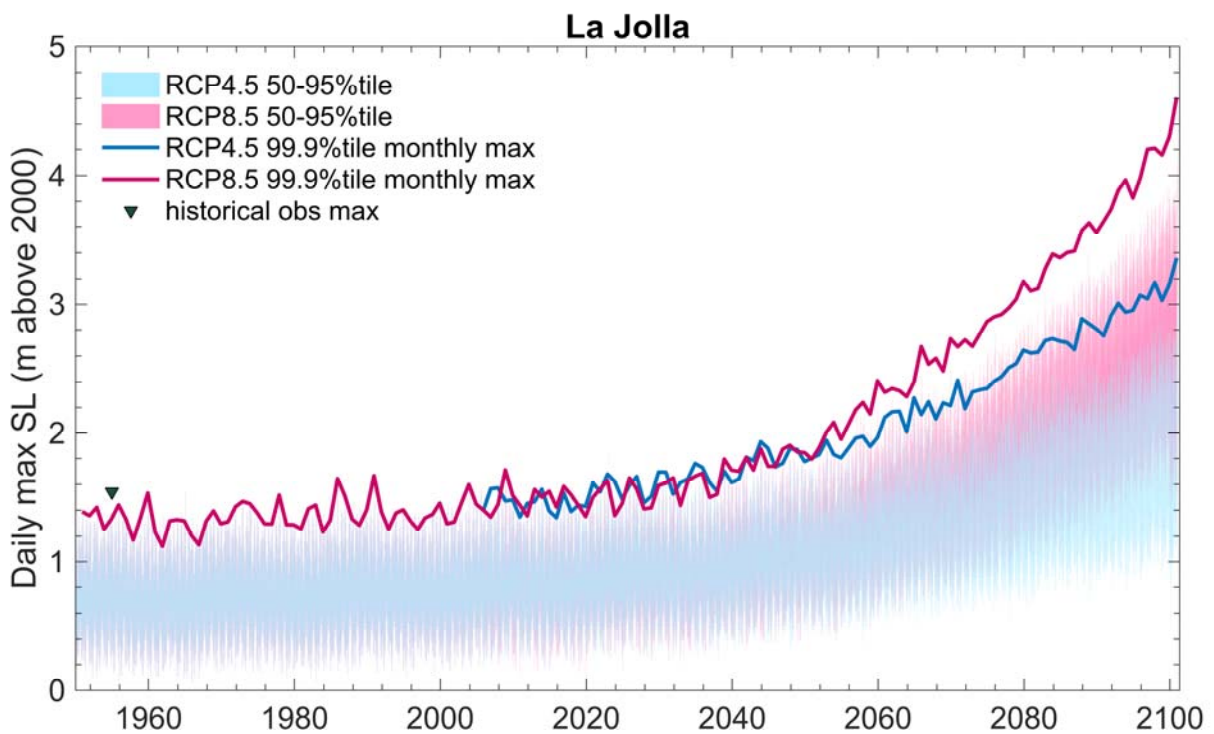


Figure 44. Projected daily maximum sea level at La Jolla constructed from the eight-model hourly simulations using the RCP 4.5 and RCP 8.5 scenarios. Envelope of 50th-95th percentile RCP4.5 and RCP 8.5 projections shown as light blue and light red shades. Maximum annual value from 99.9 percentile RCP 4.5 and RCP 8.5 projections shown as solid blue and solid red lines. Maximum observed historical sea level at La Jolla shown as blue inverted triangle.

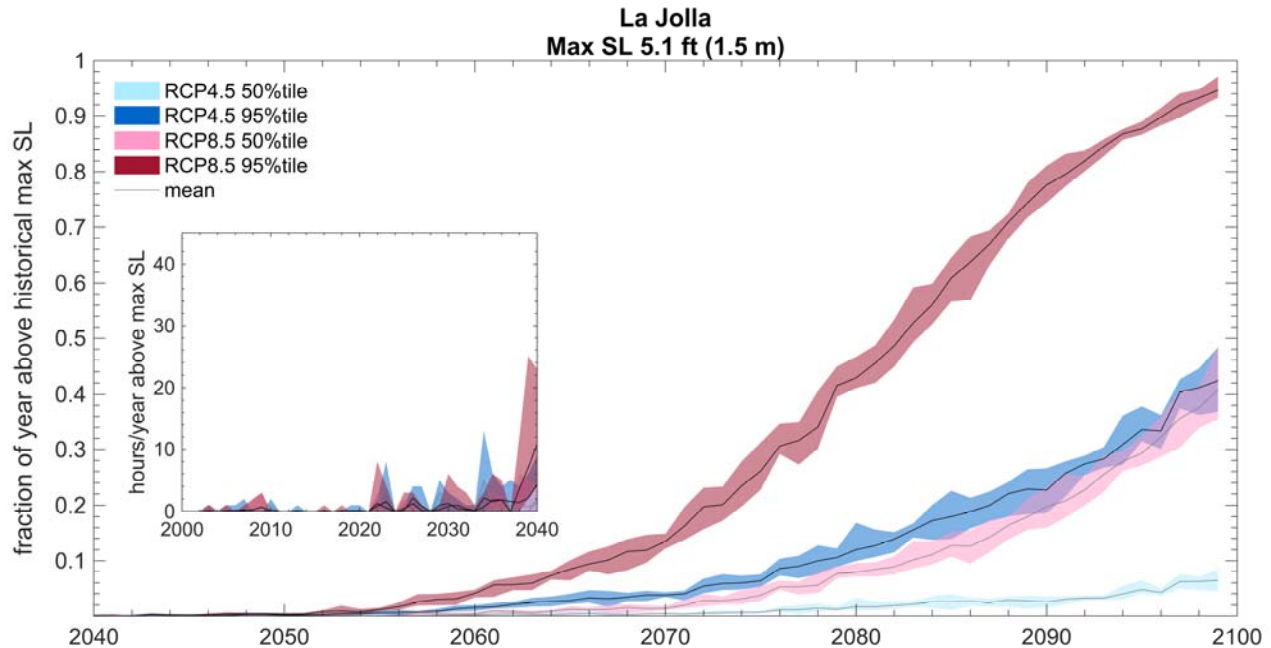


Figure 45. Projected fraction of year that sea level in La Jolla, California is over historical maximum under 50th percentile and 95th percentile SLR scenarios under RCP 4.5 (light and dark blue) and RCP 8.5 (light and dark red). Envelope shows high to low set of results from each of eight California GCMs for which hourly sea level projections were developed.

7: Conclusions and Future Directions

The purpose of this work has been to describe the procedures and methods used to construct climate data scenarios for parameters of interest to California’s energy system. These scenarios were used in California’s Fourth Climate Change Assessment to provide a consistent basis for the various analyses and facilitate cross-sectoral integration. Daily fields of precipitation, and minimum and maximum temperature were obtained from 32 global climate models (GCMs) from the most recent available archive of GCMs (CMIP5). These fields were statistically downscaled using the Localized Constructed Analogues (LOCA) method, which is designed to capture daily extreme values better than previous methods. The final downscaled fields have bearing on energy supply (hydropower, wind, and photovoltaic), demand (cooling loads), and delivery (the effect of temperatures on transmission lines), as well as wildfire, human health, ecosystems, the water supply, and agriculture.

The downscaling generated data on a 16th degree (6 km) grid covering California, spanning a historical period (1950-2005) and a future period (2006-2100) using two different projected greenhouse gas concentration pathways, RCP 4.5 (medium forcing) and RCP 8.5 (high forcing). Subsets of 10 or 4 GCMs that perform particularly well over the state were culled from the full set of 32 GCMs for Fourth Assessment teams to employ in their investigations of impacts and adaptation considerations. For the set of 10, LOCA downscaling was also applied to wind speed, specific and relative humidity, and downward solar radiation, variables that have received less attention by previous statistical downscaling efforts.

Using the downscaled fields as input, hydrological simulations were run using the Variable Infiltration Capacity (VIC) land surface model on the same 16th degree (6 km) grid. VIC estimates historical and projected future daily hydrologically relevant variables, including snow cover, soil moisture, runoff, water loss from plants, surface moisture and heat fluxes. Streamflow records were determined for selected rivers by routing the VIC runoff into the basins' channel system, then bias correcting the resultant flows using observationally based estimates of naturalized flow.

Some key findings of projected climate change, expanded further in the statewide and regional reports, include:

- Projected warming of 2-4 °C (RCP 4.5) to 4-7 °C (RCP 8.5) by the end of the century, with a strong increase in extremely hot days relative to historical norms (e.g., days with maximum temperatures above 35 °C occur with approximately twice the historical frequency over much of the state).
- Fewer wet days, increased precipitation on the wettest days, wetter winters (up to 20%), drier spring and autumn (up to 20%), and greater year-to-year precipitation variability.
- Slight decreases in wind speed over much of the state (2-8% on an annual average basis).
- Increasing relative humidity along the coast (up to 10% in summer), but decreasing in the interior (up to 10% in spring).
- Small changes in surface solar radiation, primarily composed of a 2-4% increase in the southern part of the state in spring.
- Increasing moisture deficit, with substantial (>40%) increases in the southern Sierra Nevada and northwestern coastal regions.

Broadly, the two sets of projections, following a moderate (RCP 4.5) and a high (RCP 8.5) greenhouse gas concentration trajectory, provide the user with a set of scenarios that contain lower and higher degrees of climate change along with resultant climate-related impacts, e.g., changes in hydrology and wind. (Both RCP 4.5 and RCP 8.5 produce significant changes, but those in RCP 4.5 are not as great or as fast.) For a user to decide which scenarios to include in taking adaptation measures, it is important to consider the risk imposed by extreme impacts, along with the feasibility of adaptation and project time horizons. For example, a community might accept more risk in having a bike path being flooded than in having a hospital flooded—the latter case might require attention to more extreme scenarios even though they may have low odds of occurring.

The downscaled data provide a set of meteorological variables that is physically consistent on the daily timescale across multiple variables, and has daily to multi-decadal variability within the range exhibited by historical observations. The GCMs produced amplitudes of multi-year precipitation deficits that were consistent with the observed record, so we were able to construct a northern and central California mid-21st Century 20-year dry spell from selected downscaled GCM simulations. This extended drought has a precipitation deficit comparable to the greatest precipitation deficit found historically, but with temperatures 1°C to 3°C above historical levels, depending on whether that drought occurs earlier or later in the 21st Century. Hydrological variables calculated using VIC allow us to consider the substantially diminished snowpack,

runoff, and soil moisture during the multi-year dry spell as well as the periods leading into and after the drought.

Sea level rise (SLR) projections for California to support the Fourth Assessment were generated under different greenhouse gas emission scenarios with Kopp et al.'s (2014) approach, which uses different forms of future projections to derive estimates for each of the major components that contribute to sea level rise, under a particular assumption of global climate change. The Kopp methodology (Kopp et al. 2014) produces continuous decadal projections of sea level at selected coastal locations. Using GCM-derived weather and short period climate measures, we produced hourly sea level projections that include tides, regional and local weather influences, and short period Pacific climate fluctuations in addition to the aforementioned global sea level rise scenarios. Notably, the sea level rise scenarios employed here include potential extremes as well as “middle-of-the-road” possibilities. The sea level rise projections place a heavier reliance upon recent Antarctic ice loss modeled by De Conto and Pollard (2016) than did the “Rising Seas” report (Griggs et al. 2017) produced in the recent effort by the California Ocean Protection Council (OPC) and collaborators to revise the State’s Sea Level Rise Guidance. Thus under RCP 8.5 the mid-range, 50th percentile estimate in this work is 52 cm (20 inches) greater than in Rising Seas by the end of the century (see Figure 43).

Looking forward, several awaited developments will be useful in follow-up assessments of the vulnerability of California’s energy sector to climate change, including the following:

- There is need for better understanding of the nature and causes of particular regional changes produced by GCMs and their downscaled counterparts—e.g., why some models produce, on average, wetter and some produce drier conditions in California, with the associated impacts on hydropower, water supply, agriculture, groundwater withdrawals, and pumping loads.
- Additional evaluation is needed to understand changes and causes of changes in humidity, wind, and solar radiation, and how they relate to larger scale changes in atmospheric circulation, ocean temperatures, and other variables.
- Comparison and evaluation of downscaling using dynamical methods vs. statistical methods is needed, along with evaluation of the degree to which certain historical relationships employed by statistical downscaling methods will remain valid in future decades. For example, the LOCA downscaling method used here assumes that historically observed relationships between large (synoptic to 100’s of km scale) and small (6 km scale) climate fields such as temperature, precipitation, and humidity will have the same statistics in the future as in the historically observed period.
- Hydrological simulations produced by different hydrological models are needed to augment the small number of hydrological models typically used in studies such as this. Only VIC is used here, and key aspects of future land-surface projections are likely sensitive to the land model selected. These key aspects include projected changes in potential and actual evapotranspiration, soil moisture, and the partition of precipitation between local runoff and evapotranspiration.
- Exploration of new GCMs and new climate simulations is needed. For example, new simulations from the Climate Model Inter-comparison Project Phase 6 (CMIP6)

should be investigated. Output from these new model simulations will require bias correction, evaluation, and comparison with prior generations of GCM simulations (e.g. CMIP5, CMIP3) with a focus on the California region.

8: References

- Abatzoglou, J. T. (2013), Development of gridded surface meteorological data for ecological applications and modelling. *Int. J. Climatol.*, 33: 121–131. doi:10.1002/joc.3413
- Bamber, J.L. and Aspinall, W.P. (2013) An expert judgement assessment of future sea level rise from the ice sheets. *Nat Clim Change* 3, 424-427.
- Behar, D., DeConto, R., Kopp, R., and others, 2017: Planning for Sea Level Rise: An AGU Talk in the Form of a Co-Production Experiment Exploring Recent Science AGU Invited Talk, Session ID 27225 December 2017.
- Berg, N. and A. Hall, 2015, Increased interannual precipitation extremes over California under climate change. *Journal of Climate* 28: 6324–6334.
- Bromirski PD, Miller AJ, Flick RE, Auad G (2011) Dynamical suppression of sea level rise along the Pacific coast of North America: indications for imminent acceleration. *J Geophys Res* 116:C07005. doi:10.1029/2010JC006759
- Bromirski, PD, Flick RE, Miller AJ. 2017. Storm surge along the Pacific coast of North America. *Journal of Geophysical Research-Oceans*. 122:441-457
- California Department of Water Resources, Climate Change Technical Advisory Group (2015): Perspectives and Guidance for Climate Change Analysis (2015), in: Lynn, E., Andrew Schwarz, Anderson, J., Correa, M. (Eds.), 140pp.
- Cayan, D. R., J. Kalansky, S. Iacobellis, D. Pierce, 2016, Creating Probabilistic Sea Level Rise Projections, Climate Adaptation and Resiliency, California Energy Commission, 16-IEPR-04, http://docketpublic.energy.ca.gov/PublicDocuments/16-IEPR-04/TN211806_20160614T101823_Creating_Probabilistic_Sea_Level_Rise_Projections.pdf
- Cayan, D.R., Bromirski, P.D., Hayhoe, K., Tyree, M., Dettinger, M.D. and Flick, R.E. (2008) Climate change projections of sea level extremes along the California coast. *Climatic Change* 87, S57-S73
- Cook, B.I., T.R. Ault, and J.E. Smerdon, 2015: Unprecedented 21st-century drought risk in the American Southwest and Central Plains. *Sci. Adv.*, 1, no. 1, e1400082, doi:10.1126/sciadv.1400082.
- Das, T., Hidalgo, H., Cayan, D., Dettinger, M., Pierce, D., Bonfils, C., Barnett, T.P., Bala, G., and Mirin, A., 2009, Structure and origins of trends in hydrological measures over the western United States: *Journal of Hydrometeorology*, 10, 871-892, doi:10.1175/2009JHM1095.1.
- DeConto, R.M. and Pollard, D. (2016) Contribution of Antarctica to past and future sea-level rise. *Nature* 531, 591-597.
- Gleckler, P. J., Taylor, K. E., and Doutriaux, C. 2008: Performance metrics for climate models, *J. Geophys. Res.-Atmos.*, 113, D06104, 20pp.
- Griggs, G, Árvai, J, Cayan, D, DeConto, R, Fox, J, Fricker, HA, Kopp, RE, Tebaldi, C, Whiteman, EA (California. Ocean Protection Council Science. Advisory Team Working Group).

- (2017) Rising Seas in California: An Update on Sea-Level Rise Science. California. Ocean Science Trust, April 2017.
- Guzman-Morales, J., A. Gershunov, J. Theiss, H. Li, and D. R. Cayan, 2016: Santa Ana Winds of Southern California: Their climatology, extremes, and behavior spanning six and a half decades. *Geophys. Res. Lett.*, doi:10.1002/2016GL067887.
- Hamlington, B. D., S. H. Cheon, P. R. Thompson, M. A. Merrifield, R. S. Nerem, R. R. Leben, and K.-Y. Kim (2016), An ongoing shift in Pacific Ocean sea level, *J. Geophys. Res. Oceans*, 121, 5084–5097, doi:10.1002/2016JC011815.
- Hawkins E. and R. T. Sutton, 2011: The potential to narrow uncertainty in projections of regional precipitation change, *Climate Dynamics*, 37, 407, doi: [10.1007/s00382-010-0810-6](https://doi.org/10.1007/s00382-010-0810-6)
- Iacobellis, SF, and D. R. Cayan, 2013. The variability of California summertime marine stratus: Impacts on surface air temperatures. *Journal of Geophysical Research-Atmospheres*. 118:9105-9122.
- IPCC, 2013: Climate Change 2013: The physical science basis. Working group I contribution to the IPCC fifth assessment report, T. Stocker, Q. Dahe, and G-K Plattner, coordinating lead authors. Available from <http://www.ipcc.ch/report/ar5/wg1/>.
- Kanamitsu, M., and H. Kanamaru, 2007: Fifty-seven-year California reanalysis downscaling at 10 km (CaRD10), part I: System detail and validation with observations. *J. Climate*, 20, p. 5553- 5571.
- Knutti, R., D. Masson, and A. Gettelman (2013), Climate model genealogy: Generation CMIP5 and how we got there, *Geophys. Res. Lett.*, 40, 1194–1199, doi:10.1002/grl.50256.
- Kopp, R. E., R. M. Horton, C. M. Little, J. X. Mitrovica, M. Oppenheimer, D. J. Rasmussen, B. H. Strauss, and C. Tebaldi, 2014: Probabilistic 21st and 22nd century sea-level projections at a global network of tide-gauge sites. *Earth's Future*, 2, p. 383-406
- Kopp, R. E., DeConto, R. M., Bader, D. A., Hay, C. C., Horton, R. M., Kulp, S., Oppenheimer, M., Pollard, D. and Strauss, B. H. (2017), Evolving Understanding of Antarctic Ice Sheet Physics and Ambiguity in Probabilistic Sea-Level Projections. *Earth's Future*, 5: 1217-1233. doi:10.1002/2017EF000663
- Lavers, D. A., F. M. Ralph, D. E. Waliser, A. Gershunov, and M. D. Dettinger (2015), Climate change intensification of horizontal water vapor transport in CMIP5, *Geophys. Res. Lett.*, 42, doi:10.1002/2015GL064672.
- Liang, X., D. P. Lettenmaier, E. F. Wood, and S. J. Burges (1994), A simple hydrologically based model of land surface water and energy fluxes for general circulation models, *J. Geophys. Res.*, 99, 14,415–14,428, doi:10.1029/94JD00483.
- Livneh, B., T. J. Bohn, D. W. Pierce, F. Munoz-Arriola, B. Nijssen, R. Vose, D. R. Cayan, and L. Brekke, 2015: A spatially comprehensive, hydrometeorological data set for Mexico, the U.S., and Southern Canada 1950-2013. *Scientific Data*, v. 2, article 150042 (2015). doi:10.1038/sdata.2015.42.

- Lohmann, D., R. Nolte-Holube, and E. Raschke, 1996: A large-scale horizontal routing model to be coupled to land surface parametrization schemes, *Tellus*, 48(A), 708-721
- Maurer, E. P., and D. W. Pierce, 2013: Bias correction can modify climate model-simulated precipitation changes without adverse effect on the ensemble mean. *Hydrol. Earth Syst. Sci. Discuss.*, 10, 11585-11611, doi:10.5194/hessd-10-11585-2013.
- Merrifield, M. A. (2011), A shift in western tropical Pacific sea-level trends during the 1990s, *J. Clim.*, 24, 4126–4138, doi:10.1175/2011JCLI3932.1.
- Mote, P. W., D. E. Rupp, S. Li, D. J. Sharp, F. Otto, P. F. Uhe, M. Xiao, D. P. Lettenmaier, H. Cullen, and M. R. Allen (2016), Perspectives on the causes of exceptionally low 2015 snowpack in the western United States, *Geophys. Res. Lett.*, 43, 10,980–10,988, doi:10.1002/2016GL069965.
- National Research Council (2012): *Sea-Level Rise for the Coasts of California, Oregon, and Washington: Past, Present, and Future*. The National Academies Press, Washington, DC.
- Pierce, D. W., T. P. Barnett, B. D. Santer, and P. J. Gleckler, 2009: Selecting global climate models for regional climate change studies. *Proceedings of the National Academy of Sciences*, doi:10.1073/pnas.0900094106.
- Pierce, D. W., Ed., 2012: *California Climate Extremes Workshop Report*. Scripps Institution of Oceanography, La Jolla, CA. 32 pp.
- Pierce, D. W., D. R. Cayan, T. Das, E. P. Maurer, N. L. Miller, Y. Bao, M. Kanamitsu, K. Yoshimura, M. A. Snyder, L. C. Sloan, G. Franco, and M. Tyree, 2013: The key role of heavy precipitation events in climate model disagreements of future annual precipitation changes in California. *J. Climate*, v. 26, 5879-5896.
- Pierce, D. W., D. R. Cayan, and B. L. Thrasher, 2014: Statistical downscaling using localized constructed analogs (LOCA). *J. Hydrometeorology*, v. 15, p. 2558, doi:10.1175/JFM-D-14-0082.1
- Pierce, D. W., D. R. Cayan, E. P. Maurer, J. T. Abatzoglou, and K. C. Hegewisch, 2015: Improved bias correction techniques for hydrological simulations of climate change. *J. Hydrometeorology*, v. 16, p. 2421-2442. DOI: <http://dx.doi.org/10.1175/JHM-D-14-0236.1>
- Pierce, D. W. and D. R. Cayan, 2015: Downscaling humidity with Localized Constructed Analog (LOCA) over the conterminous United States. *Climate Dynamics*, DOI 10.1007/s00382-015-2845-1.
- Polade, S. D., D. W. Pierce, D. R. Cayan, A. Gershunov, and M. D. Dettinger, 2014: The key role of dry days in changing regional climate and precipitation regimes. *Scientific Reports*, v. 4, doi:10.1038/srep04364.
- Rignot, E., Mouginot, J., Morlighem, M., Seroussi, H. and Scheuchl, B. (2014) Widespread, rapid grounding line retreat of Pine Island, Thwaites, Smith, and Kohler glaciers, West Antarctica, from 1992 to 2011. *Geophys Res Lett* 41, 3502-3509.

- Rupp, D. E., J. T. Abatzoglou, K. C. Hegewisch, P. W. Mote. 2013. Evaluation of CMIP5 20th century climate simulations for the Pacific Northwest USA, *Journal of Geophysical Research: Atmospheres* (188), doi: 10.1002/jgrd.50843.
- Swain, D. L., M. Tsiang, M. Haugen, D. Singh, A. Charland, B. Rajaratnam, and N. S. Diffenbaugh (2014), The extraordinary California drought of 2013–2014: Character, context, and the role of climate change, *Bull. Am. Meteorol. Soc.*, 95, S3–S7.
- Taylor, K. E., R. J. Stouffer, and G. A. Meehl, 2012: An Overview of CMIP5 and the experiment design. *Bull. Am. Met. Soc.*, 93, 485–498, doi:10.1175/BAMS-D-1111-00094.00091.
- van Vuuren, D. P., J. Edmonds, M. Kainuma, K. Riahi, A. Thomson, et al., 2011: The representative concentration pathways: an overview. *Climatic Change*, v. 109, p. 5–31. DOI 10.1007/s10584-0148-z
- Vaughan, D.G. and Arthern, R. (2007) Why is it hard to predict the future of ice sheets? *Science* 315, 1503–1504.
- Zhang, X., and J. A. Church (2012), Sea level trends, interannual and decadal variability in the Pacific Ocean, *Geophys. Res. Lett.*, 39, L21701, doi:10.1029/2012GL053240.